186p.

EXPERIMENTAL AND THEORETICAL STUDIES IN PLANETARY AERONOMY

FINAL REPORT

Contract No. NASw-701

PREPARED FOR

NATIONAL AERONAUTICS AND SPACE ADMINISTRATION

HEADQUARTERS

WASHINGTON, D. C.

OCTOBER 1963

GEOPHYSICS CORPORATION OF AMERICA BEDFORD, MASSACHUSETTS

NASA Headquarters
400 Maryland Avenue S.W.
Washington 25, D. C.

(NASA CR-53559 ; GCA Technical Report No. 63-30-N) TR- OTS: See Cover

EXPERIMENTAL AND THEORETICAL STUDIES IN PLANETARY AERONOMY

Prepared under

NASA Contract No. NASw-701

FINAL REPORT

Covering the Period from 2 April 1963 through 2 October 1963

by

1038512
GEOPHYSICS CORPORATION OF AMERICA
Bedford, Massachusetts

Oct. 1963 186p refs

This report has been prepared by Dr. F.F. Marmo, Project Director and Principal Investigator.

TABLE OF CONTENTS

INTRODUCTION

This is a Final Report of the work accomplished under NASA Contract No. NASw-701 covering the period from 2 April 1963 through 2 October 1963. Detailed accounts of the work accomplished during this six-month period can be found in the following six GCA Technical Reports and one technical paper (see papers accepted for publication) which are reproduced here in their entirety.

GCA TR No.	Title	Author(s)
63-3-N	PLANETARY AERONOMY XI: ABSOLUTE INTENSITY MEASUREMENTS IN THE VACUUM ULTRAVIOLET	J. Samson
63-4-N	PLANETARY AERONOMY XII: THE ROLE OF INTERPLANETARY DEBRIS IN PLANETARY ATMOSPHERES I. SODIUM IN THE EARTH'S ATMOSPHERE	F. Marmo and H. Brown
63-11-N	PLANETARY AERONOMY XIII: ELECTRON AND ION TEMPERATURES IN THE IONOSPHERE	A. Dalgarno
63-13-N	PLANETARY AERONOMY XIV: ULTRAVIOLET ABSORPTION OF SO_2: DISSOCIATION ENERGIES OF SO_2 AND SO	P. Warneck and F. Marmo
63-21-N	PLANETARY AERONOMY XV: TRANSPORT PROPERTIES AND SCATTERING IN MOLECULAR GASES	A. Dalgarno and R. Henry
63-28-N	PLANETARY AERONOMY XVI: CORPUSCULAR RADIATION IN THE UPPER ATMOSPHERE	A. Dalgarno

The scientific problems investigated under this contract not only resulted in the generation of GCA Technical Reports, but also resulted

in technical papers submitted and/or accepted for publication in accredited scientific journals and technical papers presented at scientific or professional meetings.

Technical Papers Submitted and/or Accepted for Publication in Accredited Scientific Journals

	Journal
a. Accepted for Publication	
*OBSERVED AND PREDICTED NEW AUTOIONIZED ENERGY LEVELS IN KRYPTON, ARGON AND XENON (J. Samson)	Phys. Rev. Letters (Dec. 1963)
PLANETARY AERONOMY XI: ABSOLUTE INTENSITY MEASUREMENTS IN THE VACUUM ULTRAVIOLET (J. Samson)	J. Opt. Soc. Am.
PLANETARY AERONOMY XIV: ULTRAVIOLET ABSORPTION OF SO_2: DISSOCIATION ENERGIES OF SO_2 AND SO (P. Warneck, F. Marmo and J. Sullivan)	J. Chem. Phys.
PLANETARY AERONOMY XVI: CORPUSCULAR RADIATION IN THE UPPER ATMOSPHERE (A. Dalgarno)	Annales de Geophys.
b. Submitted for Publication	
PLANETARY AERONOMY XIII: ELECTRON AND ION TEMPERATURES IN THE IONOSPHERE (A. Dalgarno)	Planetary & Space Sciences
PLANETARY AERONOMY XV: TRANSPORT PROPERTIES AND SCATTERING IN MOLECULAR GASES (A. Dalgarno and R. Henry)	Planetary & Space

Technical Papers Presented at Scientific or Professional Meetings

ABSOLUTE INTENSITY MEASUREMENTS IN THE VACUUM ULTRAVIOLET - Presented by J.A.R. Samson at OSA Meeting, Jacksonville, Florida, March 25-28, 1963.

---

*Reproduced in its entirety as it will appear in Phys. Rev. Letters.

THE ROLE OF INTERPLANETARY DEBRIS IN PLANETARY ATMOSPHERES - Presented by F.F. Marmo at AGU Meeting, Washington, D.C., April 20, 1963.

ELECTRON AND ION TEMPERATURES IN THE IONOSPHERE - Invited paper presented by A. Dalgarno at AGU Meeting, Washington, D.C., April 18, 1963.

THE FLUORESCENCE OF SOLAR IONIZING RADIATION - Presented by M. McElroy at AGU Meeting, Washington, D.C., April 20, 1963

CORPUSCULAR RADIATION IN THE UPPER ATMOSPHERE - Invited paper presented by A. Dalgarno at IUGG Meeting, Berkeley, California, August 19-24, 1963.

The material presented in this report has been divided into two categories: Section I presents the results of theoretical work, whereas Section II presents the results of experimental work accomplished under Contract No. NASw-701.

SECTION I — THEORETICAL

This section includes the results of theoretical work accomplished under Contract No. NASw-701 which have been previously published as GCA Technical Report Nos. 63-4-N, 63-11-N, 63-21-N and 63-28-N.

GCA Technical Report No. 63-4-N

PLANETARY AERONOMY XII: THE ROLE OF INTERPLANETARY DEBRIS IN PLANETARY ATMOSPHERES: I. SODIUM IN THE EARTH'S ATMOSPHERE

F. F. Marmo and H. K. Brown

March 1963

Contract No. NASw-701
and
Contract No. NASw-701*

Prepared for

National Aeronautics and Space Administration
Headquarters
Washington 25, D. C.

GEOPHYSICS CORPORATION OF AMERICA
Bedford, Massachusetts

*This work was initiated under Contract No. NASw-395 and completed under Contract No. NASw-701.

This paper was presented by F.F. Marmo at the AGU Meeting, Washington, D.C., April 20, 1963.

TABLE OF CONTENTS

LIST OF FIGURES

THE ROLE OF INTERPLANETARY DEBRIS IN PLANETARY ATMOSPHERES: I. SODIUM IN THE EARTH'S ATMOSPHERE

F. F. Marmo and H. K. Brown

I. INTRODUCTION

Interplanetary debris can be deposited in planetary atmospheres by vaporization processes brought about by the interaction of these particles with the ambient atmosphere. It is possible that these deposited chemical species can play a significant role in the aeronomy of the upper atmospheres of the terrestrial planets Venus, Earth and Mars. However, in spite of this potential, it appears that little or no detailed investigations have been directed toward this problem as far as the planets Venus and Mars are concerned. This is probably due to at least two factors: first, the aeronomy of the Martian and Venusian planets is not well known; and second, even in the Earth atmosphere the problem is not well understood since some contraversy still prevails concerning the origin of atmospheric sodium observed in the twilight and airglow. Specifically, both terrestrial (marine)[1,2] and extraterrestrial (meteoric and micrometeoric debris)[3] origins have been favored. Clearly, investigations into other planetary atmospheres are only justified on the basis of accepting the extraterrestrial origin.

In a recent article, Junge et al.[3] considered various origins for the atmospheric sodium observed above 70 km, and offered some convincing arguments to show that all terrestrial sources seem unlikely, including sea salt. Of the extraterrestrial sources considered, Junge has shown that the meteoric influx provides sufficient quantities to account for the observed sodium. In addition, they point out that the mass influx

due to micrometeorite material is considerably greater than that due to meteors. However, owing to the difficulty of estimating the fraction of incoming micrometeorite material that vaporizes, they were unable to make an accurate estimate of the contribution from this component. As a compromise, they suggest that the meteors and micrometeorites deposit equal amounts of sodium atoms in the Earth's upper atmosphere. They conclude that a flux of about 3×10^4 Na atoms/cm^2-sec can be employed as a working value, but also state that this value could be off by as much as two orders of magnitude. For the purposes of the present report, an extraterrestrial source is accepted and the role of the corresponding debris in the Earth, Venus and Mars atmospheres is investigated.

In this preliminary analysis, sodium in Earth atmosphere is examined first in order to check the validity of the model and of the parameters chosen. Then, with identical debris influx rates assumed for Venus and Mars, the distribution of sodium is calculated for their atmospheres. All the computations are presented on a relative scale for ready comparison since at this stage, only comparisons between the various planets are attempted. It is emphasized that the present effort is somewhat conjectural, so that the results should be applied with appropriate caution. However, certain qualitative features have become evident by this work which serve as a basis for further investigation.

II. QUALITATIVE DISCUSSION OF THE PROBLEM

Before any technical discussion is given, it is appropriate to give a qualitative description of the over-all problem as will become evident by the following. At first sight, it may seem premature to wonder about the role of interplanetary debris in planetary atmospheres other than Earth. Perhaps this is so, but on the other hand, a rather considerable potential exists as far as any optical probing or radar probing of these planets is concerned. For example, it can be shown that under certain conditions, the atmospheres would be easily optically thick in terms of several meteoric components and also that ionospheric electron number densities $> 10^8$ electrons cm^{-3} can be achieved at least in principle. Qualitative arguments are now given to justify these remarks.

Recent mass spectrometric[4] and twilight optical[5,6] measurements have verified the presence of Mg^+ and Ca^+ in the Earth's upper atmosphere. The mass spectrometric measurements were achieved during a meteoric shower and indicated that the Mg^+ and Ca^+ were distributed between 100 and 110 km with a maximum number density of about 10^4 cm^{-3} for Mg^+ and about 5×10^2 cm^{-3} for Ca^+. In addition, Nagy[7] has recently reported the mass spectrometric measurement of Na^+ between 90 and 120 km, but no values were given for the sodium ion number density. These measurements show that the number density of meteoric debris ions are not insignificant when compared to the ion densities of other Earth ionosphere components. It

is not only possible but almost a certainty that without the presence of atmospheric oxygen, these debris ions would, indeed, become the dominant species in the Earth atmosphere. This can be justified on the basis of previous work by Marmo[8] in which he describes the results of a series of rocket seeding experiments where Na, K, and Cs (debris-like) were ejected into the Earth upper atmosphere for the express purpose of generating highly dense artificial ionospheres. The experiments have shown that atmospheric molecular oxygen, O_2, is the dominant factor in precluding the generation of long-lived, dense ($> 10^7$ electrons cm^{-3}), artificial ionospheres at altitudes below 100 km. This was due to two factors involving molecular oxygen: (a) the high chemical consumption probability per alkali atom, and (b) the efficient formation of negative ions (O_2^-) with the subsequent removal of the alkali ion via mutual neutralization.

Although the absolute oxygen content in the atmospheres of the planets Venus and Mars has not as yet been established, there seems little doubt that oxygen is at best only a minor constituent. It can be shown that if, indeed, the atmospheres of Venus and Mars were truly oxygen-free, extremely dense ionospheres could be generated via solar photoionization of meteoric debris atoms and in addition, the atmospheres would be optically thick for several species. On the other hand, the present work will show that solar photodissociation of CO_2 in these atmospheres produces sufficient O_2 to act as an effective buffer against

the excessive buildup of free atoms. In particular, it will be shown that within the limitations of the present model, the debris atom number density-altitude distributions are somewhat similar to those for the Earth atmosphere. On the other hand, some marked differences are observed and point up the need for further investigation.

III. TECHNICAL DISCUSSION OF THE PROBLEM

The first calculations were performed for the Earth atmosphere. This was done in order to check the validity of the model, boundary conditions, and parametric values employed. Following this, calculations were performed for the planets Venus and Mars so that cogent comparisons could be made between the three terrestrial planets.

A. PHYSICAL-MATHEMATICAL MODEL

The physical-mathematical model employed was chosen to reflect the physical setup schematically shown in Figure 1. For the case of the Earth, it is presumed that atomic sodium is deposited at a single altitude of 105 km so that a delta source level is defined. Against this steady source, sinks are considered: an exospheric sink above the source level, a chemical sink below the source level, and the sink at the planet surface. In Fig. 1, the lower boundary of the exosphere sink is indicated at an altitude, $z = L$, and the chemical sink is indicated by the curve labeled $b(z) = B_o \exp(- p_o z/H)$. Concerning diffusion, two cases are considered: (a) Case I in which molecular diffusion ($\sigma_2 = 1$) prevails above the source level, whereas below the source level, eddy diffusion prevails ($\sigma_1 = 10^3$); and (b) Case II in which molecular diffusion prevails above and below the source level so that $\sigma_1 = \sigma_2 = 1$.

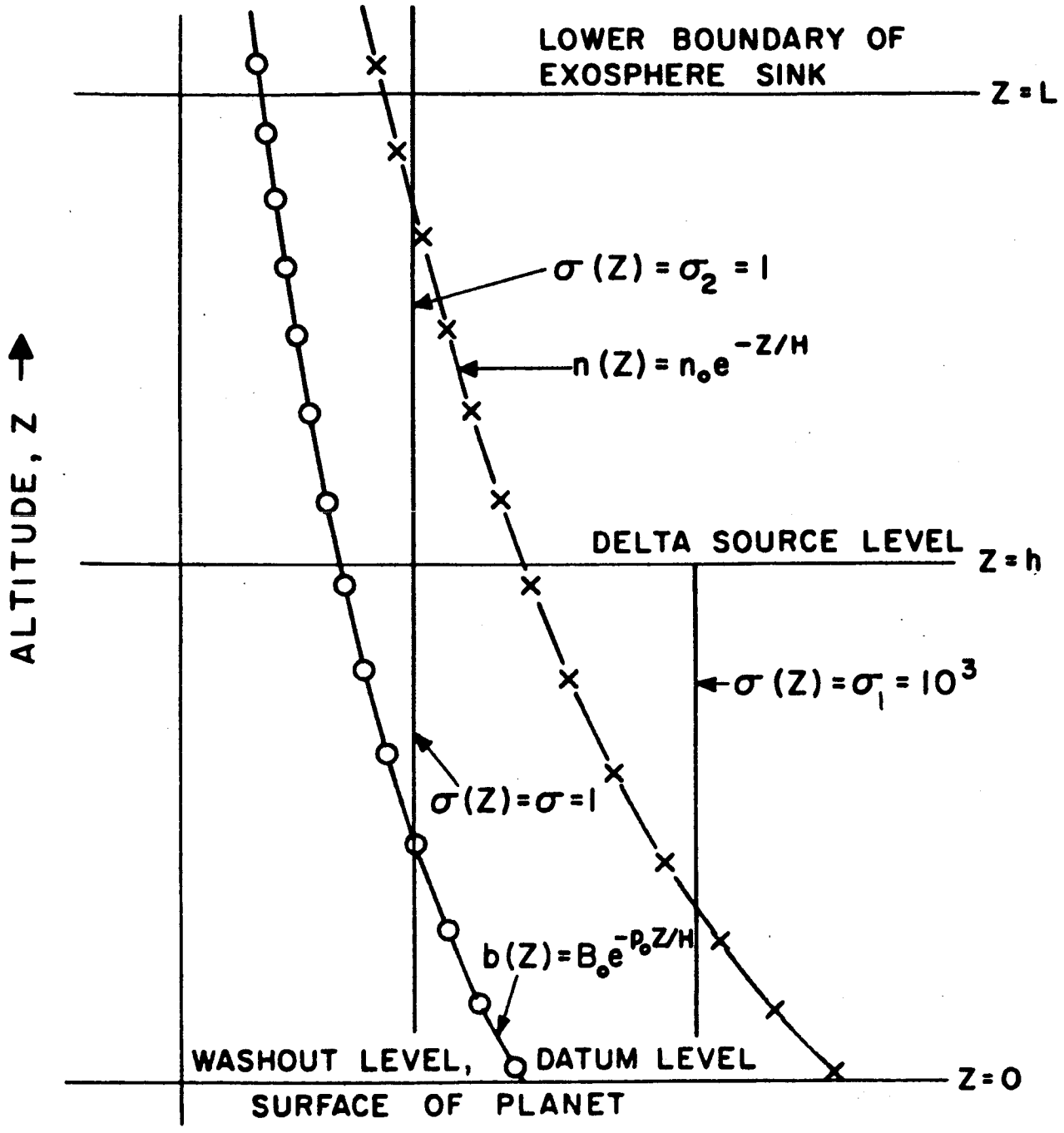

SCHEMATIC OF GENERAL PHYSICAL SET UP FOR ANY ONE OF THE TERRESTRIAL PLANETS

Figure 1

The proper mathematical model is suggested by the well-known Lettau[9] equation

$$n_s \bar{c}_s = - n_o d_o \left\{ \sigma(z) \bar{\nabla} \nu_s - \nu_s \left[\mu_s \bar{\nabla} (\ell n\ p) - \frac{m \bar{f}_s}{kT} \right] \right\} + n \nu_s \bar{V} \qquad (1)$$

which describes the mass transport of a minor constituent in a planetary atmosphere.

For our purposes, the vertical transport of the debris constituent in the isothermal atmosphere can be considered free of regular flow ($\bar{V} \equiv 0$) and external body forces ($\bar{f}_s \equiv 0$), other than gravity. In addition, at present, only a steady state solution is required; thus, Eq. (1) can be written as

$$Q_s(z) = - n_o d_o \left[\sigma(z) \frac{d\nu_s(z)}{dz} + \frac{\mu_s}{H} \nu_s(z) \right]. \qquad (2)$$

This equation defines the vertical transport flux $Q_s(z)$, particles per square centimeter per second, of the debris constituent at the height z (km) above the datum level z=0, in an isothermal atmosphere, in which the ambient number density n(z), particles/cm^3, is defined by the exponential law

$$n(z) = n_o e^{-z/H} \quad , \qquad n_o = n(0) \quad ,$$

and where H (km) is the atmospheric pressure scale height. The specific concentration is given as

$$\nu_s(z) = \frac{n_s(z)}{n\ (z)} \qquad (3)$$

of the minor constituent of number density $n_s(z)$, particles/cm^3, at the height z.

The quantity

$$\sigma(z) = \frac{D(z) + d(z)}{d(z)} \tag{4}$$

where

$$d(z) = d_o\, e^{z/H} , \qquad d_o = d(0) , \tag{5}$$

is the molecular diffusion coefficient and D(z) is the eddy diffusion coefficient.

The quantity,

$$\mu_s = \frac{m_s - m}{m} , \tag{6}$$

is the relative weight factor where m_s and m are the masses of the minor constituent (debris atom) and ambient atmospheric species, respectively.

The space gradient, dQ_s / dz, of the vertical transport flux, Q_s, satisfies the equation of continuity

$$\begin{pmatrix}\text{steady state vertical}\\ \text{flux gradient}\end{pmatrix} = \text{delta source} - \text{chemical sink} - \text{exospheric sink}$$

or

$$\frac{dQ_s}{dz} = S^{(+)}(z) - S_o^{(-)}(z) - S_L^{(-)}(z) . \tag{7}$$

Thus, the delta source

$$S^{(+)} \equiv N_o\, \delta \begin{cases} = f_o , & |z - h| < \epsilon \\ = 0 , & |z - h| > \epsilon \end{cases} , \quad \lim_{\epsilon \to 0} 2\epsilon\, f_o = N_o , \tag{8}$$

of minor constituent particles of strength N_o (particles/cm^2-sec), located at the fixed height z=h above the datum level z=0. $S_o^{(-)}$ is the steady, chemical consumption function,

$$S_o^{(-)} = b(z)\, n(z) \qquad (cm^{-3}sec^{-1}) \tag{9}$$

where

$$b(z) = B_o\, e^{-p_o z/H} \qquad (sec^{-1}) \tag{10}$$

is the probability of a chemical reaction at the height z. The exosphere exponential sink function is defined as

$$S_L^{(-)} \begin{cases} = 0 & 0 < z < L \\ = B_L\, e^{-p_L z/H}, & z > L \end{cases} \quad , \quad (particles/cm^2\text{-}sec) \tag{11}$$

where z=L is the lower boundary of $S_L^{(-)}$.

The detailed calculations for obtaining the closed analytic solutions are not repeated here. However, a brief sketch of the method of attack is included for completeness.

First, the following substitutions are made:

$$x = \frac{1}{q} \exp\left[- \frac{(1+p_o)}{2} \frac{z}{H} \right] , \tag{12a}$$

$$\nu = q^{-1/q}\, x^{-\frac{1}{2}q}\, V , \tag{12b}$$

and

$$2q = - (1+p_o) \frac{\sigma}{\mu_s} , \quad \text{where} \quad \mu_s < 0 \quad \text{and} \quad \sigma = \text{constant} \geqq 1. \tag{12c}$$

Now the H. Lettau vertical transport flux formula in Eq. (2) takes the form

$$Q_s(z) = - \frac{n_o d_o \mu_s}{2H} q^{-1/q} x^{-\frac{1}{2}q} \left[2qx \frac{dV(x)}{dx} + V(x) \right] \quad , \tag{12'a}$$

and the equation of continuity, as defined by Eq. (7), in the ν_s, z domain, is transformed into the modified Bessel differential equation,

$$L\,V \equiv \frac{d^2V}{dx^2} + \frac{1}{x}\frac{dV}{dx} - \left(c^2 + \frac{1}{4q^2x^2} \right) V = 0 \quad , \tag{12'b}$$

where

$$c^2 = \frac{\sigma B_o H^2}{d_o \mu_s^2} \quad , \quad \mu_s < 0 \quad , \quad \sigma = \text{constant} \geq 1 \quad , \tag{12'b'}$$

in the V,x domain.

The discontinuity of the flux function Q_s at the delta source level, z=h:

$$Q_s(h+0) = Q_s(h-0) + N_o \quad , \tag{13}$$

due to the presence of the delta source $N_o \delta(z,h)$ at z=h, and the piecewise definition of the step function $\sigma(z)$,

$$\sigma(z) \begin{cases} = \sigma = \sigma_1 = \text{constant} \geq 1 \, , & 0 < z < h \quad (14a) \\ = \sigma = \sigma_2 = \text{constant} \geq 1 \, , & z > h \quad , \quad (14b) \end{cases}$$

require that the V,x domain be composed of two domains, V_1, x_1 and F_2, x_2 , where

$$V(x) \equiv V_1(x_1) \, , \quad x = x_1 \quad \text{for all } z \text{ in } 0 < z < h \tag{15a}$$

and

$$V(x) \equiv V_2(x_2) \ , \quad x = x_2 \quad \text{for all } z > h. \tag{15b}$$

It is assumed that the lower boundary $z = L > h$ of the exosphere exponential sink function $S_L^{(-)}$, listed in Eq. (11), is so far removed from the delta source level, $L \gg h$, that for all practical purposes, L may be considered located at infinity: $L \approx \infty$ (if not, the V-x domain V,x would consist of three sub-domains).

The resolution of the boundary value problem in the V,x domain, which consists of the following set of conditions:

$$L\,V_1 = 0 \qquad \text{and} \qquad L\,V_2 = 0 \tag{16a}$$

$$\nu_s \to 0 \quad \text{as} \quad z \to 0 \ , \qquad \nu_s < M \quad \text{as} \quad z \to \infty \ , \tag{16b}$$

and

$$\nu_s\,(h+0) = \nu_s(h-0) \ , \qquad Q_s(h+0) = Q_s(h-0) + N_o \ , \tag{16c}$$

requires the determination of the pair of constants (A_1,B_1), and (A_2,B_2) in the general solutions,

$$V_1(x_1) = A_1\, I_{\frac{1}{2}q_1}\,(c_1x_1) + B_1 K_{\frac{1}{2}q_1}\,(c_1x_1) \tag{17a}$$

and

$$V_2(x_2) = A_2\, I_{\frac{1}{2}q_2}\,(c_2x_2) + B_2 K_{\frac{1}{2}q_2}\,(c_2x_2) \ , \tag{17b}$$

of the modified Bessel differential equations listed in Eq. (16a) of the boundary value problem, wherein

$$I_{\frac{1}{2}q}(cx) \qquad \text{and} \qquad K_{\frac{1}{2}q}(cx) \tag{17'}$$

are the modified Bessel functions, of order $\frac{1}{2}q$, of the first and second kind, respectively.

The boundary value problem stated in Eqs. (17) was evaluated for the terrestrial planets for Cases I and II with the parameter-values specified in Table 1.

1. Discussion of Parameter Values

Most of the parametric values included in Table 1 require no comments; however, some discussion is required to justify the choices for values of the following parameters: (a) delta source level, (b) lower boundary of exosphere sink, and (c) the chemical consumption probability per sodium atom.

a. Altitude Choice for Delta Source Levels of Earth, Venus and Mars

Undoubtedly, a more realistic source function is available by employing a Gaussian distribution of a specified halfwidth with maximum deposition at some selected altitude. However, for the present formulation, it is mathematically difficult to incorporate this source function, whereas the use of a delta source function made the problem tractable. The choice of a single deposition altitude is not only somewhat unrealistic, but also points up the problem of the proper choice for this altitude. It seems reasonable to consider this problem first for the planet Earth, and then

TABLE 1

PARAMETERS AND VALUES EMPLOYED IN CALCULATIONS FOR THE ATMOSPHERES OF EARTH, VENUS, AND MARS

Parameter	Earth-Value	Venus-Value	Mars-Value
delta source level, h	105 km	192 km	270 km
lower boundary of exospheric sink, L	∞	∞	∞
mass Na atom/mean mass ambient, m_s/m	2/3	2/3	2/3
total number density at surface, n_o	$2.5\times10^{19}cm^{-3}$	$6.6\times10^{20}cm^{-3}$	$2.7\times10^{18}cm^{-3}$
pressure scale height, H	6.6 km	6.7 km	20 km
local number density, n(z)	$n_o \exp(-z/H)$	$n_o \exp(-z/H)$	$n_o \exp(-z/H)$
molecular diffusion coefficient at surface, d_o	$1.8\times10^{-1}cm^2/sec$	$6.7\times10^{-3}cm^2/sec$	$1.6\times10^{0}cm^2/sec$
local molecular diffusion coefficient, d(z)	$d_o \exp(-z/H)$	$d_o \exp(-z/H)$	$d_o \exp(-z/H)$
σ-value for region below delta source level	$\sigma_1=10^3$ (for Case I) $\sigma_1=1$ (for Case II)	$\sigma_1=10^3$ (for Case I) $\sigma_1=1$ (for Case II)	$\sigma_1=10^3$ (for Case I) $\sigma_1=1$ (for Case II)
σ-value for region above delta source level	$\sigma_2=1$ (for Case I) $\sigma_2=1$ (for Case II)	$\sigma_2=1$ (for Case I) $\sigma_2=1$ (for Case II)	$\sigma_2=1$ (for Case I) $\sigma_2=1$ (for Case II)
consumption probability/Na atom, b(z)	$4.8\times10^{10}\exp(-2.2z/H)$	$4.0\times10^{10}\exp(-2.3z/H)$	$1.0\times10^{5}\exp(-2.3z/H)$

extrapolate for the other planets. This is what was done in the present case in which the Earth-value of 105 km was obtained in the following manner.

Herlofson[10] determined the following equation to describe the rate of vaporization of meteoric materials at any point along the trail:

$$q = 9/4 q_{max}(P/P_{max})[1 - 1/3(P/P_{max})]^2 \qquad (19)$$

where

q_{max} = the maximum rate of evaporization , $7 \times 10^{23} r_o^3$

P = the pressure at any point along the trail

P_{max} = pressure where q_{max} occurs , $4 \times 10^{-2} r_o$

and

r_o = the initial radius of the meteoric particle.

Dubin[11] applied Eq. (19) with the meteor number-size distribution due to Watson[12] to calculate the rate of vaporization of meteoric materials for 85 km, 100 km, and 115 km, and found that the maximum deposition could be expected at the lower altitudes. However, recent satellite measurements reported by McCracken et al.[13] show that the Watson distribution severely underestimated the component due to masses between 10^{-6} to 10^{-10} gms by as much as four orders of magnitude. Application of the McCracken distribution to Eq. (19) would result in

raising the altitude at which maximum vaporization occurs. Accordingly, an altitude of 105 km was chosen for the present work. The corresponding altitudes (on a number density basis) for Venus and Mars are 192 km and 270 km as given in Table 1.

Concerning the absolute N_o-value, Junge et al.[3] used 3×10^4 Na atoms/cm^2 sec, but state that this value may be incorrect by two orders of magnitude. In view of this uncertainty and the lack of knowledge for the planets Venus and Mars, this parameter was carried through as an adjustable value. Accordingly, the results of the present calculations will be presented as altitude profiles of the relative number density of sodium atoms for the various cases considered. Fortunately, the N_o-value enters as a factor in the analytical solution so that the calculated number density values are directly proportional to the N_o-value selected.

b. Lower Boundary of Exosphere Sink

An exospheric sink was employed as a convenient boundary condition. However, to reflect the real case, the strength of the sink is adjusted so that essentially no significant losses occur via escape. Thus, under steady state conditions, most of the loss of sodium is due to the sink at the surface of the planet. Finally, it turns out that for altitudes above a few scale heights, the position of the lower boundary of exospheric sink has relatively little effect; it is convenient to place it at infinity.

c. Chemical Consumption Probability Per Sodium Atom

Since the calculations are sensitive to this parameter, care should be exercised in choosing the proper form and value for b(z). Fortunately, there appear to be sufficient data to make a reasonable estimate for the case of Earth. On the other hand, the required data are essentially lacking in the case of the planets Venus and Mars. In any case, since b-values are required, they were calculated on the basis of available data for the Earth; and in the case of Venus and Mars, the required data were obtained by determining the amount of photochemically produced O_2 in the upper atmospheres of Venus and Mars via the solar photodissociation of CO_2. The method will be discussed and clarified below.

(1) Chemical Consumption Probability for Planet Earth

The derivation of the b-value of Earth is relatively simple since for the altitudes of interest, the dominant process for the chemical consumption of sodium atoms is

$$Na + O_2 + M = NaO_2 + M \; ; \quad k = 5 \times 10^{-30} cm^6/sec \quad \text{(Ref. 14)} \qquad (20)$$

The appropriate curve has been derived by Marmo and shown as Fig. 2 in the original report.[8] For mathematical convenience, a simplification is achieved if the probability can be expressed by the form

$$b(z) = B_o \exp(- p_o z/H) \; .$$

It can be shown that in this case the published values can be very closely approximated at all pertinent altitudes by choosing $B_o = 4.8 \times 10^{10}$ sec^{-1}, $p_o = 2.2$, and $H = 6.6$ km. These are the values employed and are shown in Table 1.

(2) Chemical Consumption Probability for Venus and Mars

The oxygen content for the upper atmospheres of these planets is not well known so that b-values could range from zero to perhaps as high as those appropriate to Earth. In order to arrive at a somewhat realistic estimate of the strength of the chemical sinks in these planets, the photochemical processes were examined in detail and are described below.

For this study, the isothermal atmospheres were assumed to consist of only nitrogen and CO_2 in which the CO_2 contents are assumed to be 2½ percent[15] and 2 percent[16] for Venus and Mars, respectively. For Venus, the atmosphere was considered isothermal at 297°K for all altitudes above the occultation level in accord with deVaucouleurs and Menzel.[17] Since it will be shown that essentially all the important photochemistry occurs above this level, this cannot be too objectionable. The surface pressure was obtained by extrapolation and found to be 27 atm.

For Mars, the temperature of the isothermal atmosphere was taken as 220°K with a surface pressure of about 64 mm Hg.

The effective photochemical reactions include:

$$CO_2 + h\nu \rightarrow CO + O \qquad \alpha_1 \qquad (21)$$

$$CO + O + M \rightarrow CO_2 + M \qquad k_1 = 5.0\times10^{-36} cc^2/molecule^2 sec \qquad (22)$$

$$O_2 + h\nu \rightarrow O + O \qquad \alpha_2 \qquad (23)$$

$$O + O + M \rightarrow O_2 + M \qquad k_2 = 2.7\times10^{-33} cc^2/molecule^2 sec \qquad (24)$$

$$O_3 + h\nu \rightarrow O_2 + O \qquad \alpha_3 \qquad (25)$$

$$O + O_2 + M \rightarrow O_3 + M \qquad k_3 = 5.0\times10^{-34} cc^2/molecule^2 sec \qquad (26)$$

$$O_3 + O \rightarrow 2O_2 \qquad k_4 = 6.8\times10^{-17} cc/molecule\ sec\ . \qquad (27)$$

At an altitude h,

$$\alpha_i = \sum_{\lambda} c_i\ I_o\ e^{-\tau}$$

where

c = total absorption cross section

τ = optical thickness = $\int_z^{\infty} \sum_i c_i\ n_i\ dz$

and

I_o = the solar flux incident at the top of the Venusian atmosphere.

Assuming photochemical equilibrium, the steady state concentrations of oxygen can be given by

$$n(O_2) = \frac{k_2\, n^2(O)\, n(N_2)\left[\alpha_3 + k_4\, n(O)\right]}{\alpha_2\alpha_3 + \alpha_2 k_4\, n(O) - k_3 k_4\, n^2(O)\, n(N_2)} \tag{28}$$

where that of atomic oxygen must be obtained from

$$n^4(O) + An^3(O) + Bn^2(O) + Cn(O) + D = 0 \tag{29}$$

where

$$A = \frac{\alpha_1 n(N_2)\left[3k_2k_3n(N_2)+2k_2k_4-k_3k_4\right]+\left[k_1n(N_2)+k_5\right]\left[\alpha_2k_4+2\alpha_3k_2n(N_2)\right]}{n(N_2)\left[k_1n(N_2)+k_5\right]\left[3k_2k_3n(N_2)+2k_2k_4-k_3k_4\right]} \tag{30}$$

$$B = \frac{\alpha_1k_4\left[\alpha_2+k_3n(N_2)n_o(CO_2)\, e^{-z/H}\right]+\alpha_3n(N_2)\left[2\alpha_1k_2+\alpha_2k_1\right]+k_5\alpha_2\alpha_3}{n(N_2)\left[k_1n(N_2)+k_5\right]\left[3k_2k_3n(N_2)+2k_2k_4-k_3k_4\right]} \tag{31}$$

$$C = \frac{\alpha_1\alpha_2\left[\alpha_3-k_4n_o(CO_2)\, e^{-z/H}\right]}{n(N_2)\left[k_1n(N_2)+k_5\right]\left[3k_2k_3n(N_2)+2k_2k_4-k_3k_4\right]} \tag{32}$$

$$D = \frac{-\alpha_1\alpha_2\alpha_3n_o(CO_2)\, e^{-z/H}}{n(N_2)\left[k_1n(N_2)+k_5\right]\left[3k_2k_3n(N_2)+2k_2k_4-k_3k_4\right]} \tag{33}$$

Solving the quartic Equation (29) for the atomic oxygen concentration enables calculation of $n(O_2)$ by Equation (28, thus describing the O_2-particle density distribution. The appropriate calculations were performed on the 1620 IBM which yielded the results shown in Figures 2 and 3 which show the resulting photochemically-produced O_2-altitude distributions on the planets Venus and Mars, respectively. It is evident that the O_2 distributions shown in Figs. 2 and 3 cannot be readily represented by a function of the form $B_o \exp(-pz/H)$ as in the case of Earth. However, for the present model, the oxygen content of the lower atmosphere is not important,

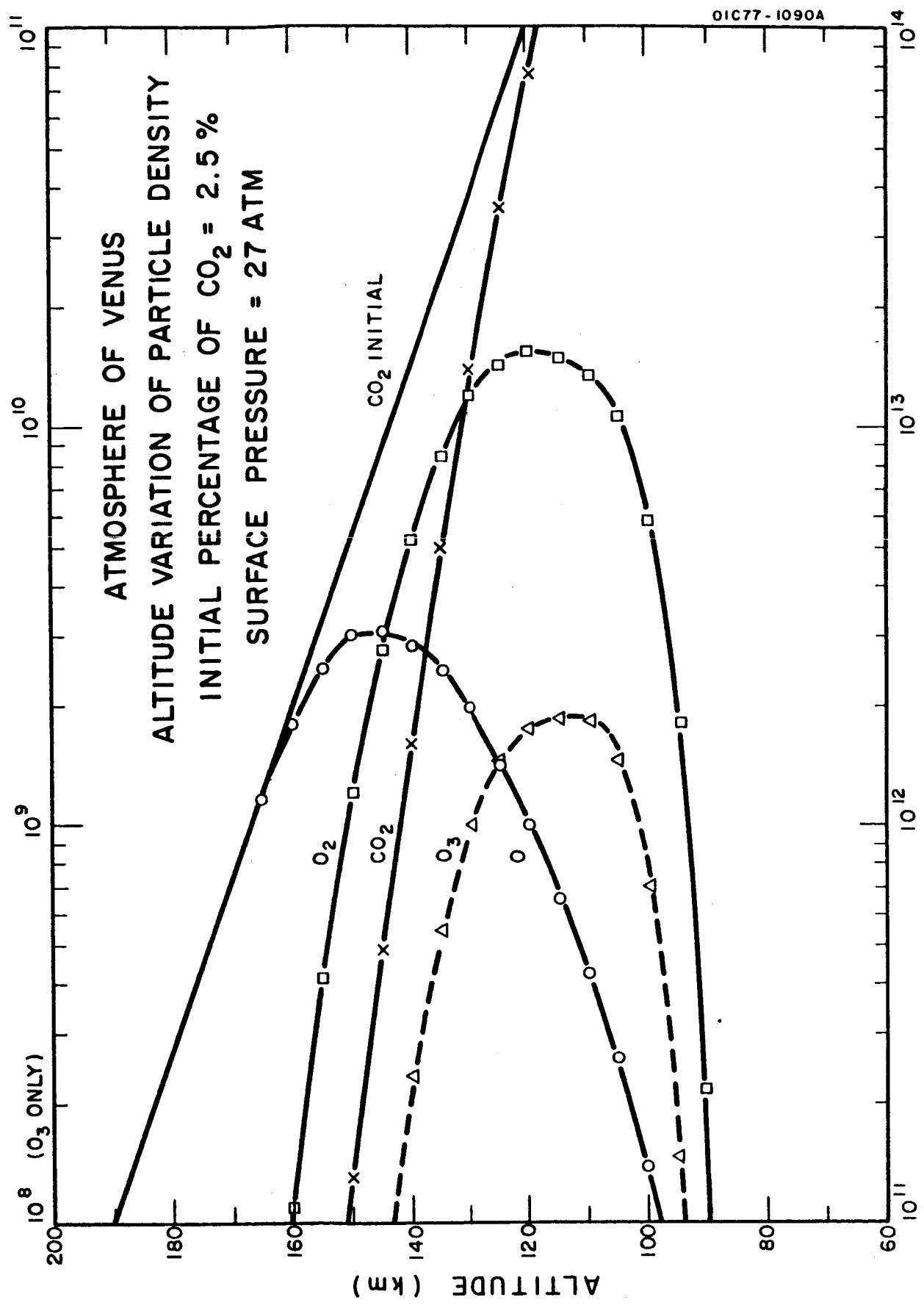
01C77-1090A
ATMOSPHERE OF VENUS
ALTITUDE VARIATION OF PARTICLE DENSITY
INITIAL PERCENTAGE OF CO_2 = 2.5 %
SURFACE PRESSURE = 27 ATM
CO_2 INITIAL
O_2
CO_2
O_3
O
10^8 (O_3 ONLY)
10^9
10^{10}
10^{11}
10^{12}
10^{13}
10^{14}
PARTICLE DENSITY (cm^{-3})
200
180
160
140
120
100
80
60
ALTITUDE (km)

Figure 2.

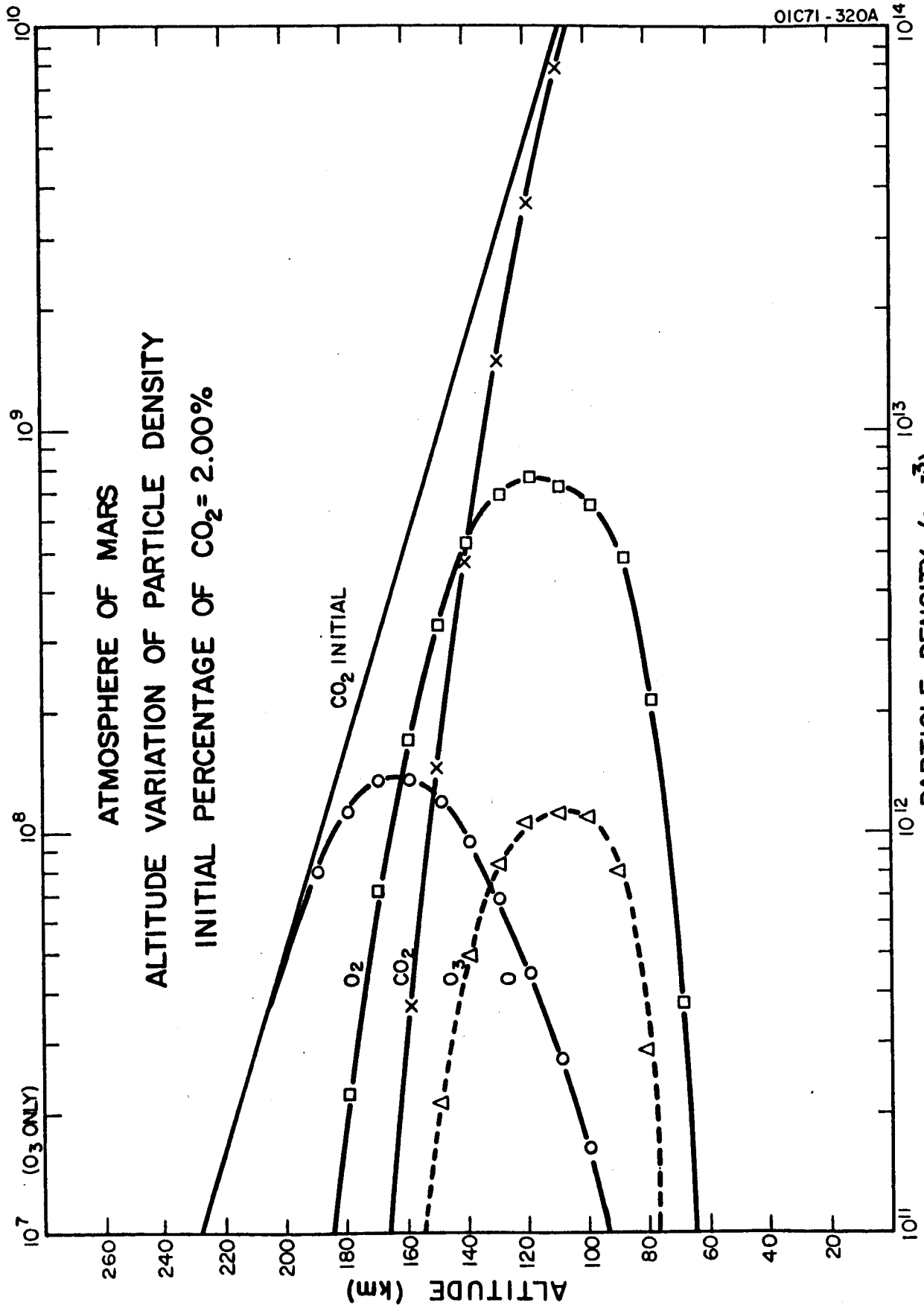
01C71-320A
ATMOSPHERE OF MARS
ALTITUDE VARIATION OF PARTICLE DENSITY
INITIAL PERCENTAGE OF CO_2 = 2.00%
CO_2 INITIAL
O_2
CO_2
O_3
O
$(O_3$ ONLY)
ALTITUDE (km)
PARTICLE DENSITY (cm^{-3})
10^{7}
10^{8}
10^{9}
10^{10}
10^{11}
10^{12}
10^{13}
10^{14}
260
240
220
200
180
160
140
120
100
80
60
40
20

Figure 3.

and at least the upper altitude region of the O_2 distributions can be closely approximated by a function of the proper form when the appropriate values shown in Table 1 are employed.

IV. RESULTS AND DISCUSSION

With the values shown in Table 1, the appropriate solutions were obtained for Eqs. (17) for Cases I and II in the planets Earth, Venus and Mars. The numerical results are summarized in Figs. 4, 5, 6, 7, 8 and 9, and are discussed in that order.

Figure 4 summarizes the numerical results for Case II in the Earth's atmosphere in which the solid curve represents the results with chemical consumption, whereas the dashed curve is the result with no chemical consumption. For the present discussion, the curves can be associated on the one hand with an oxygen-rich atmosphere and on the other hand, with an atmosphere which contains no oxygen. The figure is shown to make the following points: first, it makes evident that in the Earth's atmosphere, only a minute fraction of the total sodium content is in the free atomic form; second, if the other terrestrial planets lack oxygen, the free sodium distribution curves would be expected to be similar to the dashed curve shown in Fig. 4. It can easily be shown that if, indeed, this dashed curve does prevail, the very dense ionospheres become possible and the atmospheres take on unprecedented optical characteristics. These points were previously discussed in Section II. On the other hand, it is evident that in none of the three terrestrial planetary atmospheres does this situation actually occur. Thus, if comparable meteoric fluxes are assumed for the other planets, there probably is sufficient oxygen (or other suitable contaminant) in the Venus and Mars atmospheres to preclude

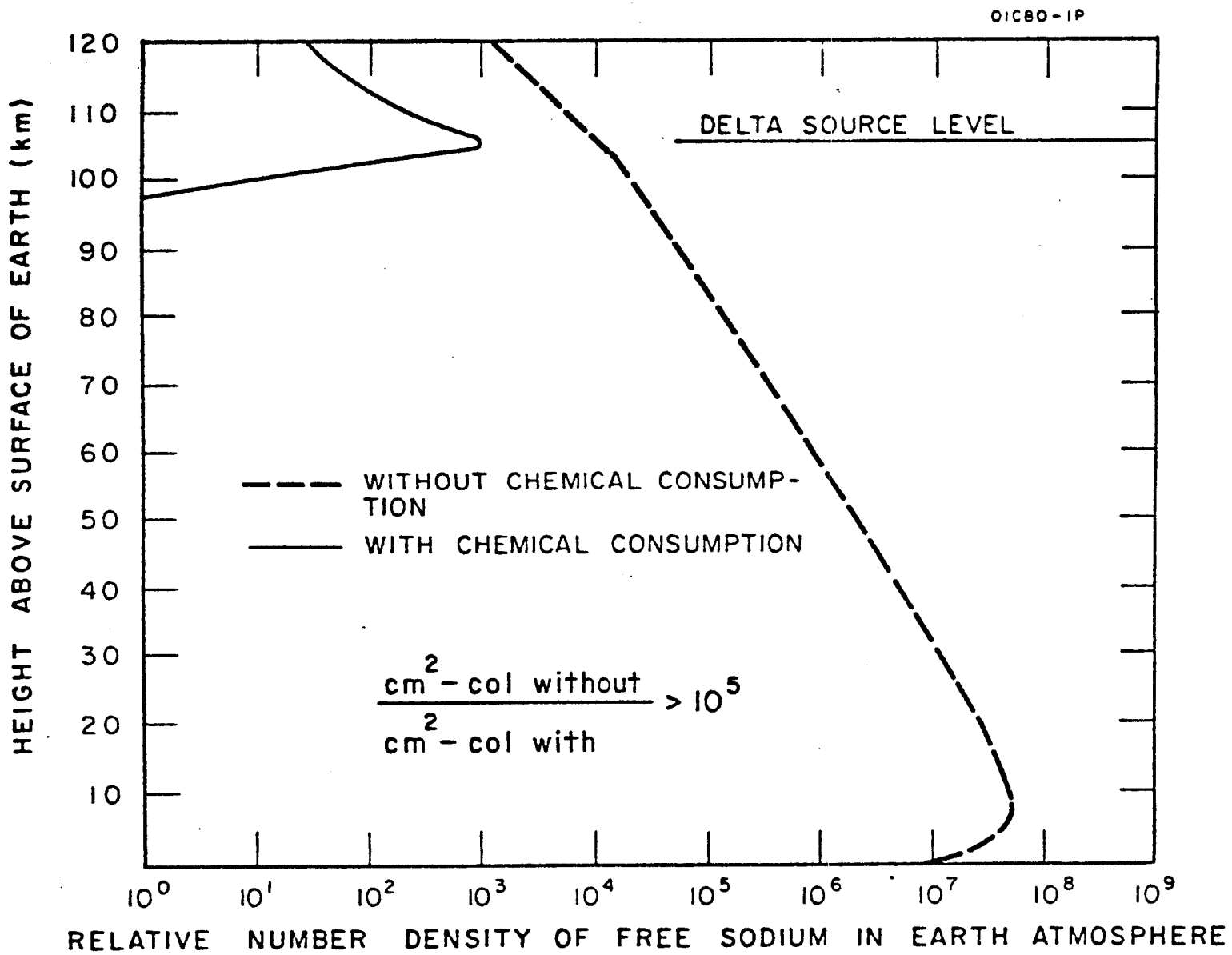
01C80-1P
HEIGHT ABOVE SURFACE OF EARTH (km)
120
110
100
90
80
70
60
50
40
30
20
10
DELTA SOURCE LEVEL
WITHOUT CHEMICAL CONSUMPTION
WITH CHEMICAL CONSUMPTION
cm² - col without / cm² - col with > 10⁵
10⁰ 10¹ 10² 10³ 10⁴ 10⁵ 10⁶ 10⁷ 10⁸ 10⁹
RELATIVE NUMBER DENSITY OF FREE SODIUM IN EARTH ATMOSPHERE

Figure 4.

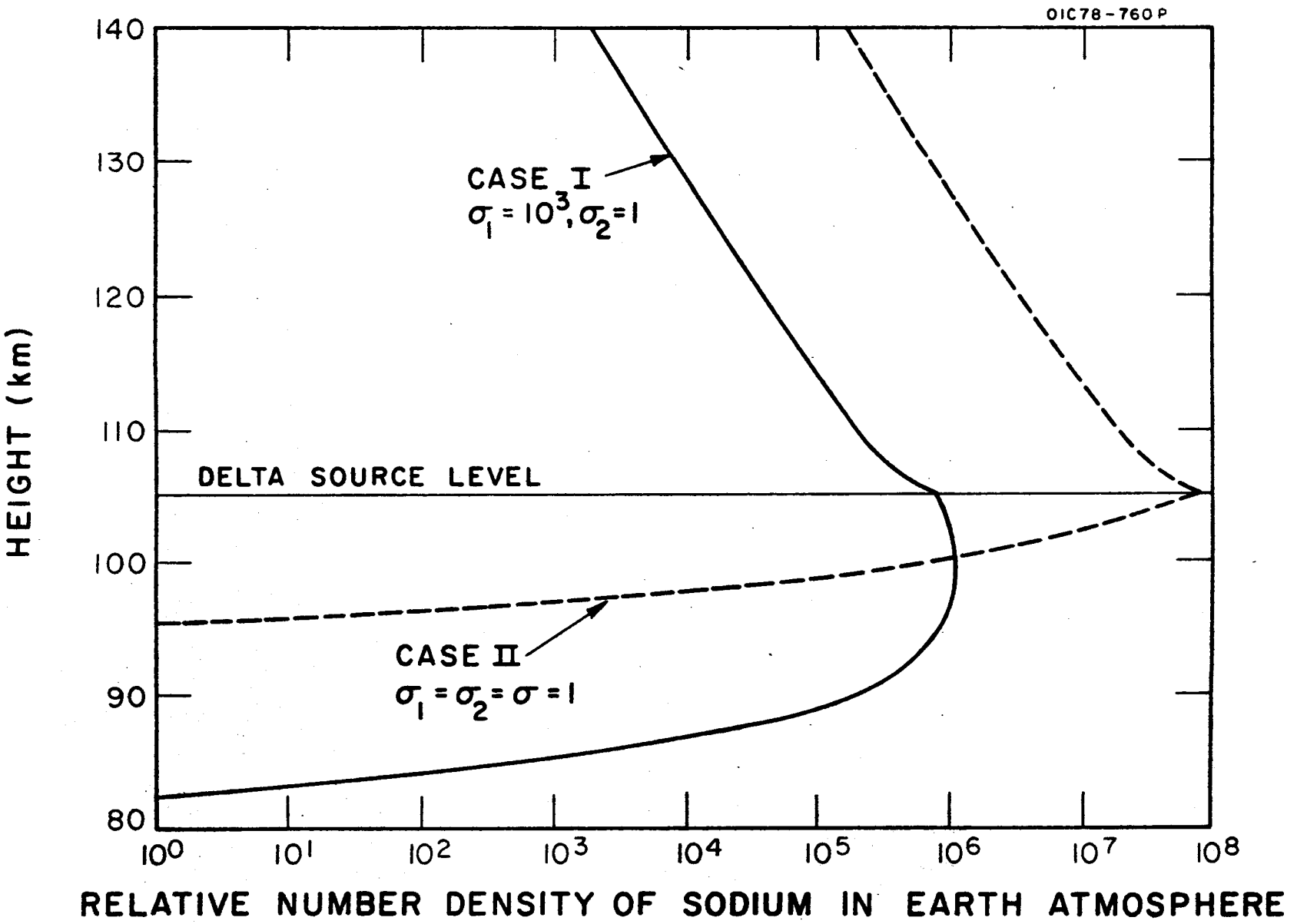
01C78-760P
140
130
120
110
100
90
80
HEIGHT (km)
CASE I
$\sigma_1 = 10^3, \sigma_2 = 1$
DELTA SOURCE LEVEL
CASE II
$\sigma_1 = \sigma_2 = \sigma = 1$
10^0
10^1
10^2
10^3
10^4
10^5
10^6
10^7
10^8
RELATIVE NUMBER DENSITY OF SODIUM IN EARTH ATMOSPHERE

Figure 5.

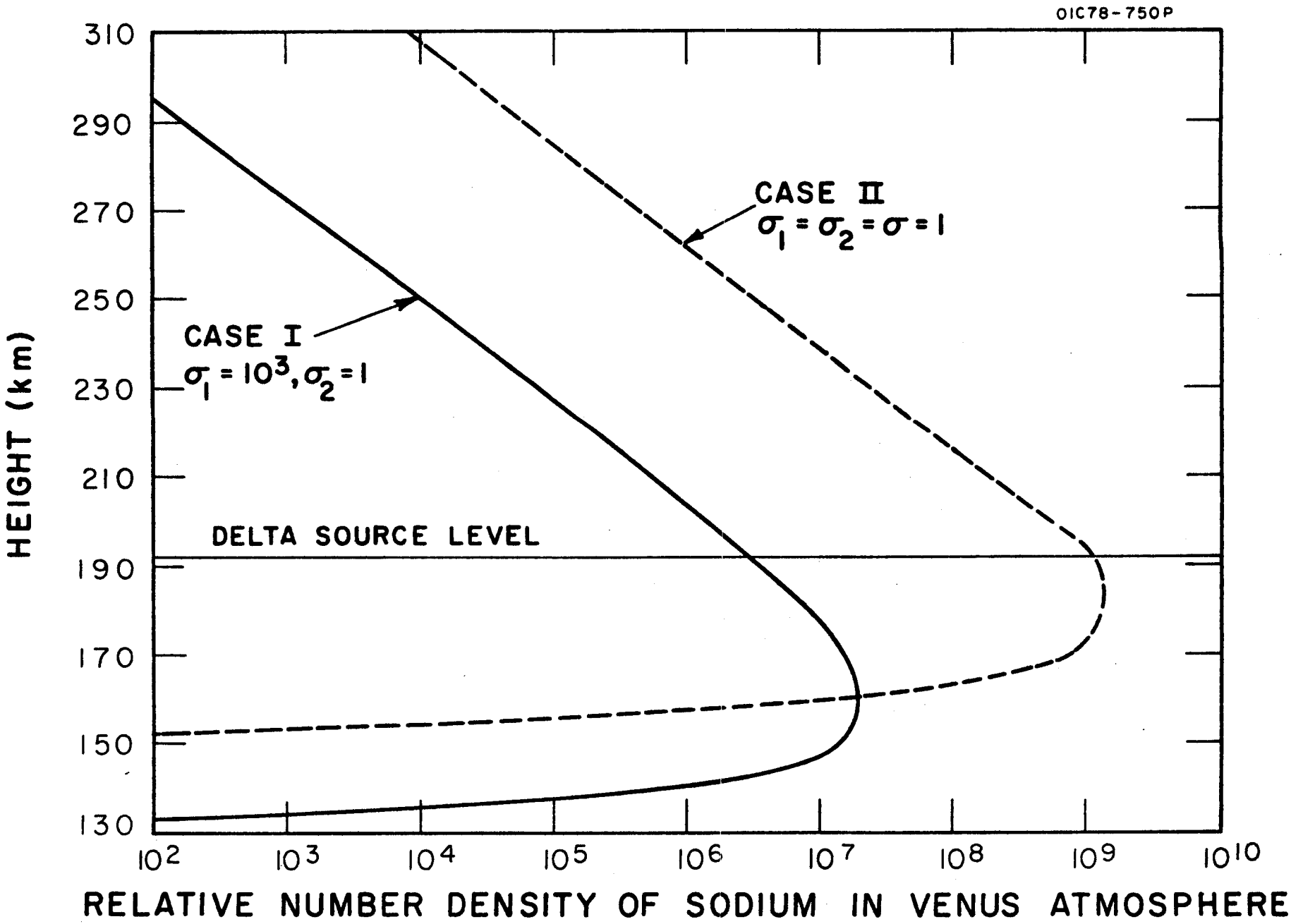
01C78-750P
310
290
270
250
230
210
190
170
150
130
HEIGHT (km)
CASE II
$\sigma_1 = \sigma_2 = \sigma = 1$
CASE I
$\sigma_1 = 10^3, \sigma_2 = 1$
DELTA SOURCE LEVEL
10^2
10^3
10^4
10^5
10^6
10^7
10^8
10^9
10^{10}
RELATIVE NUMBER DENSITY OF SODIUM IN VENUS ATMOSPHERE

Figure 6

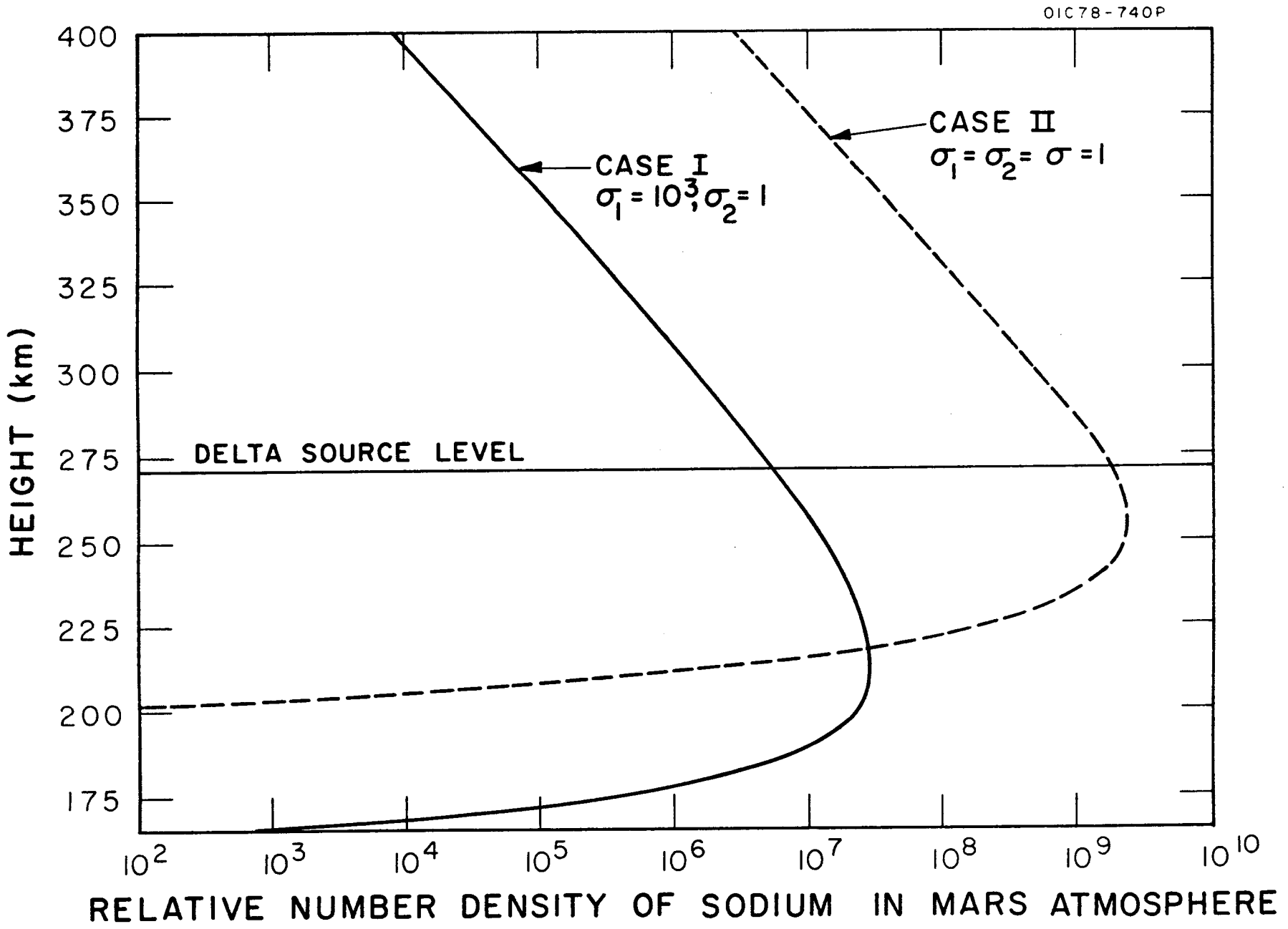
01C78-740P
400
375
350
325
300
275
250
225
200
175
HEIGHT (km)
CASE I
$\sigma_1 = 10^3, \sigma_2 = 1$
CASE II
$\sigma_1 = \sigma_2 = \sigma = 1$
DELTA SOURCE LEVEL
10^2
10^3
10^4
10^5
10^6
10^7
10^8
10^9
10^{10}
RELATIVE NUMBER DENSITY OF SODIUM IN MARS ATMOSPHERE

Figure 7.

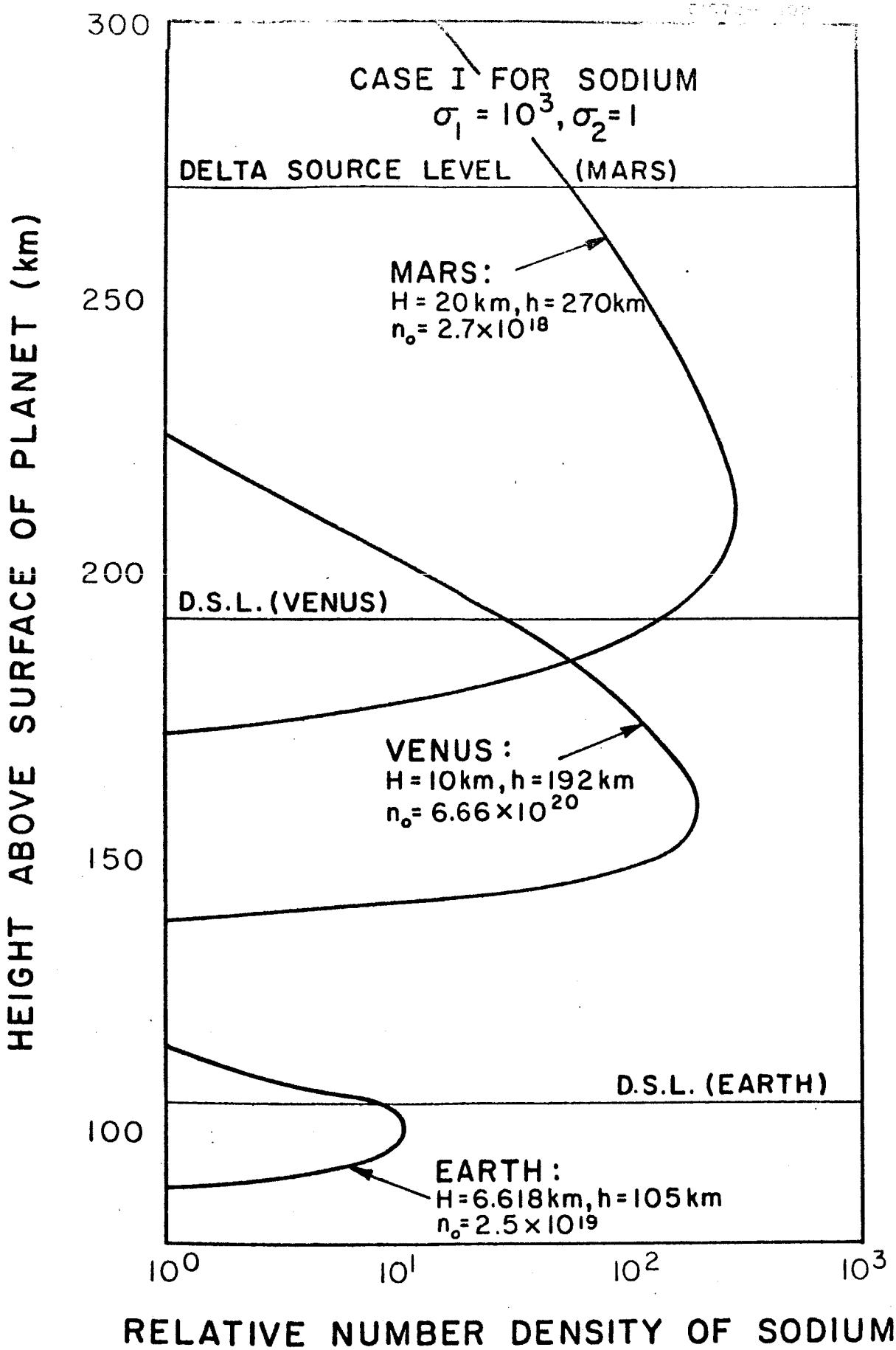
CASE I FOR SODIUM
$\sigma_1 = 10^3, \sigma_2 = 1$
DELTA SOURCE LEVEL (MARS)
MARS:
H = 20 km, h = 270km
$n_o = 2.7 \times 10^{18}$
D.S.L. (VENUS)
VENUS:
H = 10km, h = 192 km
$n_o = 6.66 \times 10^{20}$
D.S.L. (EARTH)
EARTH:
H = 6.618km, h = 105 km
$n_o = 2.5 \times 10^{19}$
300
250
200
150
100
10^0
10^1
10^2
10^3
HEIGHT ABOVE SURFACE OF PLANET (km)
RELATIVE NUMBER DENSITY OF SODIUM

Figure 8.

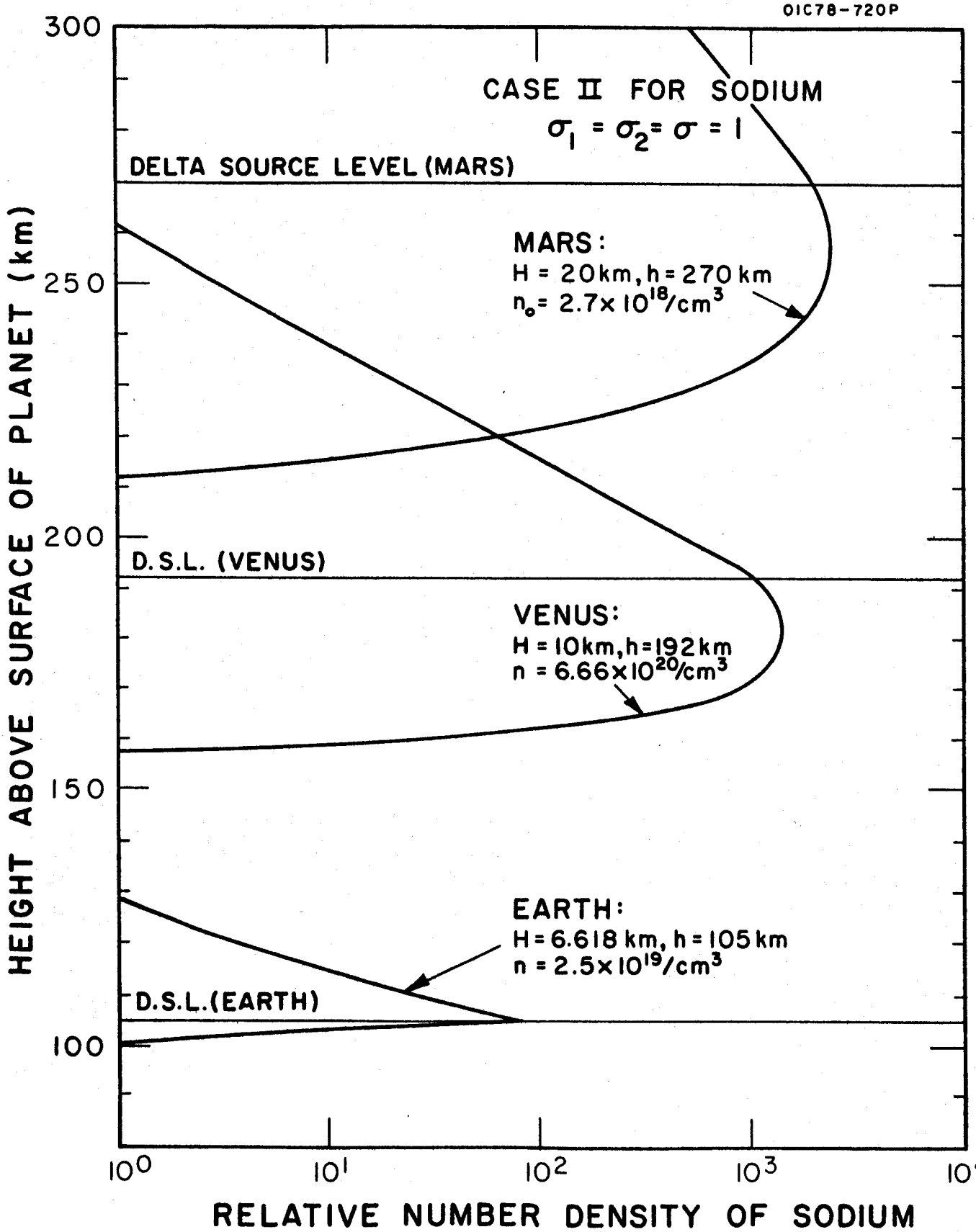
01C78-720P
CASE II FOR SODIUM
$\sigma_1 = \sigma_2 = \sigma = 1$
DELTA SOURCE LEVEL (MARS)
MARS:
H = 20km, h = 270 km
$n_o = 2.7 \times 10^{18}/cm^3$
D.S.L. (VENUS)
VENUS:
H = 10km, h = 192 km
$n = 6.66 \times 10^{20}/cm^3$
EARTH:
H = 6.618 km, h = 105 km
$n = 2.5 \times 10^{19}/cm^3$
D.S.L. (EARTH)
HEIGHT ABOVE SURFACE OF PLANET (km)
300
250
200
150
100
10^0
10^1
10^2
10^3
10^4
RELATIVE NUMBER DENSITY OF SODIUM

Figure 9.

the total conservation of free sodium. However, the role of an oxygen-poor atmosphere must still be examined, since it does not preclude that the planetary atmospheres may become optically thick in some specific spectral regions and that the meteoric debris ions may be the dominant species in the ionosphere.

In order to further investigate the possibilities discussed at the end of the previous paragraph, reference is made to Figs. 5, 6 and 7 which depict the altitude distributions of the relative number densities of sodium in the three planetary atmospheres. The solid curve represents Case I (turbulent diffusion below the delta source level), and the dotted curves represent Case II (molecular diffusion at all altitudes of interest). The three sets of curves show the effect of turbulent diffusion in lowering the entire sodium-altitude distribution curve. At the same time, this is accompanied by a corresponding decrease in the peak values for the sodium number densities. In the case of Earth, even though some pertinent data do exist, a detailed comparison of this crude model is unwarranted. This is especially true in that the subsequent effects of the solar radiation were not considered in this model. Indeed, it is quite surprising that the calculated distribution is not unlike that measured by several investigators.[1,18,19]

Perhaps the present preliminary crude results can be best employed with reference to Figs. 8 and 9. The figures can be used to make a ready comparison of Case I and Case II for the resulting relative number density

of sodium in the three terrestrial planetary atmospheres. Even a cursory comparison of these curves shows that although the total O_2-contents on the planets Venus and Mars are only about 1 part in 10^5 of that of Earth, it is sufficient to establish effective chemical sinks. However, it is also evident that there is considerably more free sodium in the planets Venus and Mars than that which exists in the Earth atmosphere. In fact, it can be noted that if the values shown in the figures are normalized against a value of 5×10^9 cm^2-column for Earth sodium, then the atmospheres of both Venus and Mars are optically thick for the sodium D-lines. This, of course, suggests that spectrographic observations be made of these planetary atmospheres in order to check the validity of this hypothesis. If an affirmative answer is obtained, this would make evident that the sea origin for Earth sodium is an unnecessary mechanism to invoke, and at the same time give critical information concerning the meteoric and micrometeoric flux. Concerning planetary ionospheres, the data in Figs. 8 and 9 are not directly applicable, since (except for the generation of photochemically-produced O_2) the model does not take account of the solar photoionizing flux or of the photodissociation of NaO_2 into free sodium and molecular oxygen. The latter process could generate a second and more dense free sodium peak in the lower atmospheres of Venus and Mars. Due to this possibility, one should not preclude the possibility of the generation of a dense (greater than 10^7 electrons cm^{-3}) ionosphere on these planets.

The more obvious improvements will be incorporated into the present model and some of the more interesting consequences of the present work

will be the subject of subsequent investigations in the role of interplanetary debris in planetary atmospheres.

REFERENCES

1. Lytle, E.A. and Hunten, D.M., J. Atmos. Terr. Phys. 16, 236 (1959).

2. Sullivan, H.M. and Hunten, D.M., Nature (London) (in press).

3. Junge, C.E., Oldenberg, O. and Wasson, J.T., J. Geophys. Res. 67, 1027 (1962).

4. Istomin, V.G., Doklady Akademii Nauk SSSR, 136, No. 5, 1066-1068 (1961).

5. Jones, A.V., Ann. Geophys. 14, 179 (1958).

6. Dufay, M., Ann. Geophys. 14, 391 (1958).

7. Nagy, E., Fizikai szemle, No. 4, 124-127 (1962).

8. Marmo, F.F., Space Research II (North-Holland Publishing Company, Amsterdam, 1961), pp. 1159-1193.

9. Lettau, H., "Diffusion in the Upper Atmosphere," pp. 320-333 of Compendium of Meteorology, Ed. T.F. Malone, Am. Meteorological Soc., Boston, Mass. (1951).

10. Herlofson, N., Phys. Soc. Rep. Prog. Phys. 11, 444 (1948).

11. Dubin, M., "Meteors" (A Symposium on Meteor Physics): Special Supplement (Vol. 2) to J. Atmos. Terr. Phys. (1955).

12. Watson, F., Between the Planets (Blakiston, 1941), pp. 140-177.

13. McCracken, C.W., Alexander, W.M. and Dubin, M., Nature, 192, No. 4801, 441-442 (Nov. 4, 1961).

14. Bawn, C.E.H. and Evans, A.G., Trans. Faraday Soc. 33, 1571, 1580 (1937).

15. Spinrad, H., Pub. A.S.P. 74, 187 (June 1962).

16. Marmo, F.F. and Warneck, P., GCA Technical Report No. 61-20-N, Final Report Contract No. NASw-395 (December 1961).

17. DeVaucouleurs, G. and Menzel, D.H., Harvard College Obs. Sci. Report No. 3 (July 1959) Reprinted from Nature, 188, 28 (1960).

18. Tinsley, B.A. and Jones, A.V., J. Atmos. Terr. Phys. 24, 345 (1962).

19. Donahue, T.M. and Blamont, J.E., Ann. Geophys. 17, 116 (1961).

GCA Technical Report No. 63-11-N

PLANETARY AERONOMY XIII: ELECTRON AND ION TEMPERATURES IN THE IONOSPHERE

A. Dalgarno

April 1963

Contract No. NASw-701

Prepared for

National Aeronautics and Space Administration
Headquarters
Washington 25, D.C.

This was an invited paper presented at the AGU Meeting, Washington, D.C., April 18, 1963. It has been submitted for publication in Planetary and Space Sciences.

GEOPHYSICS CORPORATION OF AMERICA
Bedford, Massachusetts

ABSTRACT

The relationships between the temperatures of the electrons, positive ions and neutral particles of the ionosphere are discussed. It is argued that on the basis of the heating due to solar ultraviolet radiation, the electron and ion temperatures will become equal at high altitudes and that both tend to increase above the neutral particle temperature. Anomalously high values of the electron temperature, accompanied by a red glow, are predicted to occur in the region of 400 km during the dawn period. The expected diurnal and latitudinal variations of the electron temperature are described.

TABLE OF CONTENTS

ELECTRON AND ION TEMPERATURES IN THE IONOSPHERE

A. Dalgarno

1. Introduction

The relationships between the temperatures of the electrons, the positive ions and the neutral particles which constitute the ionosphere are fundamental to the interpretation of its behavior. The theoretical studies of the effect of solar ultraviolet radiation (Hanson and Johnson 1961; Hanson 1963; Dalgarno, McElroy and Moffett 1963) show that departures from temperature equality are to be expected at altitudes above about 150 km, the difference between the electron temperature and the heavy particle temperature attaining a maximum somewhat greater than 1000°K at an altitude of about 220 km and decreasing rapidly as the altitude increases to 300 km. These conclusions are in substantial agreement with the Langmuir probe measurements (cf. Bourdeau 1963). It has been suggested (Dalgarno et al. 1963) that greater differences may occur near sunrise.

According to the theoretical studies, the difference between the electron temperature T_e and the positive ion temperature T_i should decrease rather slowly with increasing altitude above the peak of the F region. The difference may persist over several hundred kilometers, the predicted magnitude of $T_e - T_i$ depending sensitively upon the assumed density of the ambient electrons. The behavior of T_i with increasing

altitude has not been investigated except for the hypothetical situation in which T_e is taken as constant at 1800°K and the neutral particle temperature T_n is taken as constant at 1400°K. According to Hanson (1963), T_i remains equal to T_n up to an altitude of 600 km and then increases to T_e as the altitude increases to 1000 km.

Measurements of T_e and T_i at altitudes above 300 km are in apparent contradiction. Bourdeau (1963) has shown that rocket and satellite observations at mid-latitudes in quiet conditions can be satisfactorily explained assuming that T_e, T_i and T_n are approximately equal, a conclusion that is in harmony with the observations of backscatter reported by Bowles, Ochs and Green (1962), but not with the observations of backscatter by Evans (1962) who deduces that $T_e \sim 1.6\ T_i$ between 300 and 700 km or of Pineo and Hynek (1962) who deduce that $T_e \sim 2\ T_i$.

2. Electron Temperatures in the Upper F Region

Provided that $T_e < 3\ T_i$, the electrons located above the peak of the F region cool by collisions with the positive ions. If O^+ is the major positive ion, the equilibrium electron temperature T_e is determined by the equation

$$\frac{Q}{n_e^2} = 5.5 \times 10^{-7} (T_e - T_i) \Big/ T_e^{3/2} \qquad (1)$$

where Q is the heat flux density in eV cm^{-3} sec^{-1} and n_e is the electron number density. According to the calculations of Dalgarno, McElroy and Moffett (1963), the values of Q/n_e^2 which occur in the upper F region, if it is assumed that the heating takes place where the solar ultraviolet radiation is absorbed, are of the order of 10^{-9}.

The solutions of (1) for heat flux densities of the order of $10^{-9}\ n_e^2$ are shown in Figure 1 for ion temperatures of 1000°K, 1500°K and 2000°K.

It is clear from Fig. 1 that T_e-T_i is very sensitive to the values adopted for T_i, Q and n_e^2 when Q/n_e^2 is of the order of 10^{-9}. As a specific example, Table 1 lists the electron-ion temperature differences T_e-T_i corresponding to various possible electron densities for a heat flux density of 500 eV cm^{-3} sec^{-1} which is appropriate to an altitude of about 400 km during midday.

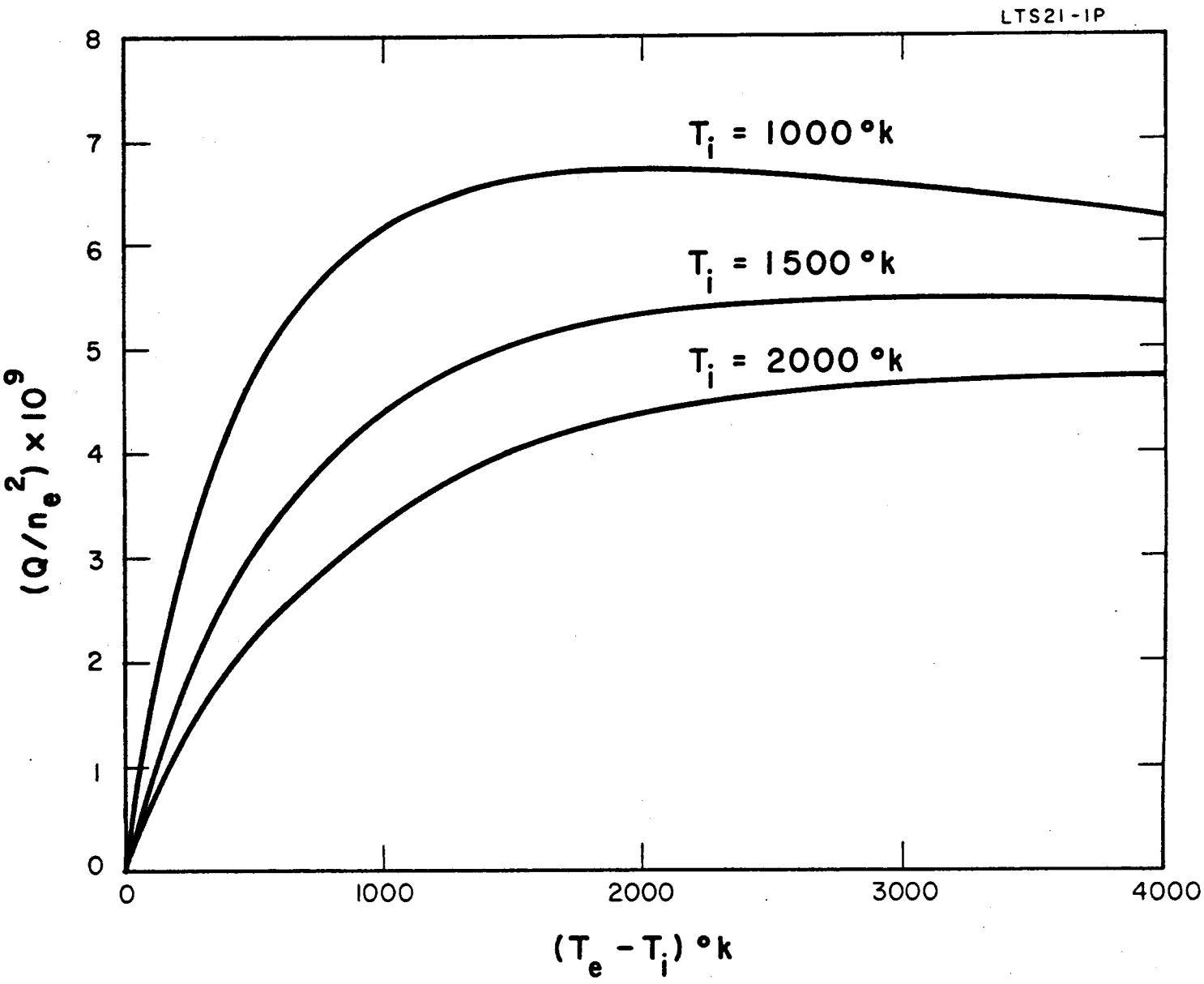

Figure 1. Equilibrium electron temperatures for various heat flux densities.

Table 1

Temperature Differences ($T_e - T_i$) at 400 km for Various Assumed Ambient Electron Densities and Ion Temperatures Corresponding to a Heat Flux Density of 500 eV cm^{-3} sec^{-1}

$n_e \times 10^{-6}$ cm^{-3} / T_i	1000°K	1500°K	2000°K
1.4	10	30	50
1.2	20	40	65
1.0	30	60	95
0.8	50	90	140
0.6	90	175	280
0.4	220	510	880
0.35	380	860	1640
0.325	490	1200	4000
0.300	720	3000	--
0.275	2000	--	--

With the assumption of local heating, the heat flux density in the upper F region where atomic oxygen is the major constituent is approximately

$$Q = 3 \times 10^{-6}\ n(0)\ \text{eV cm}^{-3}\ \text{sec}^{-1} \qquad (2)$$

where n(0) is the atomic oxygen number density. The altitude distribution of atomic oxygen may be represented by the expression of diffusive equilibrium

$$n\ (0/z) = n\ (0/r)\ \exp\ (-\ z/H) \qquad (3)$$

where H is the scale height and z is the altitude measured with respect to some reference level r at which n(0) = n (0/r). If the ions and electrons are also in diffusive equilibrium, then similarly

$$n_e(z) = n_e(r)\ \exp\ (-\ z/H') \qquad (4)$$

where the ion and electron scale height H' in an atmosphere of O, O^+ and e is related to H by

$$H' = \frac{T_e + T_i}{T_n} H \quad . \qquad (5)$$

It follows that in the upper F region,

$$\frac{Q}{n_e^2} = \frac{3\times10^{-6}\ n(0/r)}{n_e(r)^2} \exp\left\{ - \frac{z}{H}\left(\frac{T_e + T_i - 2T_n}{T_e + T_i} \right) \right\} \quad . \qquad (6)$$

If $T_n = T_i$, (6) simplifies to

$$\frac{Q}{n_e^2} = \frac{3\times10^{-6}\, n(O/r)}{n_e(r)^2} \exp\left\{ - \frac{z}{H}\left(\frac{T_e - T_i}{T_e + T_i}\right)\right\}, \qquad (7)$$

which implies that with increasing altitude, T_e and T_i will ultimately become equal. However, as Hanson (1963) notes, a small difference between T_e and T_i can persist over a considerable height range. Thus, if we assume that T_e/T_i is 1.5 at an altitude of 400 km, (7) yields the ratios listed in Table 2.

Table 2

Ratios of T_e/T_i According to (7)

Altitude (km)	400	400+H	400+2H	400+3H	400+4H
T_e/T_i	1.50	1.37	1.32	1.28	1.24

Since H is at least 75 km, (7) shows that T_e/T_i should decrease to 1.2 at an altitude of 700 km. The interpretations of the backscatter observations of Evans (1962) and of Pineo and Hynek (1962) in terms of a constant value of T_e/T_i between 300 and 700 km can not be understood on the basis of direct solar ultraviolet heating and an ionosphere in diffusive equilibrium. It is necessary to postulate either an additional heating mechanism or an electron distribution which decreases more rapidly with increasing altitude. This conclusion is strengthened

by the fact that helium and hydrogen ultimately become the major constituents with the consequence that the efficiency of heating is decreased and the efficiency of cooling is increased.

The temperate difference $T_e - T_i$ may actually decrease more rapidly than Table 2 suggests since there is a possibility that T_i is larger than T_n at great altitudes so that (6) should be used in place of (7).

3. Ion Temperatures in the Upper F Region

At high altitudes, the positive O^+ ions are heated by collisions with the electrons and cooled by collisions with the oxygen atoms, and

$$\frac{dT_i}{dt} = \frac{5.5\times10^{-7}\, n_e (T_e - T_i)}{T_e^{3/2}} - 8.6\times10^{-14}\, n(O)\, (T_i - T_n), \quad (8)$$

since the collision frequency of O^+ in O is about $10^{-9}\, n(O)\ sec^{-1}$. Therefore,

$$\frac{d}{dt}(T_e + T_i) = \frac{Q}{n_e} - 8.6\times10^{-14}\, n(O)\, (T_i - T_n) \quad . \quad (9)$$

In equilibrium,

$$T_i - T_n = \frac{1.16\times10^{13}}{n(O)} \frac{Q}{n_e} \quad . \quad (10)$$

Now using (4),

$$T_i - T_n = \frac{3.5\times10^{7}}{n_e} \quad . \quad (11)$$

This represents an upper limit since the collision frequency of O^+ in O is actually a slowly increasing function of temperature (Dalgarno 1961). It suggests that at 500 km, the ion temperature may exceed the neutral particle temperature by 100°K and at 800 km by 1000°K.

The coefficient in (11) is computed on the assumption that the heating is produced locally.† Since the major part of the heating due

†Hanson (1963) has shown that the fast photoelectrons produced at great altitude may escape from the ionosphere.

to solar ultraviolet radiation is provided by collisions of fast photoelectrons with the ambient electrons, the assumption of local heating is unlikely to be correct. Nevertheless, there is some local heating due to the photoionization processes which directly populate the ^2D metastable state of O^+. The O^+ (^2D) has a long radiative lifetime and above 200 km, it is probably deactivated by superelastic collisions

$$O^+(^2D) + e \rightarrow O^+(^4S) + e \quad . \tag{12}$$

According to Dalgarno and McElroy (1963), (12) gives rise to a heat flux density of approximately

$$Q = 6 \times 10^{-7}\ n(O)\ \text{eV cm}^{-3}\ \text{sec}^{-1} \quad , \tag{13}$$

which in the absence of heat conduction and diffusion cooling is sufficient to maintain T_i some 200°K above T_n at 800 km and some 500°K at 1000 km.

The tendency of T_i to rise above T_n increases the difficulty presented by some of the backscatter data and emphasizes the discrepancy between them and the temperatures derived from charged particle density profiles. Thus, if the heating were such that $T_e = 1.6\ T_i$ at high altitudes, then it follows from (1) and (10) that

$$T_i - T_n = \frac{2 \times 10^6\ n_e}{T_i^{\frac{1}{2}}\ n(O)} \quad . \tag{14}$$

Adopting a model atmosphere employed by Hanson (1963), it follows that at 500 km, $T_n = 1200^{\circ}K$, $T_i = 1500^{\circ}K$ and $T_e = 2400^{\circ}K$; and at 700 km, $T_n = 1200^{\circ}K$, $T_i = 2100^{\circ}K$ and $T_e = 3400^{\circ}K$.

4. Diurnal Variation of Electron Temperatures

Provided Q/n_e^2 does not exceed 10^{-9} eV cm^{-3} sec^{-1}, $T_e = T_i$ and the diurnal variation of T_e must be very similar to that of T_n. If Q/n_e^2 does exceed 10^{-9} eV cm^{-3} sec^{-1}, it is more difficult to predict the diurnal variation of T_e since it depends sensitively upon the diurnal variations of the electron and neutral particle densities. According to (7), in the upper F region $T_e - T_i$ should decrease more slowly with increasing altitude as T_n increases, but the absolute value of $T_e - T_i$ at any given altitude depends also upon $n(O/r) \,/\, n_e(r)^2$, the variation of which with increasing T_n is uncertain. In any event, the electron number density probably responds more slowly to an increase in T_n than does the neutral particle density and high values of T_e/T_i may occur during periods of geomagnetic activity. This, rather than any additional preferential heating of the electrons, may be the explanation of the observations of Spencer et al. (1962).

The diurnal variation of T_e in the lower F region is of special interest since anomalously large values may occur near sunrise. It has been suggested, in particular, that T_e may exceed $3T_i$ in which case the electron temperature increases to a new equilibrium value determined by the efficiency of cooling by collisions with the neutral particles (Dalgarno et al. 1963).

Preliminary calculations indicate that the heat flux density at dawn at an altitude of 400 km is about 700 eV cm^{-3} sec^{-1}. The resulting values of $T_e - T_i$ are shown in Table 3 for a range of concentrations n_e.

Table 3

Dawn Values of $T_e - T_i$

n_e (cm^{-3})	1×10^6	8×10^5	6×10^5	4×10^5	3.2×10^5
$(T_e - T_i)^\circ K$	50	75	130	1430	2000

If the ambient electron density at 400 km is less than 3.2×10^5 cm^{-3}, and it probably is, T_e increases above $3T_i$ and may attain a value of several thousand degrees. The principal limiting factor may be the increase in electron density.

The cooling at the high equilibrium temperatures is effected partly by collisions leading to excitation of the ^1D state of atomic oxygen, and the runaway of the electrons should become evident through the appearance of a red glow.

During the dawn period, there should occur also discontinuities in T_e as a function of altitude.* Explicit calculations are in progress to predict the altitude range of the anomalously high values of T_e.

Similar effects should occur at greater altitudes during dawn twilight. Thus, the diurnal variation of $T_e - T_i$ expected from solar

*The examination of this possibility was stimulated by a conversation with Dr. P. Molmud and Dr. S. Altshuler.

ultraviolet heating at midlatitudes consists of very high values in the region of 400 km at dawn, the magnitude and altitude of the maximum temperature decreasing with increasing time.

During the afternoon, the magnitude and altitude should increase but because the ambient electron concentration is larger, the very high dawn values are not expected to occur at sunset. After sunset, kinetic equilibrium should be rapidly established.

The diurnal variation will be less marked at high latitudes where diffusion is not inhibited by the magnetic field, especially since the faster electrons diffuse more rapidly than the slower electrons.

There is some question as to whether the dawn behavior at mid-latitudes is a stable configuration. It may be that the sunrise effect is manifested by a sharp reduction in electron density rather than by a sharp increase in electron temperature.

A departure from temperature equilibrium at dawn is suggested by a preliminary analysis of Ariel data (Willmore, Boyd and Bowen 1962) and by the backscatter observations of Bowles et al. (1962), but not by the backscatter observations of Evans (1962). There is no evidence that T_e exceeds $3T_i$ at any altitude for a short period about dawn, but this may be due to the averaging procedures which have been applied to the data.

5. Latitude Variation of Electron Temperatures

Spencer, Brace and Carignan (1962) find from rocketborne Langmuir probes that T_e is higher in auroral latitudes than at midlatitudes in quiet conditions, and the main characteristics of the Ariel data (Willmore et al. 1962, Bourdeau 1963) are a general rise in T_e and a less pronounced diurnal variation at high latitudes. It may be that the enhanced temperature is caused by corpuscular radiation (which would give rise to some preferential heating of the electrons), but higher values of T_e can be explained qualitatively as a consequence of a latitudinal decrease in the ambient electron density. The measurements of Spencer et al. (1962) show that the charged particle densities at auroral latitudes can be much lower than those occurring at midlatitudes in quiet conditions.

Willmore et al. (1962) have remarked that the Ariel data are consistent with significant atmospheric heating by particles dumped at high latitudes, but the satellite drag data do not show any important variation with latitude except during magnetically disturbed conditions (Jacchia 1963). As Bourdeau (1963) has shown, there are several uncertainties in the preliminary analysis of the Ariel electron temperatures.

REFERENCES

Bourdeau, R.E., 1963, Space Science Reviews, March issue.

Bowles, K.L., Ochs, E.R. and Green, J.L., 1962, J. Res. NBS A66, 395.

Dalgarno, A. and McElroy, M.B., 1963, Planetary Space Sci., in press.

Dalgarno, A., McElroy, M.B. and Moffett, R.J., 1963, Planetary Space Sci., April issue.

Evans, J.V., 1962, J. Geophys. Res. 67, 4914.

Hanson, W.B., 1963, Space Physics III, in press.

Hanson, W.B. and Johnson, F.S., 1961, Mémoires Soc. R. Liège, Series 5, 4, 390.

Jacchia, L., 1963, Rev. Mod. Phys., in press.

Pineo, V.C. and Hynek, D.P., 1962, J. Geophys. Res. 67, 5119.

Spencer, N.W., Brace, L.H. and Carignan, G.R., 1962, J. Geophys. Res. 67, 157.

Watanabe, K. and Hinteregger, H.E., 1962, J. Geophys. Res. 67, 999.

Willmore, A.C., Boyd, R.L.F. and Bowen, S.J., 1962, Conference on the Ionosphere, London, July.

GCA Technical Report No. 63-21-N

PLANETARY AERONOMY XV: TRANSPORT PROPERTIES AND SCATTERING IN MOLECULAR GASES

A. Dalgarno and R.J.W. Henry

June 1963

Contract No. NASw-701

Prepared for

National Aeronautics and Space Administration
Headquarters
Washington 25, D. C.

GEOPHYSICS CORPORATION OF AMERICA
Bedford, Massachusetts

This paper has been submitted for publication in Planetary and Space Sciences.

ABSTRACT

Experimental data on transport properties and scattering in molecular gases are usually interpreted assuming a spherically symmetric interaction potential and single channel (elastic) scattering. This procedure is analyzed and shown to be justifiable as a first approximation provided it is recognized that the generalization of transport theory to molecular gases involves the replacement of elastic cross sections by total cross sections and that the beam scattering data refer to total cross sections and not elastic cross sections. The distinction between total and elastic cross sections is especially significant for ion-molecule interactions at thermal velocities, since it implies a form for the long range interaction different from that which has been adopted. Some consequences of this difference in long range behaviour are described.

Explicit calculations are presented for the scattering of atomic hydrogen by molecular deuterium.

TABLE OF CONTENTS

FIGURE CAPTIONS

Figure 1. Angular distribution for collisions between an H atom and D_2 molecule with incident energy 0.0625 eV;

curve A: elastic differential scattering cross section plotted against scattering angle;

curve B: inelastic differential scattering cross section plotted against scattering angle (the scale of inelastic cross section is $\frac{1}{20}$ scale of elastic cross section).

Figure 2. Elastic angular distributions for collisions between an H atom and D_2 molecule.

curve A: incident energy = 0.00625 eV;

curve B: incident energy = 0.03125 eV;

curve C: incident energy = 0.0625 eV.

Figure 3. Angular distributions for collisions between an H atom and D_2 molecule with incident energy 0.0625 eV.

Viscosity distribution = $2\pi\ I\ (\theta)\ \sin\theta\ (1 - \cos^2\theta)$

curve A: elastic contribution;

curve a': inelastic contribution;

Diffusion distribution = 2π I (θ) sin θ (1 - cos θ)

curve B: elastic contribution;

curve b': inelastic contribution.

TRANSPORT PROPERTIES AND SCATTERING IN MOLECULAR GASES

A. Dalgarno and R.J.W. Henry

1. Introduction

According to the Chapman-Enskog theory, the transport properties of dilute spherically symmetric gases depend upon the coefficients of diffusion, viscosity, thermal conductivity and thermal diffusivity. These transport coefficients may be expressed in terms of collision cross sections

$$Q_s = 2\pi \int_o^\pi I(\theta) (1 - \cos^s \theta) \sin \theta \, d\theta$$

where $I(\theta)$ is the differential cross section for the elastic scattering of one gas atom by another through an angle θ measured in the centre of mass system. The total elastic cross section is

$$Q = 2\pi \int_o^\pi I(\theta) \sin \theta \, d\theta.$$

Measurements of the scattering of beams of particles refer to the differential cross section $I(\theta)$ or to the total cross section for scattering through angles greater than some minimum angle θ_o:

$$Q(\theta) = 2\pi \int_{\theta_o}^\pi I(\theta) \sin \theta \, d\theta.$$

The differential cross section $I(\theta)$ can be evaluated from a knowledge of the interaction potential $V(r)$ as a function of the separation r of the colliding particles. It is customary in the analysis of experimental data on transport coefficients and beam scattering to adopt an

analytic representation of V (r) containing a number of disposable parameters and to choose the parameters so that the experimental data are reproduced. Having determined V (r) it may be used to predict other transport coefficients over wider temperature ranges and the procedure has proved very useful in extending experimental measurements.

It has also been followed in the analysis of molecular gases for which the interaction potential is not spherically symmetric and the scattering is not single channel (elastic) scattering. A detailed study is necessary in order to assess the significance of such analyses and of the effective interaction potentials that are derived.

2. Theory of Scattering

The scattering channels appropriate to a collision between two molecules can be labelled by the rotational angular momentum quantum numbers j_1 and j_2, characterizing the internal motions of the molecules, and the orbital angular momentum quantum number ℓ, characterizing the relative motion of the colliding pair. The interaction potential $V(\underset{\sim}{r})$ is a function of the position vector $\underset{\sim}{r}$ joining the two molecules, and it can usefully be written in the form

$$V(\underset{\sim}{r}) = v_o(r) + v_c(\underset{\sim}{r})$$

where $v_o(r)$ is obtained from $V(\underset{\sim}{r})$ by averaging over all orientations assuming that they are equally probable. The potential $v_c(\underset{\sim}{r})$ couples together different scattering channels $(\underline{j}_1, \underline{j}_2, \underline{\ell})$ and $(\underline{j}_1', \underline{j}_2', \underline{\ell}')$ such that

$$\underline{j}_1 + \underline{j}_2 + \underline{\ell} = \underline{j}_1' + \underline{j}_2' + \underline{\ell}' = \underline{J}$$

and gives rise to the possibility of inelastic rotational transitions.

The coupled equations which result from a partial wave expansion in angular wave functions corresponding to the total angular momentum quantum numbers J have been written down by Arthurs and Dalgarno[1] for atom-molecule collisions and by Gioumousis and Curtiss[2] for molecule-molecule collisions. We need not reproduce them here.

2.1 Weak Coupling

Arthurs and Dalgarno[1] have shown that if the coupling between channels is weak, the elastic cross sections Q and Q_s differ from those corresponding to scattering by the central field $v_o(r)$ in second order in the coupling strengths, the first order changes vanishing essentially because $v_c(\underset{\sim}{r})$ vanishes when averaged over all orientations. The inelastic cross sections are clearly of second order in $v_c(\underset{\sim}{r})$. Thus, the assumptions of spherical symmetry and of single channel elastic scattering lead to second order errors only and the derived interaction potential can be identified as $v_o(r)$, the average of the actual potential $V(\underset{\sim}{r})$ over all orientations.

However, the coupling is weak only for light molecules at low temperatures and a more typical situation involves a considerable range of impact parameters for which the coupling is strong.

2.2 Strong Coupling

The case of strong coupling has been discussed by Bernstein, Dalgarno, Massey and Percival.[3] They show that in the strong coupling region the <u>total</u> scattering cross section is insensitive to the details of the intermolecular potential and it has the same form as the <u>elastic</u> scattering cross section corresponding to a strong spherically symmetric potential. It follows that the analysis of experimental data on the basis of a spherically symmetric potential should not lead to gross

error provided it is recognized that the cross sections occurring in the definitions of the transport coefficients and in the measurements of beam scattering are total cross sections, not elastic cross sections.

Some error may occur because the angular distributions of elastic and inelastic scattering are different. Whereas the inelastic angular distribution will not be very different from isotropic, the elastic angular distribution has a sharp forward peak associated with the shadow scattering (compare Figures 1, 2 and 3). Most beam scattering measurements refer to angles outside the shadow region so that the conventional analysis should be only slightly less accurate than for atomic gases when used for the prediction of the coefficients of diffusion and viscosity at high temperatures, which also do not involve any important contribution from the shadow region. Much greater error may result if the same potential is used to predict transport coefficients at lower temperatures at which the shadow region does contribute significantly to the collision cross sections. It should be stressed that the error does not arise from a mere lack of flexibility of the form of V (r) as for the atomic gas, but from the essential failure of the concept of an intermolecular (velocity-independent) potential.

Small errors may occur at lower temperatures in inferring one transport coefficient from measurements of another, since the associated collision cross sections weight differently the shadow and isotropic scattering regions. In particular, the use of viscosity data tends to

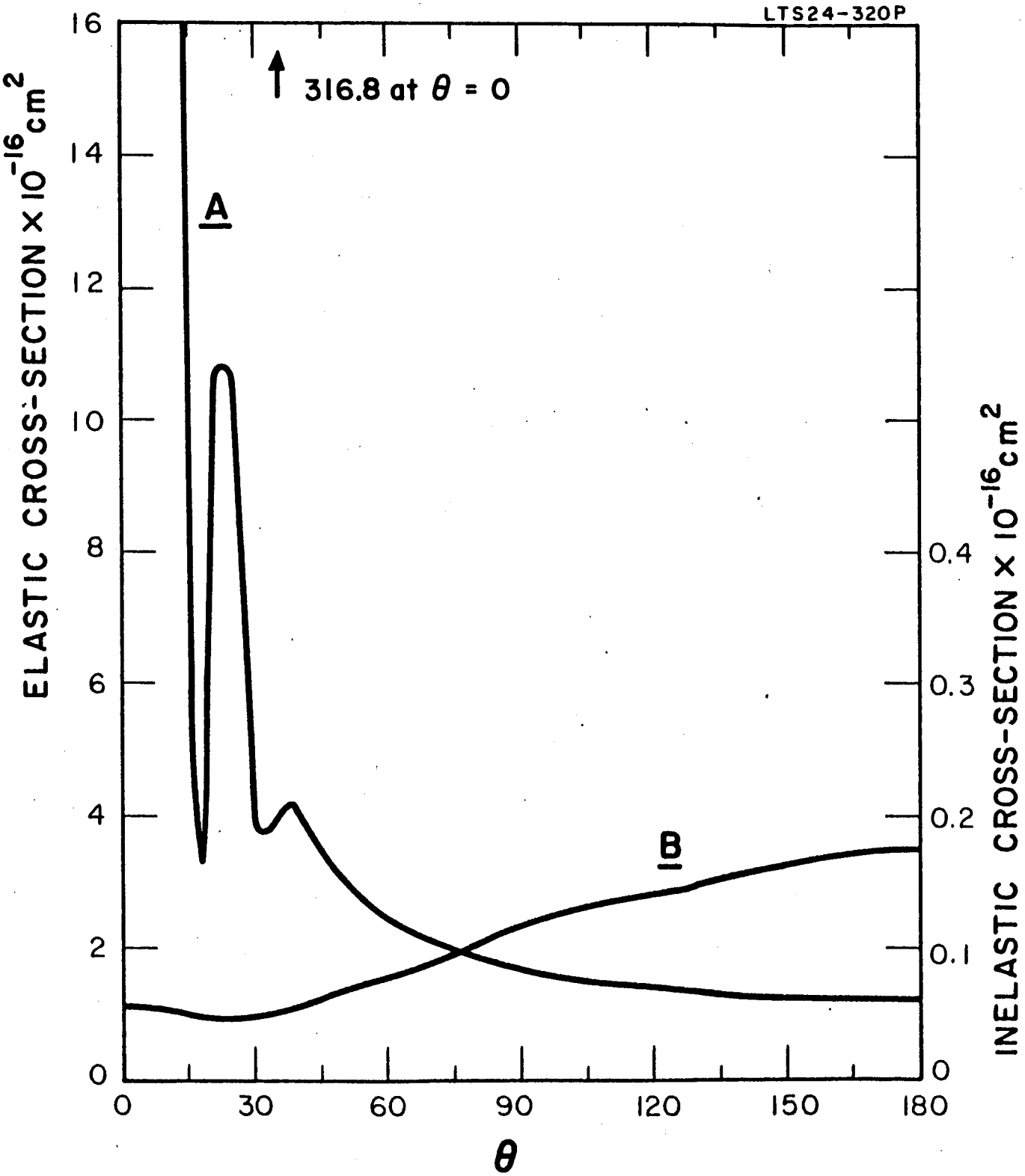
LTS24-320P
316.8 at θ = 0
A
B
ELASTIC CROSS-SECTION X 10^-16 cm^2
INELASTIC CROSS-SECTION X 10^-16 cm^2
θ
0
2
4
6
8
10
12
14
16
0
0.1
0.2
0.3
0.4
0
30
60
90
120
150
180

Figure 1.

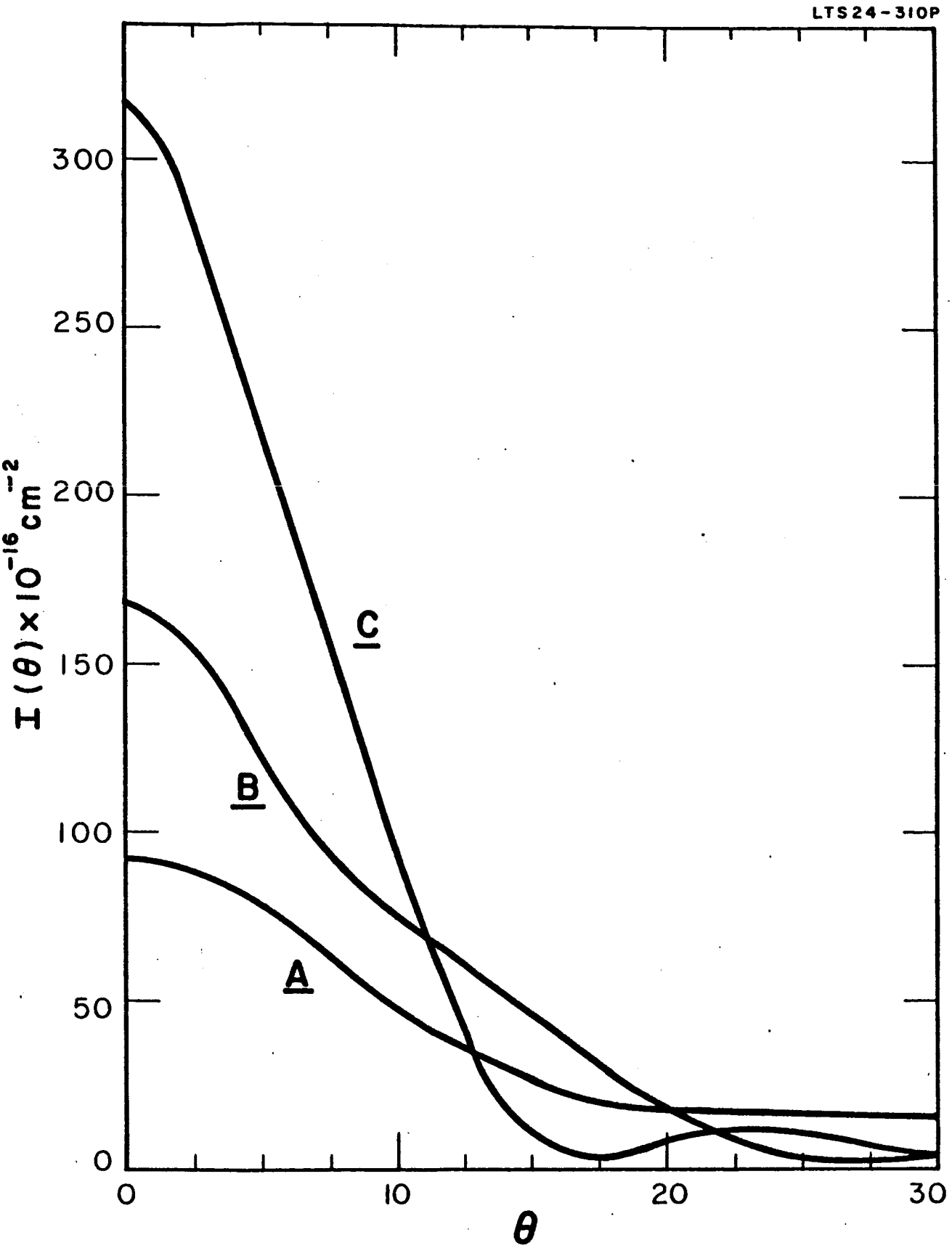

Figure 2.

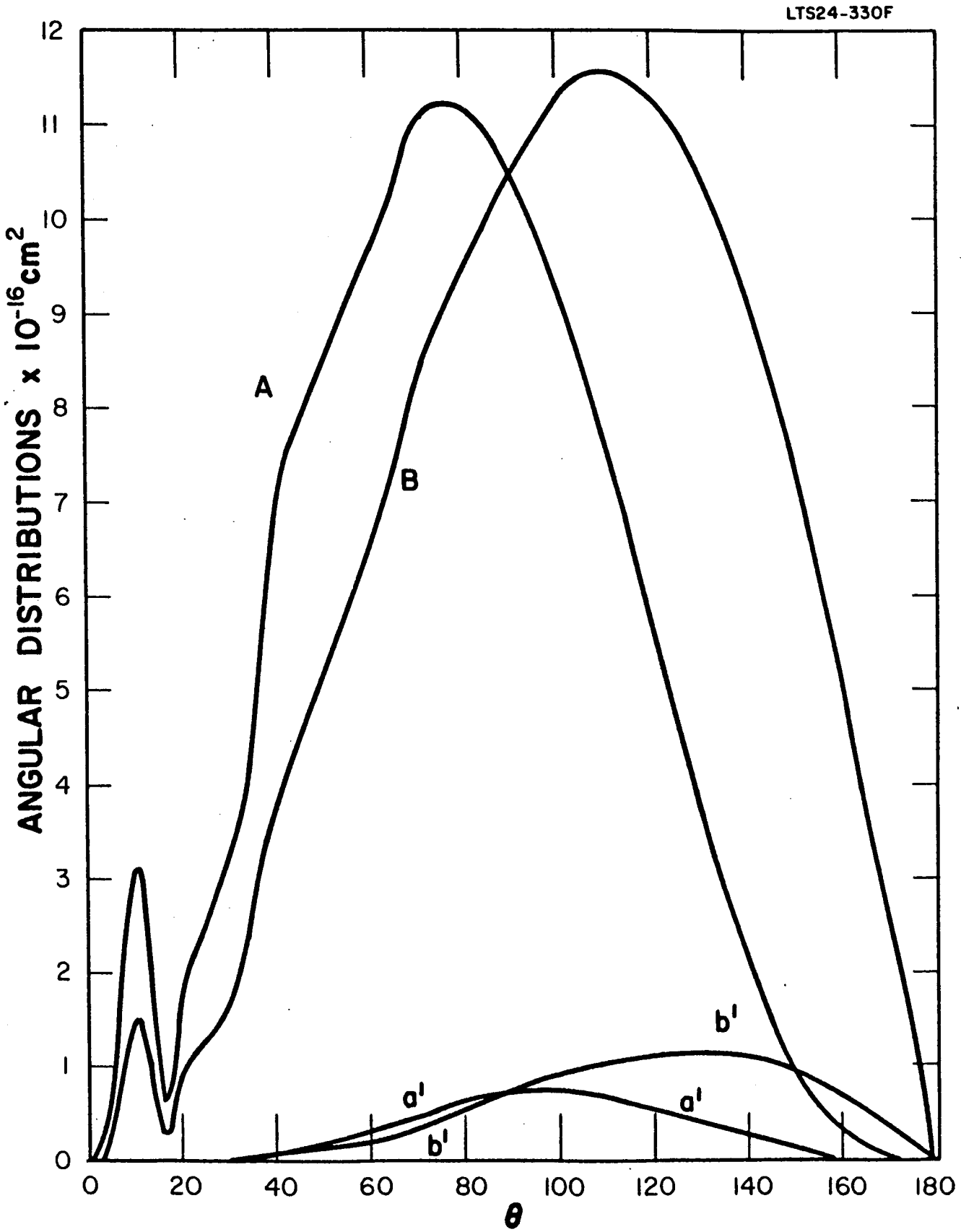
LTS24-330F
ANGULAR DISTRIBUTIONS x 10^{-16}cm^2
θ
A
B
a'
a'
b'
b'
0
1
2
3
4
5
6
7
8
9
10
11
12
0
20
40
60
80
100
120
140
160
180

Figure 3.

overestimate diffusion coefficients. This is opposite in sense to the observed discrepancies of Amdur, Ross and Mason,[4] Walker and Westenberg,[5] Westenberg and Frazier,[6] and Amdur and Shuler[7], the origin of which may be rather in the inappropriateness of the adopted analytic representations of V (r).

Thus, at large separations, the leading term of V ($\underset{\sim}{r}$) for a pair of neutral diatomic molecules decreases as r^{-3}, r^{-4} or r^{-5} depending upon whether both one or neither of the molecules has a permanent dipole moment. On averaging equally over all orientations, these terms vanish and the leading term is the spherically symmetric r^{-6} term that is usually adopted. If the scattering were mainly elastic in the important range of scattering angles, the choice could perhaps be justified (except at very low temperatures).* However, according to Bernstein et al.[3] up to half the total scattering may be inelastic and for the inelastic scattering there occurs no cancellation of the contributions from v_c ($\underset{\sim}{r}$).

There is a case of special interest which should be accessible to experimental verification. In the long range interaction of a positive or negative ion with a diatomic molecule, v_o (r) decreases as r^{-4} and v_c ($\underset{\sim}{r}$) as r^{-2} or r^{-3}. If the effective interaction has the form of v_o (r), then just as for an atomic gas, the mobility of an ion in a molecular gas tends to become independent of the gas temperature as the

*An interesting analysis of the effect of the orientation-dependent terms on the viscosity and second virial coefficient of hydrogen at very low temperatures has been presented by Niblett and Takayanagi.[10]

temperature decreases while if the effective interaction has the form of $v_c(\underset{\sim}{r})$, the mobility will tend to zero as the temperature decreases.

This marked difference between atomic and molecular gases was predicted by Arthurs and Dalgarno[8] from a consideration of elastic scattering only. The effect of $v_c(\underset{\sim}{r})$ on the elastic scattering is small until very low temperatures are reached. From the recognition that inelastic scattering is significant, it follows that the decrease of the mobility towards zero should set in at much higher temperatures than those implied by the formula given by Arthurs and Dalgarno.[8]

The predicted behaviour has been observed by Chanin, Phelps and Biondi,[9] for an ion, probably O_2^-, in O_2. The interpretation of this case is complicated by the possibility of charge transfer and measurements of the mobilities of various ions in unlike gases would provide a more certain test of the theoretical arguments.

3. Scattering in H_2 and D_2

The scattering of neutral particles in molecular hydrogen and in molecular deuterium at thermal velocities can be described by a weak-coupling approximation. Calculations of the inelastic angular distribution corresponding to the j = 0 to j = 2 rotational transitions have been carried out by Dalgarno, Henry and Roberts[11] using the formal scheme of Arthurs and Dalgarno.[1] Their results for the process

$$H + D_2\ (j=0) \rightarrow H + D_2\ (j=2)$$

at an impact energy of 0.0625 eV are reproduced in Figure 1.

We have computed the elastic angular distribution corresponding to scattering by D_2 in the j = 0 state and the results are shown in Figures 1 and 2. The elastic angular distribution is characterized by a sharp forward peak which decreases in angular extent as the impact velocity increases. The contributions of elastic and inelastic scattering at 0.0625 eV to the cross sections Q_1 and Q_2 effective in determining, respectively, the coefficients of diffusion and viscosity are shown in Figure 3. The contribution of the shadow scattering is suppressed and the contribution of the inelastic scattering is enhanced in comparison. Thus, whereas the total inelastic cross section is 2.5% of the total scattering cross section, the contribution of inelastic scattering to Q_1 is 7.5% of Q_1 and to Q_2 is 5.4% of Q_2.

An experiment in which a property of molecular hydrogen was carefully compared as a function of temperature with the same property of molecular deuterium would be of great interest. Because of the closer rotational spacing in D_2, the effect of inelastic scattering should become manifest at a lower temperature for D_2 than for H_2.

REFERENCES

1. A. M. Arthurs and A. Dalgarno, Proc. Roy. Soc., A256, 540 (1960).
2. G. Gioumousis and C. F. Curtiss, J. Math. Phys., 3, 1059 (1962).
3. R. B. Bernstein, A. Dalgarno, H.S.W. Massey and I. C. Percival, Proc. Roy. Soc. A (in press).
4. I. Amdur, J. Ross and E. A. Mason, J. Chem. Phys., 20, 1620 (1952).
5. R. E. Walker and A. A. Westenberg, J. Chem. Phys., 32, 436 (1962).
6. A. A. Westenberg and G. Frazier, J. Chem. Phys., 36, 3499 (1962).
7. I. Amdur and L. M. Shuler, J. Chem. Phys., 38, 188 (1963).
8. A. M. Arthurs and A. Dalgarno, Proc. Roy. Soc., A256, 552 (1960).
9. L. M. Chanin, A. V. Phelps and M. A. Biondi, Phys. Rev., 128, 219 (1962).
10. P. D. Niblett and K. Takayanagi, Proc. Roy. Soc., A250, 222 (1959).
11. A. Dalgarno, R.J.W. Henry and C. Roberts (to be published).

GCA Technical Report No. 63-28-N

PLANETARY AERONOMY XVI:
CORPUSCULAR RADIATION IN THE UPPER ATMOSPHERE

A. Dalgarno

October 1963

GEOPHYSICS CORPORATION OF AMERICA
Bedford, Massachusetts

Contract No. NASw-701

Prepared for

NATIONAL AERONAUTICS AND SPACE ADMINISTRATION
HEADQUARTERS
WASHINGTON, D. C.

Invited paper presented at IUGG Meeting held in Berkeley, California, on August 19-24, 1963. This paper has been accepted for publication in Annales de Geophysique.

ABSTRACT

The efficiencies of fast electrons and protons in producing luminosity and heating by collisions with the atmosphere are discussed and upper limits to the fluxes of corpuscular radiation are obtained. A possible explanation of high-altitude red auroras is advanced. The effects of the photoelectrons produced in the ionization of the atmosphere by extreme solar ultraviolet radiation are examined and it is noted that the electron temperature at high altitudes may be anomously large at dawn, the phenomenon being accompanied by a red glow.

It is suggested that the source of 1304Å dayglow radiation postulated by Donahue and Fastie is excitation by impact of fast photoelectrons and that fast photoelectrons may lead to a large dayglow intensity of the first positive system of nitrogen through resonance scattering by metastable molecules.

TABLE OF CONTENTS

CORPUSCULAR RADIATION IN THE UPPER ATMOSPHERE

A. Dalgarno

1. INTRODUCTION

It is clear from the occurrence of visible auroras and of polar cap and auroral absorption that corpuscular radiation is an important energy source in the upper atmosphere at high latitudes and various indirect arguments have suggested that it is also an important energy source at middle and low latitudes. Some of the consequences of a flux of corpuscular radiation are examined in this review.

2. LUMINOUS EFFICIENCY OF FAST ELECTRONS

2.1 Emission from N_2^+

There is an important argument (Omholt [1]) which relates the energy flux of a beam of fast electrons absorbed by the atmosphere to the resulting intensity of the first negative system of molecular nitrogen. Stewart [2] has measured the cross sections for production of the 0-0, 0-1 and 0-2 bands

$$e + N_2(X'\Sigma_g^+) \rightarrow e + N_2^+(B^2\Sigma_u^+) + e \qquad (1)$$

by the impact of electrons with energies up to 200 eV and finds that the variation with energy is very similar to that of the total ionization cross section

$$e + N_2(X'\Sigma_g^+) \rightarrow e + N_2^+ + e \qquad (2)$$

(Tate and Smith [3], Fite and Brackmann [4]). The cross sections for the production of the 0-0, 0-1 and 0-2 bands are respectively about 2%, 0.7% and 0.2% of the total ionization cross section. Since the mean energy expended in the production of an ion pair by a beam of fast electrons absorbed in nitrogen is 35 eV (cf. Valentine and Curran [5]), it follows that the efficiency with which energy is converted into radiation is about 2×10^{-3} for the 0-0 band at 3914Å, about 7×10^{-4} for the 0-1 band at 4278Å and about 2×10^{-4} for the 0-2 band at 4709Å.

When the initial energies of the fast electrons fall below perhaps 100 eV, these efficiencies must decrease sharply (cf. Dalgarno and Griffing [6]).

Hartman and Hoerlin [7] have measured the efficiency of energy conversion into 3914Å radiation of a beam of electrons absorbed in air at sea level. They obtained an efficiency of 3.3×10^{-3}, independent of the electron energy which was varied from 200 eV to 1000 eV. Correcting for the oxygen content, the efficiency for absorption in nitrogen is about 4×10^{-3}, a value which is twice that derived from cross section data. Some of the discrepancy may be attributed to the deactivation of more highly vibrating molecules through processes such as

$$N_2^+(B^2\Sigma_u^+, v) + N_2(X'\Sigma_g^+, 0) \rightarrow N_2^+(B^2\Sigma_u^+, 0) + N_2(X'\Sigma_g^+, v) \quad . \tag{3}$$

The value of the energy conversion coefficient appropriate to the upper atmosphere depends upon the fractional content of N_2 at the altitude at which the electrons are absorbed. To avoid complicating the argument, I shall adopt 1×10^{-3} for the efficiency with which energy is converted into 3914Å radiation so that a flux of ζ erg cm^{-2} sec^{-1} gives rise to 200 ζ rayleighs. I am indebted to Dr. Roach for the remark that 60 rayleighs of 3914Å emission would not occur undetected from which it follows that the possible flux of fast electrons at middle

and low latitudes cannot exceed 0.3 erg cm^{-2} sec^{-1}. It might be possible to place a smaller upper bound if a systematic search for N_2^+ emissions were made at middle and low latitudes. Indeed, Galperin [8] has stated that for the long night exposures in Zvenigorod at a geomagnetic latitude of 51.1°N, the absence of observable emission shows that the intensity of the 4278Å band does not exceed 1.5 rayleighs. Adopting an energy conversion coefficient of 3×10^{-4}, it follows that the flux of energetic electrons cannot exceed 2×10^{-2} erg cm^{-2} sec^{-1}, a result in close agreement with the limits derived by Galperin [8]. The derived upper limit is comparable to the value of the average flux of dumped electrons with energies greater than 1 keV at midlatitudes over North America, estimated by O'Brien [9] from Injun 1 data on outer zone electrons, and to the average fluxes recorded by Antonova and Ivanov-Kholodny [10] and by Kazachevskaya and Ivanov-Kholodny [11] at altitudes between 70 km and 100 km. The intensity of the electron fluxes fluctuates markedly in time (Ivanov-Kholodny[12])

Ivanov-Kholodny and Antonova [13], Antonova and Ivanov-Kholodny [14], Danilov [15] and Ivanov-Kholodny [16] have advanced the hypothesis that the persistence of the ionosphere through the night is due to a flux of energetic electrons. According to their analysis, the required flux is greater than 1 erg cm^{-2} sec^{-1} which considerably exceeds the derived limits. Thus, either the nocturnal ionization hypothesis or the theoretical analysis must be rejected.

A corpuscular flux has also been invoked by Mariani [17] in order to explain the correlation of maximum electron density in the F region at noon

with solar activity. For high-solar activity, Mariani postulates a flux of about 0.1 erg cm^{-2} sec^{-1} of electrons with energies of the order of 1 keV, peaking at geomagnetic latitudes between 55° and 65°. It is of interest to note that if the maxima of the outer radiation belt at 1000 km are projected along local magnetic lines of force, the maximum at 100 km occurs at a magnetic latitude between 56°N and 57°N (Winkler [18]). The distribution with latitude is broadly similar to that found by O'Brien [9] for the time average of electrons with energies above 40 keV precipitated into the atmosphere at an altitude of 1000 km, which also peaks between about 60°N and 65°N. However, the shapes of the distributions at higher latitudes are very different, as are the electron energies involved.

The flux derived by Mariani gives rise to at least 20 rayleighs of 3914Å emission and it is of interest to compare this intensity with those observed at night in the absence of auroras. It may be relevant to note that O'Brien [19] found that the flux of geomagnetically trapped electrons with energies greater than 40 keV at an altitude of 1000 km shows little diurnal variation for magnetic latitudes less than about 63°N (strictly for $L \leq 5$, where L is the coördinate introduced by McIlwain [20]).

Observing at a magnetic latitude of 60.5°N, Lytle and Hunten [21] found a permanent intensity of about 30 rayleighs during 1960 and probably less than 20 rayleighs during 1961. Russian workers (cf. Galperin [8], Mulyarchik and Shcheglow [22]) found greater intensities at Loparskaya at the slightly higher geomagnetic latitude of 63.7°N, the associated fluxes

being about 1 erg cm^{-2} sec^{-1} at maximum solar activity and 0.3 erg cm^{-2} sec^{-1} at minimum solar activity. These observations are consistent with the view that corpuscular radiation is an important source of ionization in the F region at geomagnetic latitudes near 60°.

Van Allen and his collaborators [23] have observed a permanent flux of electrons at low altitudes, the maximum intensity occurring between 65°N and 70°N. Most of the electrons have energies between 10 keV and 100 keV and the maximum energy flux lies between 0.1 and 1 erg cm^{-2} sec^{-1}. The energy spectrum is consistent with Mariani's analysis which suggests that corpuscular radiation is not an important source of ionization in the F layer at latitudes much above 60°N so that the incident particle flux should not include a large component of electrons with energies of less than 1 keV.

The conversion efficiency for producing 3914Å radiation has been used by Sharp et al. [24] in an analysis of satellite measurements of particle fluxes during auroras. From ground-based observations of 3914Å emission (Belon et al. [25]), they conclude that the energy flux was at least 100 erg cm^{-2} sec^{-1} whereas the measured flux of electrons with energies greater than 2 keV indicated a total intensity of only 10 erg cm^{-2} sec^{-1}. Thus, either the energy spectrum rises very steeply at low energies or an acceleration mechanism is operating [24].

2.2 Other Emissions

There are few quantitative data on the efficiencies for converting electron kinetic energy into radiations other than those of the first

negative system. Hartman and Hoerlin [7] have obtained an efficiency of 1.5×10^{-2} for converting the energy of 200 eV - 1000 eV electrons absorbed in air at sea level into radiation between 3000Å and 10,000Å. About one-third of the energy is emitted in the first positive band system of $N_2(C^3\pi_g \rightarrow A^3\Sigma_u^+)$ (Hartman and Hoerlin, private communication 1963). The measured efficiency is unexpectedly high, for very little intensity is to be expected from molecular band systems of O_2 and O_2^+ or from atomic lines and a deactivation mechanism such as (3) is probably rapid enough to present any observable emission of the infrared Meinel bands of $N_2^+(A^2\pi_g - X^2\Sigma_g^+)$, the 0-0 band of which is located at 11,036Å. Presumably, a considerable fraction of the luminosity must be emitted in the second positive system of $N_2(C^3\pi_u - B^3\pi_g)$ in the region between 3000Å and 4000Å and in particular at 3371Å, 3577Å and 3805Å corresponding respectively to the 0-0, 0-1 and 0-2 bands.

Because of the lower frequency of quenching collisions, larger values of the conversion efficiency should be appropriate in the upper atmosphere. The value of 2×10^{-3} derived by McIlwain [26] from an analysis of simultaneous observations of particle fluxes and luminosity intensity in a quiescent auroral glow at an altitude of about 120 km is therefore unexpectedly low. Thus, the first negative system of N_2^+ should alone contribute more than 2×10^{-3} and a comparable amount is to be expected from the green line of atomic oxygen at 5577Å, for it has been observed that the ratio of the intensity of 5577Å line to that of the 3914Å band is nearly constant at a value between 1 and 2 over a wide

range of auroral intensities, for various auroral forms and probably over a wide height interval (cf. Chamberlain [27]). Chamberlain [27] has suggested that the smallness of the ratio of 5577Å to 3914Å may be due to the removal of electrons, that would otherwise excite the green line, by excitation of the nitrogen bands in exchange collisions. However, there is another mechanism which may also contribute to the low ratio.

Fast electrons of energy E eV lose energy in elastic collisions with the ambient thermal electrons at a rate

$$\frac{dE}{dx} = - \frac{2 \times 10^{-12}}{E} n_e \text{ eV cm}^{-1} \tag{4}$$

where n_e is the number density of the thermal electrons whereas they lose energy in exciting O('S) at a rate of about

$$\frac{dE}{dx} = - 2 \times 10^{-17} n(O) \text{ eV cm}^{-1} \tag{5}$$

where n(O) is the number density of atomic oxygen (Dalgarno, McElroy and Moffett [28]). Thus, for a bright aurora of IBC III for which $n_e \sim 5 \times 10^6$ cm^{-3} at an altitude of 120 km where $n(O) \sim 5 \times 10^{10}$ cm^{-3}, fast electrons lose energy more rapidly in heating the ambient electron gas than in exciting the green line whenever their energy falls below 10 eV.

An appreciable contribution to the energy conversion coefficient should also appear in the second positive bands of N_2 but uncertainty

as to the spectral sensitivity curve of the photometer employed prohibits any estimate of the importance of the first positive bands of N_2, the Meinel bands of N_2^+ and the atmospheric bands of O_2, all of which are probably produced with high intensities.

McIlwain [27] remarked that the probable error in his estimate of 2×10^{-3} is about a factor of two and that it is unlikely to be in error by more than a factor of four. A value of 6×10^{-3} seems a reasonable compromise with an approximately equal distribution in the first negative system of N_2^+, the first positive system of N_2 and the green line of atomic oxygen.

Anderson and DeWitt [29] observed 60 kilorayleighs of green line emission from a widespread auroral glow over Alaska, implying an energy flux of about 250 erg cm^{-2} sec^{-1}. Taken together with their balloon measurements of X-rays, this suggests that only 1 percent of the luminosity is contributed by electrons with energies of more than 25 keV.

3. LUMINOUS EFFICIENCY OF FAST PROTONS

3.1 Emission from N_2^+

The cross sections for allowed transitions are approximately equal for fast electrons and protons of the same velocity and explicit confirmation of this theoretical prediction has obtained for the ionization of N_2 (Hooper, Harmer, Martin and McDaniel [30]). Since a considerable fraction of the excitation and ionization produced by the absorption of fast protons is due to the secondary electrons, the coefficient for the conversion of the proton kinetic energy into radiation in the N_2^+ first negative system should be much the same as for fast electrons. It may actually be somewhat greater because of the additional contribution from charge transfer excitation

$$H^+ + N_2(X'\Sigma_g^+) = H + N_2^+(B^2\Sigma_u^+) \quad . \tag{6}$$

Thus, the relationship between the intensity of 3914Å radiation and the incident energy flux given in Section 2.1 is largely independent of the nature of the fast particles involved.

3.2 Emission from H

The most recent analysis of the absorption of a beam of fast protons in air is that of Chamberlain [27] who shows that about 60 quanta of H_α and about 16 quanta of H_β are produced. These values are independent of the initial energy (provided it is large enough) because the probability

of capture decreases very rapidly at high velocities. Accordingly, observations of Doppler-shifted hydrogen lines yield information only on the particle flux and additional data are required to determine the energy flux.

Measurements by McIlwain [20] of protons in a quiescent auroral glow using rocket-beam detectors yield a proton energy flux of

$$j(>E) = 2.5 \times 10^{6} \exp(-E/30)\ \mathrm{cm}^{-2}\mathrm{sec}^{-1}\mathrm{ster}^{-1} \qquad (7)$$

for proton energies between 80 and 250 keV, E being measured in keV. By assuming that (7) may be extrapolated to zero energy and that the angular distribution is isotropic, McIlwain obtains a particle flux of $1.6 \times 10^{7}\ \mathrm{cm}^{-2}\ \mathrm{sec}^{-1}$ which on comparison with the ground-based observations of H_β (Montalbetti [31]) yields a value of $4H_\beta$ quanta for each incident proton. In view of the many uncertainties, the agreement with the theoretical value of 16 quanta is satisfactory.

The additional information required to determine the energy flux cannot be provided directly by the measurements of the intensity ratio of N_2^+ and H emissions because the former is also produced by electron impact, but it can be provided by observations of the emission altitudes. Thus, it has been shown (Omholt [1,32], Chamberlain [27]) that in an aurora produced by monoenergetic protons at an altitude of about 120 km, the ratio of the intensities of 3914Å and H_β emission is about unity and it decreases as the altitude of the aurora increases. The observed ratio

is nearly always, and often much greater than ten, and it is therefore highly improbable that any ordinary aurora is produced mainly by proton bombardment ([1], [32], [27]). It may also be shown [27] that for bright auroras above an altitude of 100 km with a flux of 10 kilorayleighs of H_α (which is near the maximum observed), the energy flux of fast protons is about 10 percent of the total energy deposited as evidenced by the emission rate of 3914Å. The discrepancy does not necessarily imply a significant difference between the fluxes of electrons and protons in an aurora since a large proportion of the incident protons could have low velocities and produce no radiation. If present, the undetected slow protons may be an important source of atmospheric heating during an aurora.

According to Galperin [8], the intensity of Doppler-shifted H_α emission does not exceed 3 rayleighs at low and middle latitudes. He concludes that the proton energy flux must be less than 6×10^{-4} erg cm^{-2} sec^{-1} and that the associated heat flux must be smaller still. This argument does not take account of the low efficiency for producing radiation of protons with energies less than 1 keV, an efficiency which is anomously low because of the accidental resonance

$$H^+ + O \rightarrow H + O^+ \quad . \tag{8}$$

4. HEATING EFFICIENCY OF ELECTRONS

4.1 Recombination Heating

A fast electron loses energy in exciting and ionizing the atmospheric constituents. The electrons ultimately become thermalized and are removed mainly by processes of dissociative recombination, which yield atoms with excess kinetic energy. There have been several discussions of the fraction of total electron kinetic energy which is converted into heat energy but neither the arguments nor the conclusions differ in any substantial way from those put forward by Bates [33], who concludes that the fraction is probably about 0.2. However, a value as high as 0.5 cannot be excluded.

It follows that a flux of S rayleighs of 3914Å emission is associated with a heat flux of about 10^{-3} S erg cm^{-2} sec^{-1} from recombination heating. Adopting the estimate of Galperin [8] for the maximum intensity of 3914Å emission, the heat flux at middle and lower latitudes due to fast corpuscular radiation in the nocturnal atmosphere is less than 8×10^{-3} erg cm^{-2} sec^{-1}. This upper limit is much greater than the heat flux postulated by Paetzold and Zschörner [34], Paetzold [35], Harris and Priester [36] and Jacchia [37]. The postulated heat flux is usually identified as arising from the dissipation of hydromagnetic waves (Dessler [38]) but it is useful nevertheless to note that it cannot be attributed to fast particles colliding in the upper atmosphere.

At the higher latitude of Loparskaya at 63.7 N, the heat flux in the absence of auroras varies from about 0.2 erg cm^{-2} sec^{-1} at maximum solar activity to about 0.07 erg cm^{-2} sec^{-1} at minimum solar activity. Except at high altitudes where diffusion is important, the distribution with altitude of the recombination heat source will be similar to those of the production of ionization and the production of N_2^+ radiation. Using the measurements of Grün [39], which are in harmony with the theoretical predictions of Spencer [40], Rees [41] has computed the altitude profiles of the ionization and N_2^+ emission produced by fast electrons. The influence of the magnetic field is not taken into account and the calculations are strictly appropriate only to high latitudes, as Rees notes.

The calculations by Rees show that for monoenergetic electrons with energies greater than about 5 keV, most of the heat energy is deposited in regions of limited altitude extent below 140 km and that as the energy decreases, the minimum altitude and the altitude extent of significant heat deposition increase. Thus, 1 keV electrons penetrate to an altitude of 150 km and the heat deposition per unit volume decreases by only a factor of four as the altitude increases from 180 km to 280 km.

The importance of the heat source implied by the observations of N_2^+ emission at high latitudes is accordingly strongly dependent upon the energy spectrum of the incident corpuscles. Satellite drag data do not show any large increase in the exospheric temperature at high latitudes (Jacchia [42]) which suggests that the energy spectrum of the incident corpuscles in quiet conditions does not contain a significant

component of soft electrons. A corpuscular heat source may be responsible for the apparent increase with latitude of the rotational temperature of the OH airglow band system, but it may be an altitude effect (cf. Hunten [43], Wallace [44]).

There is evidence from direct measurements of corpuscular radiation (McIlwain [20]; Meredith, Davis, Heppner and Berg [45]; Anderson and DeWitt [29]; Sharp et al. [24]) that the energy spectrum during auroras often contain large components of soft electrons and significant local heating must occur. For 1 keV electrons, the initial rate of temperature rise is constant above 240 keV and equals 10^{-9}°K per minute for unit flux of electrons. Thus, in a bright aurora the initial rate of temperature rise will exceed 100°K per minute.

Measurements of the Doppler width of the oxygen red line during auroras by Mulyarchik [46] have shown a correlation between the intensity and width of the red line, suggesting that the heating increases with auroral intensity. For a strong bright red aurora, the width was equivalent to a temperature of 3500°K. Some care is needed in interpreting the observed temperature since, should the O('D) atoms be produced by dissociative recombination, they would initially possess excess kinetic energy. At altitudes above 350-400 km, the O('D) atoms will radiate before they are thermalized by elastic collisions.

An upper limit to the kinetic temperature of the high atmosphere can be obtained from observations of the red line. The intensity of

the red line from thermal excitation at a kinetic temperature of 2000°K above 200 km is about 200 rayleighs and at a kinetic temperature of 3000°K it is about 20 kilorayleighs. The red line in the night airglow has typically an intensity of between 50 and 100 rayleighs (cf. Chamberlain [47]).

Occasionally, the red line appears with enormous intensity. Thus, in the great red aurora of February 11, 1958, the ratio of 6300Å to 5577Å was about 2.5×10^3 and the intensity of the 6300Å line attained a value of 10^5 kilorayleighs at one time (Manring and Pettit [48]). As Chamberlain [27] has argued, the green line had an intensity corresponding to IBC II so that the total particle flux and associated heating were presumably not unusually large. A possible explanation of such events emerges from an examination of heating by direct impact processes.

4.2 Impact Heating

Fast electrons which penetrate deeply into the atmosphere lose energy initially in exciting and ionizing the atmospheric constituents. As they are slowed down to energies of less than 7 eV, they lose energy predominantly in vibrational excitation of molecular nitrogen and less efficiently in exciting atomic oxygen into the ^1D and ^1S levels. The last electron volt of energy is usually lost by elastic collisions with the ambient electrons which provide a means of selectively heating the electron gas. The slowing down by excitation of the vibrational levels of nitrogen may also provide a path for selective heating of the electron gas depending

upon which mechanism prevails for deactivating the vibrationally excited molecules [28]. However, because of the efficiency of cooling mechanisms at low altitudes, no large departure from equality of the electron temperature and the neutral gas temperature is to be expected (unless electric fields are present) in the altitude region near 110 km where most auroras are located.

The situation is very different for slower electrons which do not penetrate deeply into the atmosphere and which lose a large fraction of their energy in elastic collisions. Thus, 400 eV electrons penetrate to an altitude of 215 km [41] in producing excitation, ionization and secondary electrons. The distribution is approximately uniform over an altitude extent of perhaps 200 km. At these altitudes, the secondary electrons lose almost all their energy in elastic collisions with the ambient electrons leading to an energy conversion coefficient of about 0.1.

A convenient parameter for assessing the possible effect on the electron temperature T_e is the critical heat flux density Q_c eV cm^{-3} sec^{-1}, defined by

$$Q_c = \frac{2 \times 10^{-7} \, n_e^{\,2}}{\sqrt{T_i}} \tag{9}$$

where T_i is the positive ion temperature [28]. If the actual heat flux density exceeds Q_c, T_e is not limited by energy transfer to the positive ions (Hanson and Johnson [49]) and it moves to a new equilibrium value

determined by the efficiency of cooling by collisions with the neutral particles [22]. At high altitudes, the new equilibrium value of T_i will exceed $3T_i$. In order that such high values of T_i may occur between, say, 320 km and 420 km, it is sufficient to deposit there a heat energy of about 6×10^9 eV cm^{-2} sec^{-1} for an assumed mean electron density of 3×10^5 cm^{-3}. Such a heat source can be supplied by a flux of 400 eV electrons of about 0.2 erg cm^{-2} sec^{-1}.

Above 300 km, the most efficient cooling mechanism at the high equilibrium value of T_i, which is in the region of 5000°K, is electron impact excitation of the ^1D level of atomic oxygen. Thus, a flux of 0.2 erg cm^{-2} sec^{-1} of 400 eV electrons may produce 3 kilorayleighs of red line emission.

Large fluxes are required to explain the great red auroras. To produce 10^4 kilorayleighs of red line emission, a flux of about 600 erg cm^{-2} sec^{-1} is required of which 30 erg cm^{-2} sec^{-1} appear as 6300Å photons. Because the efficiency of cooling increases rapidly with increasing electron temperature, the larger flux will not cause any great increase in T_e. The postulated mechanism for the production of the red line gives rise to essentially no green line emission. The observed green line intensity can be attributed to incident electrons with higher energies penetrating more deeply into the atmosphere, the required flux being about 20 erg cm^{-2} sec^{-1}.

The slow secondary electrons produced below 300 km will lose energy in exciting the vibrational levels of N_2 rather than in elastic collisions with the ambient electrons. This may be reflected in an unusual vibrational development of the first negative system of nitrogen which is apparently a feature of low latitude, high altitude red aurora ([27]).

An alternative explanation of the red auroras has been proposed by Megill and Carleton [50] who remark that they are almost certainly caused by local electric fields.

In normal aurora, the red line intensity is less than 15 kilorayleighs so that the incident flux of soft electrons should not exceed 1 erg cm^{-2} sec^{-1}.* Similarly in the undisturbed airglow, for which the intensity is less than 100 rayleighs, the flux of soft electrons should not exceed 0.2 erg cm^{-2} sec^{-1}.*

Limits to the flux of soft electrons may also be derived from the observed equality of the electron and ion temperatures at night. I shall return to this possibility in Section 6.2.

---

*There is some question as to whether a configuration in which the electron temperature is essentially a discontinuous function of altitude is stable. The limits on the possible fluxes are correspondingly tentative.

5. HEATING EFFICIENCY OF PROTONS

5.1 Recombination Heating

It follows from arguments similar to those presented in Section 3.1 that the efficiency of recombination heating due to fast protons is comparable to that due to fast electrons so that the heat fluxes given in Section 4.1 are largely independent of the nature of the incident particles. If the permanent N_2^+ emission at high latitudes is due mainly to fast protons, the associated heat flux is unimportant since the protons necessarily penetrate deeply into the atmosphere. Of greater significance to the heating of the upper atmosphere is the possible flux of slow protons which do not produce radiation but instead lose energy through process (8) and by elastic collisions. As for electrons, the absence of a large increase in the exospheric temperature at high latitudes suggests that the component of soft protons is small. A quantitative examination of the possible heating would be of value.

5.2 Impact Heating

The energy loss of protons by elastic collisions with the charged particles of the ionosphere is inefficient compared to the energy loss in elastic collisions with the neutral particles.

6. EFFECTS OF FAST PHOTOELECTRONS

The photoelectrons produced by the absorption of extreme solar ultraviolet radiation in photoionizing processes constitute a source of corpuscular radiation in the daytime ionosphere.

6.1 Luminosity

The fast photoelectrons slow down through collisions with the neutral particles and some of the collisions lead immediately to radiation. The most intense features in the visible spectrum arising from direct impact excitation are presumably those mentioned earlier in Section 2.2, though the contribution to the allowed first negative and Meinel band systems of N_2^+ will be negligible compared to resonance scattering and to fluorescence scattering (Dalgarno and McElroy [51]).

Resonance scattering will also provide the major contribution to the resonance transitions of N_2 and O which appear in the ultraviolet. However, from an analysis of dayglow observations of the oxygen line at 1304Å, Donahue and Fastie [52] have concluded that, in addition to resonance scattering and to Ly-β fluorescence, there is a weak source located in the F region near 190 km. Donahue and Fastie have tentatively suggested that the excited atoms may be produced by dissociative recombination of O_2^+ or NO^+ in highly excited vibrational levels but impact excitation by photoelectrons may be a more efficient mechanism. Although detailed calculations are required in order to test the hypothesis of impact excitation,

there seems little difficulty in obtaining the required flux of 1304Å radiation. Preliminary calculations suggest an intensity profile peaking near an altitude of 250 km for a solar elevation angle of 30° rather than near 200 km as Donahue and Fastie require.

The origin of a weak line at 1355Å, observed by Donahue and Fastie and tentatively identified by them as the oxygen multiplet $(2p)^4\ ^3P - (2p^3)\ 3s^5S$, may also be electron impact excitation. Other weak oxygen lines, such as the auroral lines 7774Å and 8446Å, should be present in detectable intensities. An additional source of the line at 8446Å, which has been observed during twilight by Shefov [53], is absorption of solar Ly-β radiation (Swings [54], Shlovskii [55], and Brandt [56]).

Fast photoelectrons may also produce dayglow luminosity indirectly by populating metastable levels, an example of special interest being the helium line at 10830Å observed during twilight by Shefov and by Scheglow and during a solar eclipse by Shaiskaya (cf. Shefov [57]). Krassovsky [58] and Shefov [59] have attributed the line to resonance scattering by metastable 2^3S helium atoms. The main production mechanism is apparently impact excitation by fast photoelectrons (Shefov [57]) and the main loss mechanism is apparently the Penning ionization process (Ferguson [60]). Preliminary calculations suggest that the observed intensity of 1 kilorayleigh can be explained only by postulating helium concentrations greater than those given by Kockarts and Nicolet [61].

Resonance scattering by the metastable $A^3\Sigma_u^+$ state of nitrogen may lead to a considerable intensity of the first positive band system; the measured lifetime of the $A^3\Sigma_u^+$ state has been reported variously as 2.0 ± 0.9 sec (Carleton and Oldenberg [62]), 0.08 ± 0.04 sec (Dunford [63]) and 0.9 sec (Zipf [64]).

6.2 Electron and Ion Temperatures

The relationships between the temperatures of the electrons, the positive ions and the neutral particles which constitute the ionosphere are fundamental to the interpretation of its behavior. The theoretical studies of the effect of solar ultraviolet radiation and the fast photoelectrons it produces ([49], [28], Hanson [65] and Dalgarno [66]) show that departures from temperature equality are to be expected at altitudes above about 150 km, the difference between the electron temperature and the heavy particle temperature attaining at midday a maximum somewhat greater than $1000^{\circ}K$ at an altitude of about 220 km and decreasing rapidly as the altitude increases to 300 km. These conclusions are in substantial agreement with the Langmuir probe measurements (cf. Bourdeau [67]).

According to the theoretical studies, the difference between the electron temperature T_e and the positive ion temperature T_i should decrease rather slowly with increasing altitude above the peak of the F region. The difference may persist over several hundred kilometers, the predicted magnitude of $T_e - T_i$ depending sensitively upon the assured density of the ambient electrons ([65], [66]).

It has been suggested ([28]) that near sunrise the heat flux density may exceed the critical value (9) and preliminary calculations by Dalgarno [66] and Bourdeau [68] support the conjecture. Dalgarno [66] has pointed out that the anomalous rise of T_e to a value greater than $3T_i$ should be accompanied by a red glow. A preliminary calculation suggests that the glow is located between 400 and 500 km and may attain an intensity of several hundred rayleighs. There is evidence from satellite observations (cf. [68]) and from equational backscatter observations (Bowles, Ochs and Green [69]) that $T_e - T_i$ is large at sunrise but the reported magnitudes do not exceed $2T_i$.

Measurements of T_e and T_i at altitudes above 300 km are in apparent contradiction. Bourdeau [67] has shown that rocket and satellite observations at mid-latitudes in quiet conditions can be satisfactorily explained by assuming that T_e, T_i and the neutral gas temperature T_n are approximately equal, a conclusion that is in harmony with the observations of backscatter at the equator reported by Bowles, Ochs and Green [69] but not with the observations of backscatter by Evans [70] and Pineo and Hynek [71] at higher latitudes. Evans (private communication, 1963) and Bourdeau [68] have emphasized that there may be a significant variation of T_e with latitude as was indeed suggested by the rocket measurements of Spencer, Brace and Carignan [72].

The electron temperature in the ionosphere is very sensitive to small disturbances [66] and the flux of electrons postulated by Mariani

(cf. Section 2.1) may well be sufficient to explain the results of the recent analysis by Evans (private communication, 1963) of backscatter data at a geomagnetic latitude of 54°N, which show that the ratio of T_e to T_i reaches a maximum value of nearly 2.4 at an altitude of 450 km. That T_e should considerably exceed T_i at these altitudes appears to preclude a possible explanation involving electric fields.

If the values of T_e/T_i obtained by Evans are correct, then in addition T_i may exceed T_n by several hundred degrees in the altitude region between 500 and 600 km (Dalgarno [66]).

The backscatter observations and the rocket and satellite measurements are consistent in showing that temperature equality normally prevails at night. The possible flux of soft electrons is accordingly less than 0.03 erg cm^{-2} sec^{-1}.

REFERENCES

1. A. Omholt, Geophys. Publikasjoner 20 (11), 1 (1959).

2. D. T. Stewart, Proc. Phys. Soc. A69, 437 (1956).

3. S. H. Tate and P. T. Smith, Phys. Rev. 39, 270 (1932).

4. W. L. Fite and R. T. Brackman, Phys. Rev. 112, 815 (1959).

5. J. M. Valentine and S. C. Curran, Rep. Progr. Phys. 21, 1 (1958).

6. A. Dalgarno and W. G. Griffing, Proc. Roy. Soc. A248, 415 (1958).

7. P. L. Hartman and H. Hoerlin, Bull. Am. Phys. Soc. Ser. II, 7, 69 (1962).

8. Yu. I. Galperin, Bulletin (Izvestiya) Acad. Sci. USSR, Geophys. Series No. 2, 174 (1962).

9. B. J. O'Brien, J. Geophys. Res. 67, 3687 (1962).

10. L. A. Antonova and G. S. Ivanov-Kholodny, Izv. Akad. Nauk SSSR, ser. geofiz. No. 5, 756 (1960).

11. J. V. Kazachevskaya and G. S. Ivanov-Kholodny, Isk. sput. Zemli 15, 81 (1962).

12. G. S. Ivanov-Kholodny, Planetary Space Sci. 10, 219 (1963).

13. G. S. Ivanov-Kholodny and L. A. Antonova, Dokl. A.N. SSSR 140, 1062 (1961).

14. L. A. Antonova and G. S. Ivanov-Kholodny, Geomagnetic i Aeronomiya 1, 164 (1961).

15. A. D. Danilov, Space Research III (North-Holland: Amsterdam), Ed. W. Priester, 1963.

16. G. S. Ivanov-Kholodny, Space Research III (North-Holland: Amsterdam), Ed. W. Priester, 1963.

17. F. Mariani, J. Atmos. Sci. (in press).

18. J. R. Winkler, Radio Propagation 66D, 127 (1962).

19. B. J. O'Brien, J. Geophys. Res. 68, 989 (1963).

20. C. E. McIlwain, J. Geophys. Res. 66, 3681 (1961).

21. E. A. Lytle and D. M. Hunten, Canad. J. Phys. 40, 1370 (1962).

22. T. M. Mulyarchik and P. V. Shcheglow, Planetary Space Sci. 10, 215 (1963).

23. L. H. Meredith, M. B. Gottlieb and J. A. VanAllen, Phys. Rev. 97, 201 (1955); J. A. VanAllen, Proc. Nat. Acad. Sci. Wash. 43, 57 (1957).

24. R. D. Sharp, J. E. Evans, W. L. Imhof, R. G. Johnson, J. B. Reagan and R. V. Smith (in press).

25. A. E. Belon, L. Owren, G. J. Romick, J. L. Hook, C. S. Deehr and M. H. Rees, J. Geophys. Res. (in press).

26. C. E. McIlwain, J. Geophys. Res. 65, 2727 (1960).

27. J. W. Chamberlain, Physics of the Aurora and Airglow (Academic Press: London) 1961.

28. A. Dalgarno, M. B. McElroy and R. J. Moffett, Planetary Space Sci. 11, 463 (1963).

29. K. A. Anderson and R. DeWitt, J. Geophys. Res. 68, 2669 (1963).

30. J. W. Hooper, D. S. Harmer, D. W. Martin and E. W. McDaniel, Phys. Rev. 125, 2000 (1962).

31. R. Montalbetti, J. Atmos. Terr. Phys. 14, 200 (1959).

32. A. Omholt, Astrophys. J. 126, 461 (1957).

33. D. R. Bates, Proc. Phys. Soc. B64, 805 (1951).

34. H. K. Paetzold and H. Z. Schörner, Space Research I (North-Holland: Amsterdam), Ed. H. Kallman-Bijl, 1960.

35. H. K. Paetzold, J. Geophys. Res. 67, 2741 (1962).

36. I. Harris and W. Priester, J. Geophys. Res. 67, 4585 (1962); J. Atmos. Sci. 19, 286 (1962); Space Research III (North-Holland: Amsterdam), Ed. W. Priester, 1963.

37. L. G. Jacchia, Space Research III (North-Holland: Amsterdam), Ed. W. Priester, 1963.

38. A. J. Dessler, J. Geophys. Res. 64, 397 (1959).

39. A. E. Grün, Z. Naturforsch, 12a, 89 (1957).

40. L. V. Spencer, N.B.S. Monograph No. 1, 1959.

41. M. H. Rees, Planetary Space Sci. (in press).

42. L. G. Jacchia, Rev. Mod. Phys. (in press).

43. D. M. Hunten, Annales de Geophys. 17, 249 (1961).

44. L. V. Wallace, J. Atmos. Sci. 19, 1 (1962).

45. L. H. Meredith, L. R. Davis, J. P. Heppner and D. E. Berg, IGY Rocket Report Series No. 1, 169 (1958).

46. T. M. Mulyarchik, Izv. Akad. Nauk SSSR, Ser. Geofiz. 3, 449 (1960).

47. J. W. Chamberlain, Annales de Geophys. 17, 90 (1961).

48. E. R. Manring and H. B. Pettit, J. Geophys. Res. 64, 149 (1958).

49. W. B. Hanson and F. S. Johnson, Mém. Soc. Sci. Liège Ser. 5, 4, 390 (1961).

50. L. R. Megill and N. P. Carleton, J. Geophys. Res. (in press).

51. A. Dalgarno and M. B. McElroy, Planetary Space Sci. 11, 6 (1963).

52. T. M. Donahue and W. G. Fastie, Space Research IV (North-Holland: Amsterdam, in press) (COSPAR Meeting, Warsaw, Poland, June 1963).

53. N. N. Shefov, Aurorae and Airglow (USSR Acad. Sci.) 9, 55 (1962).

54. P. Swings, Aurorae and Airglow (Pergamon Press: London) Ed. E. B. Armstrong and A. Dalgarno, 1956.

55. I. S. Shlovskii, Astr. J. (Moscow) 34, 127 (1957).

56. J. C. Brandt, Astrophys. J. 130, 228 (1959).

57. N. N. Shefov, Planetary Space Sci. 10, 73 (1963).

58. V. I. Krassovsky, Proc. XIth International Astronautical Congress, Stockholm, 1960.

59. N. N. Shefov, Planetary Space Sci. 5, 75 (1961); Aurorae and Airglow (USSR Acad. Sci.) 5, 49 (1961).

60. A. E. Ferguson, Planetary Space Sci. 9, 286 (1962).

61. G. Kockarts and M. Nicolet, Annales de Geophys. 18, 269 (1962).

62. N. P. Carleton and O. Oldenberg, J. Chem. Phys. 36, 3460 (1962).

63. H. B. Dunford, J. Phys. Chem. 67, 258 (1963).

64. E. C. Zipf, J. Chem. Phys. 38, 2034 (1963).

65. W. B. Hanson, Space Research III (North-Holland: Amsterdam) Ed. W. Priester, 1963.

66. A. Dalgarno, National Aeronautics and Space Administration CR-8 (1963).

67. R. E. Bourdeau, Space Science Reviews 1, 683 (1963).

68. R. E. Bourdeau, Proc. Roy. Soc. A (in press).

69. L. K. Bowles, E. R. Ochs and J. L. Green, J. Research (National Bureau of Standards) A66, 395 (1962).

70. J. V. Evans, J. Geophys. Res. 67, 4914 (1962).

71. V. C. Pineo and D. P. Hynek, J. Geophys. Res. 67, 5119 (1962).

72. N. W. Spencer, L. H. Brace and G. R. Carignan, J. Geophys. Res. 67, 157 (1962).

ACKNOWLEDGMENTS

This manuscript was begun at the Joint Institute of Laboratory Astrophysics in Boulder, Colorado, and completed at the Goddard Institute for Space Studies in New York. The work was supported by the National Aeronautics and Space Administration under Contract No. NASw-701.

I am indebted to Dr. L. Branscom and Dr. R. Jastrow for their hospitality. I am indebted also to Mr. J. Walker for some valuable discussions.

SECTION II — EXPERIMENTAL

This section includes the results of experimental work accomplished under Contract No. NASw-701 which have been previously published as GCA Technical Report Nos. 63-3-N and 63-13-N and which have been accepted for publication in scientific journals. Also reproduced in this section is the technical paper entitled "Observed and Predicted New Auto-ionized Energy Levels in Krypton, Argon and Xenon" which has been accepted for publication in Physical Review Letters.

GCA Technical Report No. 63-3-N

PLANETARY AERONOMY XI: ABSOLUTE INTENSITY MEASUREMENTS IN THE VACUUM ULTRAVIOLET

J.A.R. Samson

March 1963

Contract No. NASw-395
and
Contract No. NASw-701*

GEOPHYSICS CORPORATION OF AMERICA
Bedford, Massachusetts

Prepared for

NATIONAL AERONAUTICS AND SPACE ADMINISTRATION
Headquarters
Washington 25, D. C.

*This work was initiated under Contract No. NASw-395 and completed under Contract No. NASw-701.

This paper has been accepted for publication in the Journal of the Optical Society of America (January 1964), and was presented at the Spring Meeting of the Optical Society of America, Jacksonville, Florida, 1963.

TABLE OF CONTENTS

Absolute Intensity Measurements in the Vacuum Ultraviolet*

JAMES A. R. SAMSON
Physics Research Division, Geophysics Corporation of America
Bedford, Massachusetts

ABSTRACT

Photoionization of the rare gases is proposed as a method to measure the absolute intensities of radiation below 1022 Å, the ionization potential of xenon. The method is based on the assumption that the photoionization yield of the rare gases is unity. Experimental evidence is presented to justify this assumption. The relative quantum yield of sodium salicylate is measured and shown to be constant between 400 - 900 Å. Finally, the photoelectric yield of gold "black" has been measured and found to be about 1% at 1215 Å rising to 4% at 850 Å and remaining constant from there down to 500 Å.

*Presented at the Spring Meeting of the Optical Society of America, Jacksonville, Florida, 1963.

INTRODUCTION

Techniques to measure the absolute intensity of radiation in the visible and infrared region of the spectrum are well established. The techniques usually involve the calibration of the response of a thermopile or some other detector to radiation emitted from a standard lamp. This calibration is made at wavelengths far removed from the vacuum ultraviolet (VUV) region of the spectrum. The assumption is then made that the thermopile has a "flat" response to all wavelengths; that is, its quantum efficiency is constant. These "secondary" standards are then used to determine the absolute intensity of the unknown radiation. Unfortunately, in the vacuum ultraviolet region of the spectrum, the flux density emitted by many light sources is far weaker than in the visible, especially after transmission through a monochromator where the initial radiation intensity is greatly attenuated by the poor reflectivity of gratings.[1,2] This necessitates the use of wide slits in a monochromator to obtain sufficient light intensity for a measurable signal from the thermopile. Wavelength resolution is sacrificed for this increased intensity. A third and more sensitive standard, typically a sodium salicylate-coated photomultiplier, is then calibrated against the thermopile. With this more sensitive standard, the monochromator slits can be narrowed and a higher wavelength resolution achieved. Using the above technique, Watanabe et al.[3] measured the photoelectric yield of nitric oxide, among many other gases. Of

particular interest is the yield of NO at Lyman-α (1215.7 Å) which has recently been remeasured by Watanabe and found to be about 81 to 85%.[4] This value for the yield of NO has been used as a standard to determine the absolute intensity of the hydrogen Lyman-α line emitted from the sun using nitric oxide ionization chambers in rockets and satellites.[5-7] The many steps involved in reaching the photoelectric yield of NO increases the chance for error in the value of the yield. However, the main assumption is that the thermopile does have a "flat" response to all wavelengths. It is calibrated in the visible region of the spectrum and then used to determine absolute intensities in the vacuum ultraviolet region.

The metallic "blacks" with which the receivers of a thermopile are coated are actually pure metallic droplets which have been evaporated onto the receivers under appropriate conditions to form spherical droplets of suitable radii to provide minimum reflection of visible and infrared radiation. The receivers thus appear black and essentially absorb all of the incident radiation. The work of Harris et al.[8] on the optical properties of gold "black" shows that a highly absorbing deposit of gold is obtained for the visible and infrared when the gold spheroids have a diameter of the order of 100 Å. For VUV radiation, the wavelengths are reduced by about an order of magnitude or more; thus, the spherical drops will appear larger to this type of radiation and presumably the blackness does not necessarily hold in this region of the spectrum. In fact, Harris does find that the reflected light at

4000 Å is slightly greater than in the red. However, due to the fact that most materials have poor reflectances in the VUV,[9,10] this may offset the fact that the metallic spheres have a larger ratio of radii/wavelength and the receivers may thus be truly black to VUV radiation. A further point is that all metals show a photoelectric yield in the vicinity of 5 to 10 per cent at wavelengths below 1000 Å.[11] This certainly means a loss of photons for the production of heat and thus an error in the determination of the absolute energies.

To circumvent these problems the thermopile should be calibrated as a function of wavelength to determine the extent the flatness of response deviates in the VUV. A program of this nature is currently under way at the National Bureau of Standards, Washington, under the direction of Dr. R. Madden. The standard light source in this case is the continuous radiation emitted from a 180 Mev synchrotron. The absolute intensity of the synchrotron radiation can be calculated knowing the electron beam density and other instrumental parameters.[12] The validity of the theoretical treatment of the synchrotron radiation has been checked experimentally by Tomboulian and Hartman[13] in the extreme ultraviolet and excellent agreement obtained. A useful feature of the synchrotron radiation is that it is plane polarized with the electric vector parallel to the electron orbit. The major advantage of the synchrotron radiation is that it provides a continuous and calculable radiation intensity from the visible to the X-ray region of the spectrum. However, for normal laboratory research synchrotrons are not readily available for calibration work.

It is the purpose of this paper to investigate the photoelectric yield of gold black and to present a simple but extremely accurate and reproducible method for measuring absolute intensities in the vacuum ultraviolet; namely, photoionization of the rare gases. The one assumption made is that the photoionization yield, γ, of the rare gases is unity. γ is defined as the ratio of ions formed per second to the number of incident photons absorbed per second within the gas. If the assumption is accepted, the method resolves itself to the determination of an electron current (ions/sec), which is then equal to the absolute number of photons/sec absorbed by the gas. Theoretically, γ is expected to be unity for the rare gases, even in the regions of autoionization which generally occur between the $^2P_{3/2}$ and $^2P_{1/2}$ states.

For an autoionized energy level the atom may be de-excited with the emission of a photon or by a radiationless transition into the adjacent ionization continuum with the release of a photoelectron. The ratio of the number of photoelectrons emitted to the total number of atoms in the autoionized state is equal to $\alpha/(\beta+\alpha)$, where α and β are, respectively, the probabilities for radiationless and radiative transitions. The probability for a given transition is equal to the inverse of the mean lifetime of that state. Therefore, since the lifetime of radiationless transitions into the ionization continuum is of the order of 10^{-13} to 10^{-15} secs compared to 10^{-8} secs for a radiative transition, then $\alpha/(\beta+\alpha)$ is essentially unity. Thus, the photoionization yield of the rare gases is expected to be unity in an autoionized level.

Using photoionization of the rare gases, direct calibration of the absolute intensity of a source can be made only at wavelengths shorter

than 1022 Å, the ionization potential of xenon. However, a thermopile may be calibrated against the rare gases for use above 1000 Å.

EXPERIMENTAL TECHNIQUES

An experimental approach to the measurement of γ for the rare gases is to measure their yields relative to one another. If these yields all turn out to be constant, even in regions of autoionization, then this is excellent evidence that the constant γ must be unity.

Ionization chambers. Three ionization chambers were designed and constructed to measure the photoionization yields of the rare gases. Figure 1 shows a drawing of a double ion chamber which, as far as can be ascertained, was first used to measure photoionization yields by Weissler and associates.[14] Two new designs, one a modified double ion chamber and the other a single ion chamber, are illustrated in Figs. 2 and 3.

With the aid of Fig. 1 an analysis of the double ion chamber is given. Denote I_o as the incident light intensity to be measured; then, with a gas in the cell at some suitable pressure, say P, denote I_1 and I_1' as the intensities entering and leaving plate 1, and denote I_2 and I_2' as the intensities entering and leaving plate 2. The three small plates alternating with the ion collection plates are guard rings to provide a uniform field between the parallel plates and are all at ground potential. The repeller plate is held a few volts positive to drive the ions to the collector plates 1 and 2. Now at plate 1, the total number of ions produced per second is equal to i_1/e, where i_1 is the electric current flow

in amperes and e is the electronic charge measured in coulombs; and, further, the total number of photons absorbed per second is equal to $(I_1 - I_1')$. Using Lambert's law this becomes

$$I_1 - I_1' = I_o e^{-\mu L_1}(1 - e^{-\mu d}) ,$$

where μ is the absorption coefficient of the gas measured at a pressure P, while L_1 and d are the dimensions shown in Fig. 1. From the definition of the photoionization yield, we get

$$\gamma = \frac{i_1/e}{I_o e^{-\mu L_1}(1-e^{-\mu d})} ,$$

or in terms of the experimentally determined quantity

$$I_o\gamma = \frac{i_1/e}{e^{-\mu L_1}(1-e^{-\mu d})} . \qquad (1)$$

Similarly, for plate 2

$$I_o\gamma = \frac{i_2/e}{e^{-\mu L_2}(1-e^{-\mu d})} . \qquad (2)$$

From the ratio of Eqs. (1) and (2) and solving for μ, we get

$$\mu = \frac{\ell n(i_1/i_2)}{L_2 - L_1} . \qquad (3)$$

Substituting μ into Eq. (1) and assuming $\gamma = 1$, I_o can be found from measurements of L_1, L_2, d, and the ion currents i_1 and i_2.

The same procedure is used to measure γ in other gases. When I_o is known, Eq. (1) is again used and the value of the photoionization yield determined. It should be noted that the absolute value of the gas pressure is not required in these measurements.

Implicit in the double ion chamber method is the use of measured absorption coefficients, and thus the accuracy of the method depends upon the measured absorption coefficients obeying Beer's law which states that the amount of light absorbed is proportional to the number of absorbing molecules through which the light passes. Incorporated into Lambert's law, this gives

$$I = I_o e^{-kx} ,$$

where k is the absorption coefficient at S.T.P., while x is the path length reduced to S.T.P. and is given by

$$x = L \frac{P}{760} \frac{273}{T} .$$

Thus, to obey Beer's law, k must be independent of both pressure, P, and path length, L. This will not be the case in regions of discrete absorption when the absorption lines are narrower than the band pass of the photoionizing radiation. Thus, in using the double ion chamber to measure absolute intensities or photoionization yields one must vary the pressure to check that k is pressure independent.

The major advantage of the double ion chamber lies in the fact that all the variables, viz., the two ion currents and, if desired, a

secondary standard output, can be measured simultaneously, thereby eliminating any discrepancies due to light source fluctuations.

Referring to Fig. 2 for an analysis of the single ion chamber, we define I_o as the light intensity at the exit slit of the monochromator and I as the transmitted intensity at the end of the ion chamber. Then,

$$\gamma = \frac{\text{ions formed/sec}}{\text{photons absorbed/sec}}$$

$$= \frac{i/e}{I_o - I}$$

$$= \frac{i/e}{I_o(1-I/I_o)}$$

$$\therefore I_o\gamma = \frac{i/e}{(1-I/I_o)} \qquad (4)$$

The ratio I/I_o is measured by the detector which must lie exactly at the end of the ion chamber. This ratio is independent of absolute intensities and any detector which has a linear response with respect to intensity may be used. This method requires that all the ions formed from the exit slit to the detector be collected and counted. To achieve this, it is necessary to connect the exit slit electrically to the positive repeller plate. The ion chamber will then have a field distribution as shown in Fig. 2 and all ions formed within the ion chamber system will be collected. The major advantage of this system is that no measurement of an absorption coefficient is made which must obey Beer's law. Actually, I_o is independent of the pressure used and in the limit when $I/I_o \rightarrow 0$, Eq. (4) becomes

$$I_o\gamma = i/e \ . \qquad (5)$$

The modified double ion chamber, shown in Fig. 3, is obtained by letting L_1 and L_2 in Fig. 1 go, respectively, to zero and d. In this case, Eq. (1) becomes

$$I_o\gamma = \frac{i_1/e}{1-e^{-\mu d}}$$

or

$$I_o\gamma = \frac{(i_1)^2/e}{i_1-i_2} \ , \qquad (6)$$

since

$$\mu = \frac{1}{d} \ln(i_1/i_2) \ . \qquad (7)$$

As in the case of the single ion chamber, the exit slit of the monochromator must be at the same positive potential as the repeller plate. When the gas pressure is sufficiently high for total absorption of the incident radiation, the modified double ion chamber acts as a single ion chamber with $I_o\gamma = i_1/e$.

With each ionization chamber the experimentally determined quantity is the product of the absolute intensity and the photoionization yield. Knowledge of one, therefore, provides the other.

Experimental difficulties. The use of photoionization techniques for absolute intensity measurements is far from being straightforward. To begin with, since there are no windows available in this spectral

region, one must take care that the main vacuum system of the monochromator is maintained at a high vacuum to insure that the photon intensity at the exit slit of the monochromator is the same before and after the calibrating gas is allowed to flow into the ion chamber. Another problem associated with a flow system is to assure that the gas is uniformly at the same pressure throughout the ion chamber. Any pressure gradients would be detrimental when using the double ion chamber. To check the uniformity of the pressure the following technique was employed: Using the double ion chamber and a sodium salicylate-coated photomultiplier, as in Fig. 1, the absorption coefficient of argon was measured with the 584 $\mathring{A}$ radiation from a D.C. helium light source. This wavelength was chosen since argon has no discrete absorption peaks there and the measured absorption coefficient will, therefore, obey Beer's law. The two methods gave an absorption coefficient of 990 cms^{-1} with 4% of each other. Further, the absolute intensity of the 584 $\mathring{A}$ line was measured with each of the three ion chambers and with a range of pressures including total absorption of the radiation; a constant value was obtained within one or two per cent. It is concluded, therefore, that no appreciable pressure gradients exist with these flow type ion chambers with the narrow slit openings used here; namely, 50 microns wide by 1 cm in length.

Probably one of the most important precautions to take is to be certain one is using the proper collector voltage on the ion plates. That is, one must operate in the plateau region of the ions vs. voltage curve; in fact, one must ascertain that there actually is a plateau

for the particular ion chamber, calibrating gas, and wavelength used. For example, if xenon were ionized by 461.5 Å (26.86 ev), an electron could be ejected with an energy, E, given by:

$$E = h\nu - I(Xe) , \qquad (8)$$

where I(Xe) is the ionization potential of xenon and is equal to 12.13 ev. $h\nu$ is the energy of the incident photon which, in this example, is 26.86 ev. Substituting these values into Eq. (8) gives E = 14.73 ev. Thus, the electron is emitted with sufficient energy to cause secondary ionization. With the addition of a collector voltage this energy is increased. It is, therefore, impossible to achieve a plateau with xenon at 461.5 Å and at a pressure which would give a measurable ion current. The top curve in Fig. 4 illustrates this point for a particular ion chamber.

A further competing process is the collection of electrons as well as ions. This can occur if an insufficiently high electron retarding potential is used. Reference to Fig. 5 illustrates possible electron trajectories. Now these electrons all have the same energies, but those travelling at an angle to the field lines can be retarded at lower voltages than those travelling parallel to, but opposing, the field lines. That is, the important quantity is the component of the electron energy normal to the collector plate. It has been shown by Sommerfeld[15] that the probability for an electron to be ejected at an angle θ to the direction of propagation of the incident radiation is proportional to $\sin^2\theta$; thus, the most probable direction is at right

angles to the path of the incident radiation. For a given geometry, this will result in an energy spread between some minimum and maximum energy. Therefore, a curve of ion current versus voltage should indicate a plateau at voltages lower than that necessary to retard the electrons of minimum energy. In this region, all the ions and a fraction of the electrons are collected. At a voltage high enough to retard the electrons of minimum energy, the ion current should start to increase and continue increasing until the voltage is sufficiently high to retard all electrons at which point the true plateau should start. The bottom two curves in Fig. 4 show typical curves for krypton and neon illustrating this point. The arrows indicate the values of the calculated ion chamber voltages to provide the necessary minimum and maximum voltages to retard the electrons.

As can be seen in Fig. 5, the ionizing radiation is made to pass as closely to the ion repeller plate as possible without actually striking it. The reason for this is to provide a maximum retarding potential for electrons travelling towards the collector plate while giving a minimum acceleration to electrons travelling towards the +V plate and thereby decreasing the chance of providing the electrons with sufficient energy to cause secondary ionization.

Apparatus. The major apparatus consisted of a McPherson model 235, 1/2 M Seya-type monochromator. The monochromator was used with a 600 L/mm platinized replica grating blazed for normal incidence at

1500 Å. The entrance and exit slits were 50μ wide which gave a wavelength resolution of 2.5 Å. Differential pumping was employed between the light source and monochromator.

The light source consisted of a high voltage (5Kv) repetitive spark discharge in a low pressure gas, the discharge taking place through a 3 mm diameter ceramic capillary about 5 cm long. This produced a many lined spectrum characteristic of the gas used. Since migration of the light source gas into the ion chamber would be an impurity and a possible error, argon was chosen as the light source gas. The useful range of the light source was from 400 - 1000 Å; however, above 800 Å care had to be taken to avoid second order lines. A hydrogen D.C. discharge was used to provide radiation from 900 - 1300 Å. Actually, the many lined hydrogen spectrum continues to 1650 Å; however, the ionization potential of xenon is at 1022 Å and the photoelectric yield of metals is already very low, around 1300 Å, so it was unnecessary to go to longer wavelengths in this investigation.

RESULTS

Intensity measurements of VUV radiation have been made by the technique of photoionizing rare gases and assuming that their photoionization yield, γ, is unity. We have set out to show that this assumption is indeed a good one. Data have also been obtained on the quantum efficiency of sodium salicylate in the previously unexplored region between 400 Å and 900 Å, and on the photoelectric yield of gold black.

Photoionization. Using photoionization of the rare gases to determine absolute radiation intensities the experimentally determined quantity, as given by Eqs. (1), (4), (5), or (6), is the product of the absolute radiation intensity with the photoionization yield; that is, $I_o\gamma$. Now if the light source intensity is kept constant - and hence I_o - and the quantity $I_o\gamma$ measured for each of the rare gases which will ionize in that region, then the ratio of these values will give the relative photoionization yield γ_1/γ_2 of the rare gases. Should the rare gases all have identical yields, this ratio will be unity. Figure 6 shows a plot of the relative yields of argon, xenon, krypton, and neon, with respect to wavelength. The ratio of the yields is unity with an error spread of $\pm$ 5%. This is true even in the autoionized lines of krypton where its yield was measured relative to xenon. It is extremely unlikely that the photoionization yield curves can show structure which is identical for all the rare gases. Thus, the most probable value for the photoionization yield of the rare gases is unity even in the regions of autoionization. This result agrees with what one expects theoretically. Watanabe, using a calibrated thermopile, has determined the yield of xenon in the range 850 - 1000 Å which includes the autoionized structure, and found that the yield is indeed unity.[4] Curves similar to Fig. 6 were obtained using the double and single ion chambers and also using the single ion chamber with total absorption. This latter method greatly simplifies the data reduction.

The scatter of points in Fig. 6 is due mainly to fluctuations in the light source during the time it takes for a run in each gas. If a single wavelength is selected and various rare gases passed through the ion chamber one after the other, the value of $I_o\gamma$ remains constant to within 1%.

Sodium salicylate. The research presented here is not intended to be an exhaustive investigation of sodium salicylate; rather it points up some of the problems involved when sodium salicylate is used as a detector with a "flat" response to VUV radiation. Several researchers have investigated the relative quantum yield of sodium salicylate in various spectral regions from 3500 Å down to 900 Å.[16-21] Of particular interest is the work in the VUV of Johnson et al.,[16] Watanabe and Inn,[17] and Smith.[18] The two former references report a relatively constant yield between 900 - 2300 Å with a tendency for the yield to peak around 1500 Å. This increase amounted to approximately 20% above the constant yield value. In each case the results were obtained using fresh coatings of sodium salicylate.[4] The results reported in reference (18) were made with fresh and aged coatings between 900 - 1600 Å. As in references (16) and (17) a fresh coating exhibited a relatively constant yield up to 1300 Å, then increased to a maximum around 1500 Å. However, as the coating aged, the relative quantum yield progressively decreased. The decrease was more rapid at the shorter wavelengths; in fact, for a 40-day-old coating the yield at 900 Å was three times less than at 1600 Å.

Results on the constancy of the yield of sodium salicylate for the unexplored region between 400 - 900 Å and verification of its nature between 900 - 1600 Å are given below.

Grade U.S.P. sodium salicylate was dissolved in methyl alcohol to form a saturated solution, then was sprayed onto a glass slide or window with an atomizer. A heat gun blew hot air continually onto the window to facilitate the evaporation of the alcohol. This produced a fine crystalline layer of sodium salicylate. The spraying continued until the glass surface was all covered.

Figure 7 gives the relative quantum yield of sodium salicylate between 400 - 1020 Å. The coating was of undetermined age but certainly older than seven days. The yield, determined using the rare gas technique to calibrate the light intensity, is defined as the output current of a sodium salicylate-coated photomultiplier divided by $I_o\gamma$. It can be seen that the yield remains constant between 400 - 900 Å at which point it begins to increase. Figure 8 presents data between 400 - 800 Å for a coating 1, 24, and 48-hours old. This coating was continually under vacuum during the test period. There is a small overall decrease in quantum yield from day to day; however, the yield remained constant within $\pm$ 6% for any given day.

A Reeder-type uncalibrated thermopile was used in the range 900 - 1600 Å to measure the yield of sodium salicylate. The thermopile elements were coated with gold black by evaporating pure gold in an

atmosphere of dry nitrogen at a pressure of 1 Torr. The elements appeared extremely black to the eye. The scattered light in the monochromator as seen by the thermopile and coated photomultiplier was very small. Figure 9 gives the results of the yield of two different coatings, one less than an hour old and the other approximately eleven days old. The fresh coating has a constant yield between 900 - 1250 Å, then rises to a maximum in the vicinity of 1500 Å. The old coating shows the characteristics decrease towards the shorter wavelengths.

It appears, therefore, that the quantum yield of sodium salicylate decreases with age and that the decrease is a function of wavelength at least above 900 Å. Between 400 - 900 Å the yield seems to be constant within $\pm$ 6% and although decreasing with age this constancy remains. However, care must be exercised in the use of sodium salicylate as a detector of VUV radiation. The sensitivity of the detector depends on the thickness of the crystalline coating and on the age of the coating. The ageing process is not well understood and may depend on the history of a particular coating; e.g., its exposure to a vacuum, continual or intermittently, and possibly to vacuum contaminants such as pump oil. The quantum yield of a fresh coating of sodium salicylate does appear to have the following consistent characteristics: a constant yield from 400 - 1250 Å; then the yield increases by 20 - 50% up to 1500 Å where it again remains constant to 1600 Å.

Photoelectric yields. To determine the possible effects of the photoelectric process on the performance of a thermopile, the photoelectric yield of gold black was measured between 400 and 1216 Å. The gold black was prepared by evaporating pure gold onto a microscope slide in an atmosphere of nitrogen at a pressure of approximately 1 Torr. The resulting coating was extremely black to the eye with a velvet-like texture. Figure 10 shows the yield of gold black with and without any collector voltage and, for comparison, the yield of pure gold evaporated at a pressure of 10^{-5} Torr. The evaporated gold had a mirror-like surface. The open circle data points were taken relative to a sodium salicylate freshly coated photomultiplier, and then normalized to fit the curve. The remaining data points were all taken relative to the rare gas ionization chambers. The important yield curve as far as the effects on the thermopile are concerned is that of gold black with zero collector voltage since this is the condition under normal operation of the thermopile. It can be seen from Fig. 10 that the effective yield of gold black is about 4% from 800 Å to 450 Å, to longer wavelengths it decreases steadily to about 1% at Lyman-α (1215.7 Å).

The yield of gold black is less than that of smooth evaporated gold although the two samples were made from the same batch of 99.99% pure gold wire. All other conditions were identical with the exception of the residual nitrogen pressure during evaporation. The reduced yield of gold black is to be expected since for any micrograin surface the

photoelectrons released in a direction other than close to the normal will have a high probability of striking the spheroids which make up the surface of the material and therefore be retained by the metal.

The loss of photons in the production of photoelectrons results in a lower output of the thermopile. The photoelectric yield for gold black given in Fig. 10 probably represents an upper limit to the loss since not all of the photon energy goes into the kinetic energy of the electron. Over and above the normal work function barrier an electron released within the volume of the metal loses energy by multiple collisions before reaching the surface.[22] Photoelectrons are thus released with a wide spread of energy by radiation of fixed energy. An analysis of the energy distribution of photoelectrons released from gold has been made by Walker and Weissler.[23] They find, for example, that for radiation of 704 Å (17.6 ev) nearly all of the photoelectrons have energies uniformly distributed from zero to 7.5 ev.

To verify directly the effect of photoelectrons on the thermopile output, a retarding potential of -90 volts/cm was applied between the thermopile elements and the monochromator slits. Using the 584 Å radiation an increase of approximately 2% in the output was detected with the retarding field on. No effect was observed at 1216 Å. This is in excellent agreement with the discussion above.

The reflectance of gold black has been measured by Smith[18] between 900 and 1600 Å and found to be less than one-third of one per cent.

CONCLUSIONS

The relative photoionization yields of the rare gases with respect to one another is unity. Thus, absolute intensity measurements will be independent of which rare gas is used, provided proper experimental care is observed; for example, measurements must be made on the plateau region of the ions vs. voltage curve, no stray electrons should be collected, and measurements in the vicinity of discrete absorption peaks should be avoided unless the single ion chamber is used.

It appears as if sodium salicylate can be used as a detector having a quantum efficiency which is constant within $\pm$ 10% between 400 - 1250 Å if a fresh coating is used each time.

When a thermopile is used in the vacuum ultraviolet region of the spectrum, a small correction of a few per cent is necessary, especially below 1000 Å, to account for photons lost in the production of photoelectrons. However, on the whole a thermopile apparently maintains its "flatness" of response throughout the vacuum ultraviolet region.

ACKNOWLEDGEMENTS

The author wishes to thank Dr. F. F. Marmo, Director of the Laboratory, for his interest and encouragement in this work, and also F. Kelley for his help in the reduction of the data.

REFERENCES

1. J. A. R. Samson, J. Opt. Soc. Am. 52, 525 (1962).

2. H. M. O'Bryan, Phys. Rev. 38, 32 (1931).

3. K. Watanabe, F. F. Marmo, and E.C.Y. Inn, Phys. Rev. 91, 1155 (1953).

4. K. Watanabe, University of Hawaii, Honolulu (private communication).

5. H. Friedman, Physics of the Upper Atmosphere, edited by J. A. Ratcliffe (Academic Press, Inc., New York, 1960).

6. T. A. Chubb and H. Friedman, Rev. Sci. Instr. 26, 493 (1955).

7. J. E. Kupperian, E. T. Byram, T. A. Chubb, and H. Friedman, Planetary Space Sci. 1, 3 (1959).

8. L. Harris, R. T. McGinnies, and B. M. Seigel, J. Opt. Soc. Am. 38, 582 (1948).

9. G. B. Sabine, Phys. Rev. 55, 1964 (1939).

10. W. C. Walker, O. P. Rustgi, and G. L. Weissler, J. Opt. Soc. Am. 49, 471 (1959).

11. W. C. Walker, N. Wainfan, and G. L. Weissler, J. Appl. Phys. 26, 1366 (1955).

12. J. Schwinger, Phys. Rev. 75, 1912 (1949).

13. D. H. Tomboulian and P. L. Hartman, Phys. Rev. 102, 1423 (1956).

14. N. Wainfan, W. C. Walker, and G. L. Weissler, J. Appl. Phys. 24, 1313 (1953).

15. A. Sommerfeld, Wave Mechanics (Methuen & Co., Ltd., London, 1930), p. 181.

16. F. S. Johnson, K. Watanabe, and R. Tousey, J. Opt. Soc. Am 41, 702 (1951).

17. K. Watanabe and E.C.Y. Inn, J. Opt. Soc. Am. 43, 32 (1953).

18. A. Smith, Thesis, University of Rochester, 1961.

19. J. F. Hammann, Z. Angew. Physik 10, 187 (1958).

20. E. Krokowski, Naturwissenschaften 45, 509 (1958).

21. W. Slavin, R. W. Mooney, and D. T. Palumbo, J. Opt. Soc. Am. 51, 93 (1961).

22. H. Hinteregger, Phys. Rev. 96, 538 (1954).

23. W. C. Walker and G. L. Weissler, Phys. Rev. 97, 1178 (1955).

LIST OF FIGURES

Figure 9. Relative quantum yield of sodium salicylate in the spectral range 900 - 1600 Å. The yield was measured for two different coatings relative to a thermopile: Coating A less than one hour old; Coating B approximately 280 hours old.

Figure 10. The photoelectric yield of gold. The gold samples were all made from 99.99% pure gold wire. The evaporated gold sample had a metallic lustre and was prepared at a pressure of 10^{-5} Torr while the gold black was evaporated in an atmosphere of nitrogen at a pressure of 1 Torr and had a black velvet-like texture. The numbers in parenthesis represent the electron collector voltages. The open circle data points were obtained relative to a sodium salicylate freshly coated photomultiplier while all other data points were obtained using the rare gas ionization chamber.

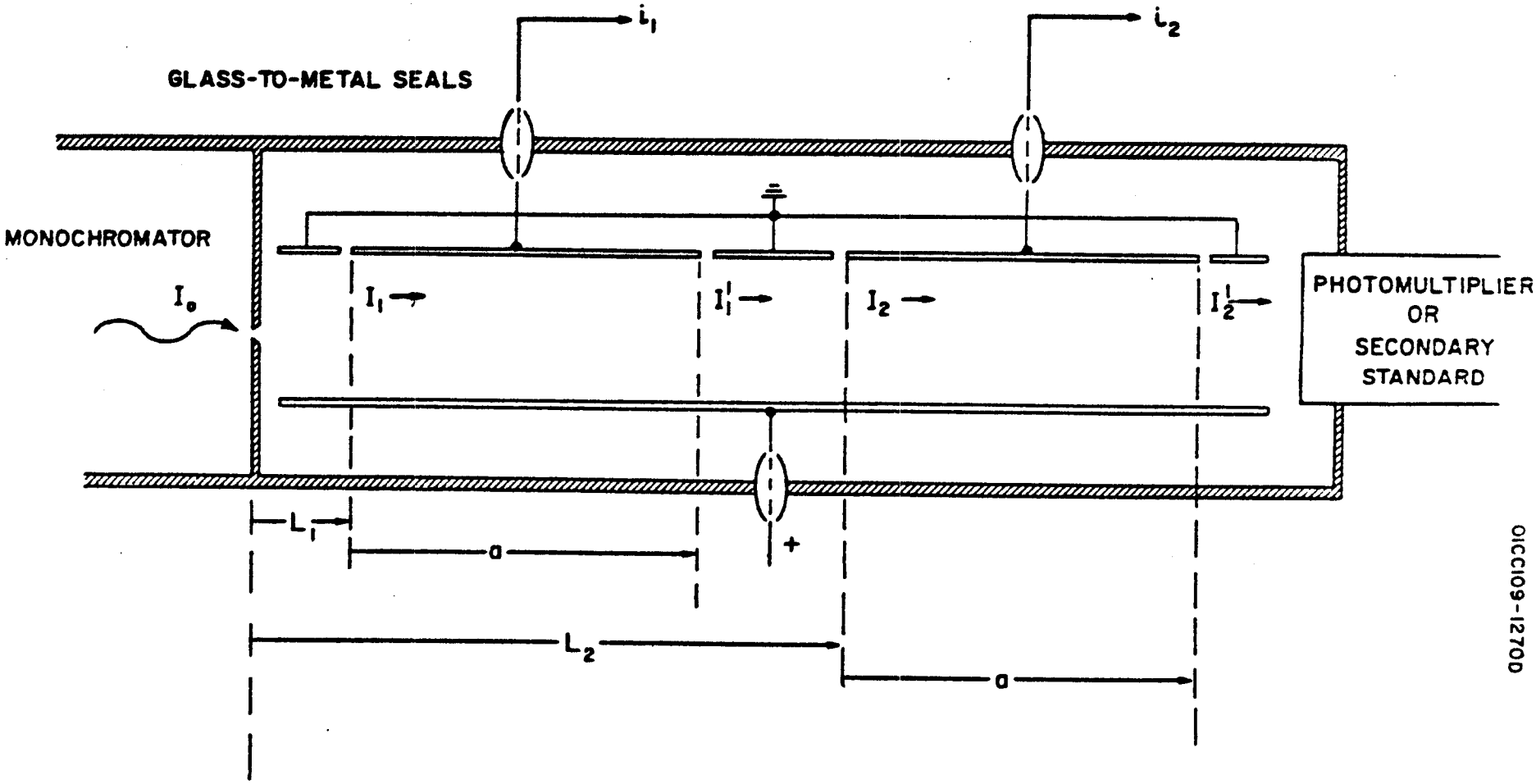

Figure 1. The double ion chamber. I_o is the flux passing through the exit slit of the monochromator. I_1 and I_2 are the fluxes entering, and I_1' and I_2' are the fluxes leaving the ion collector regions of Plate 1 and Plate 2, respectively.

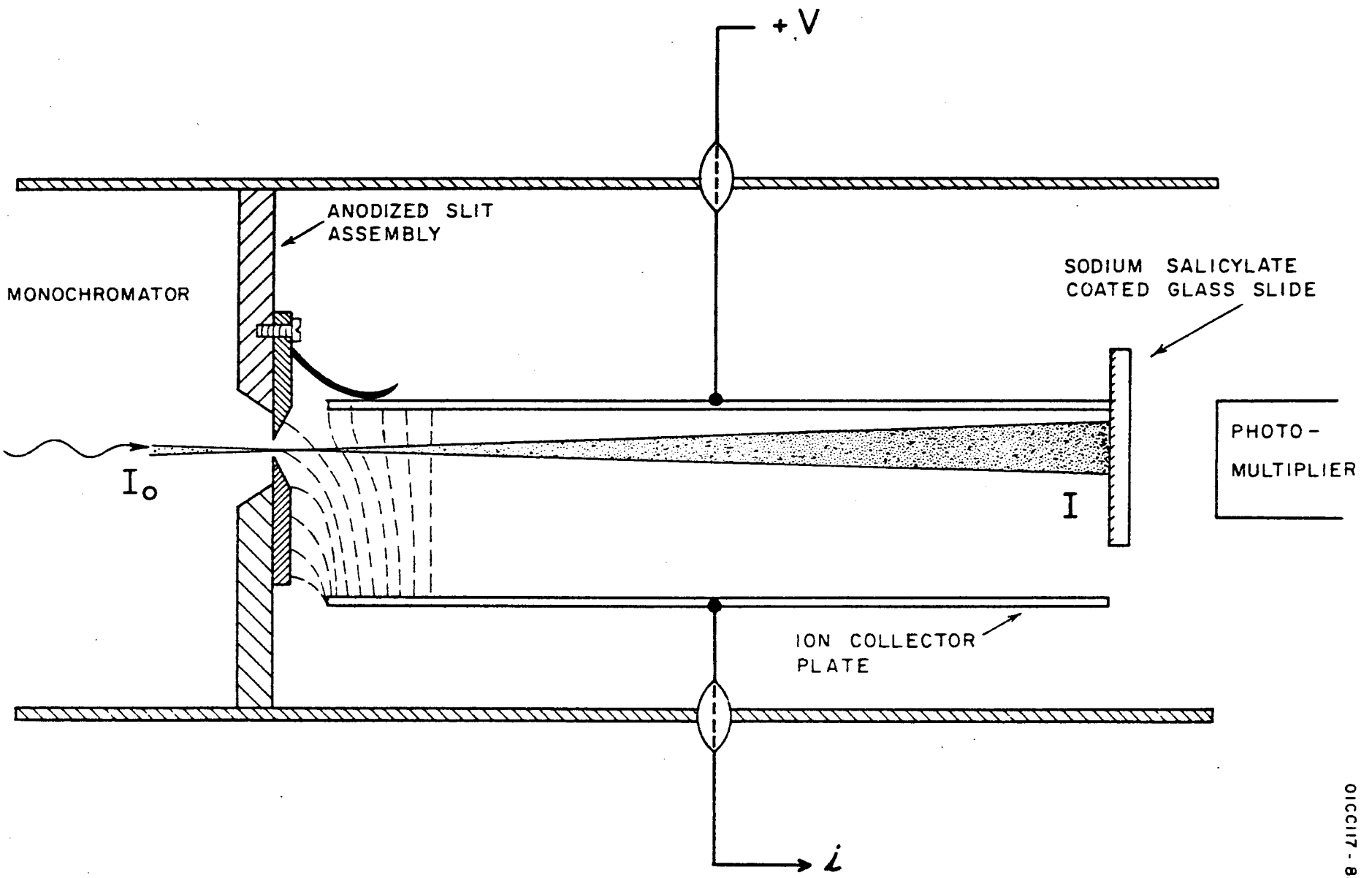

Figure 2. The single ion chamber. I_o is the flux passing through the exit slit of the monochromator while I is the flux at the detector. The exit slit of the monochromator is held at the same potential as the repeller plate. The dashed lines indicate typical electric field lines.

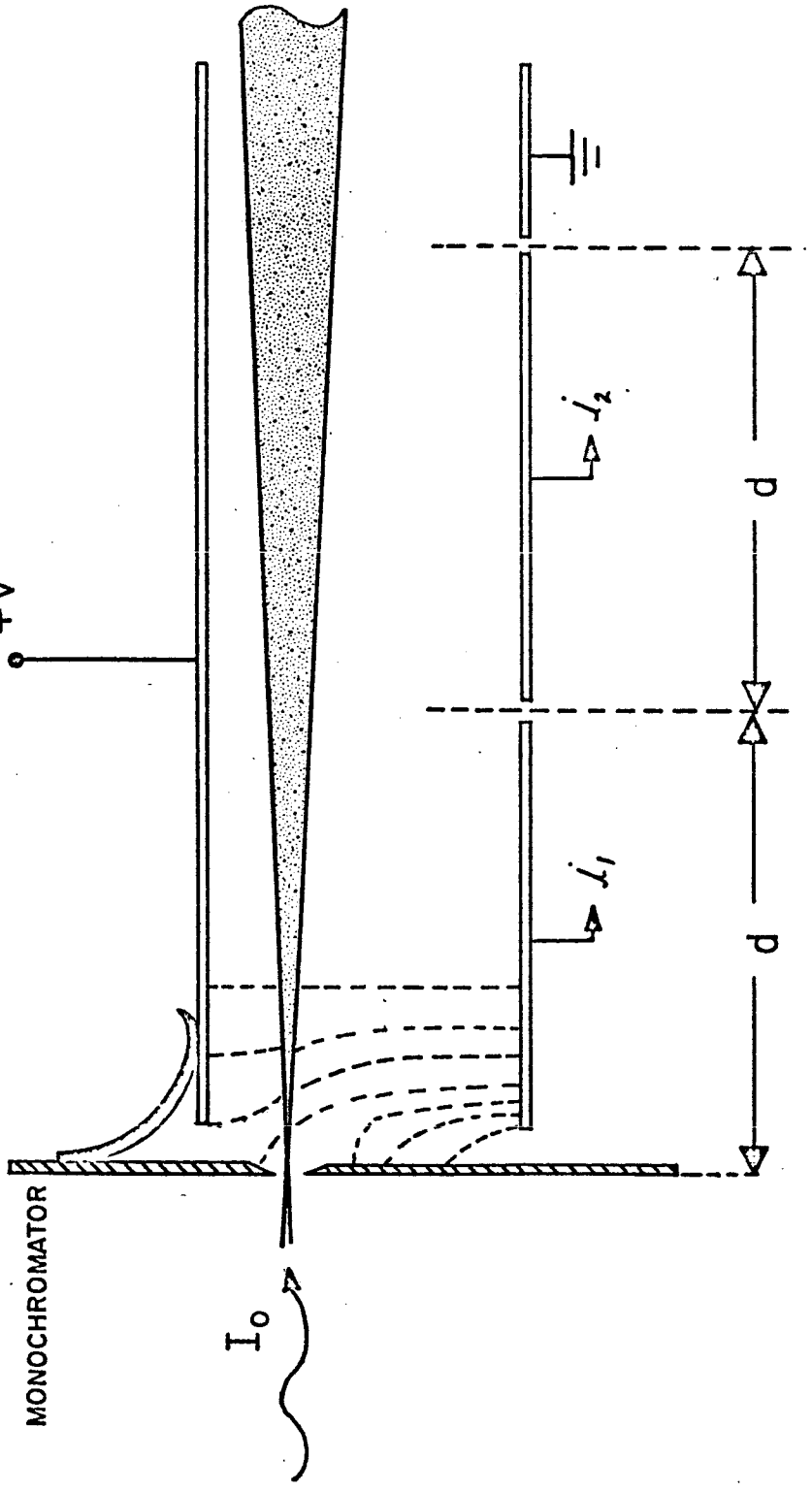

Figure 3. Modified double ion chamber. The exit slit is held at the same potential as the repeller plate. The grounded guard plate at the end of the ion chamber provides a uniform field at the end of the second collector plate. Thus, the ions collected by the two collector plates are formed over equal distances.

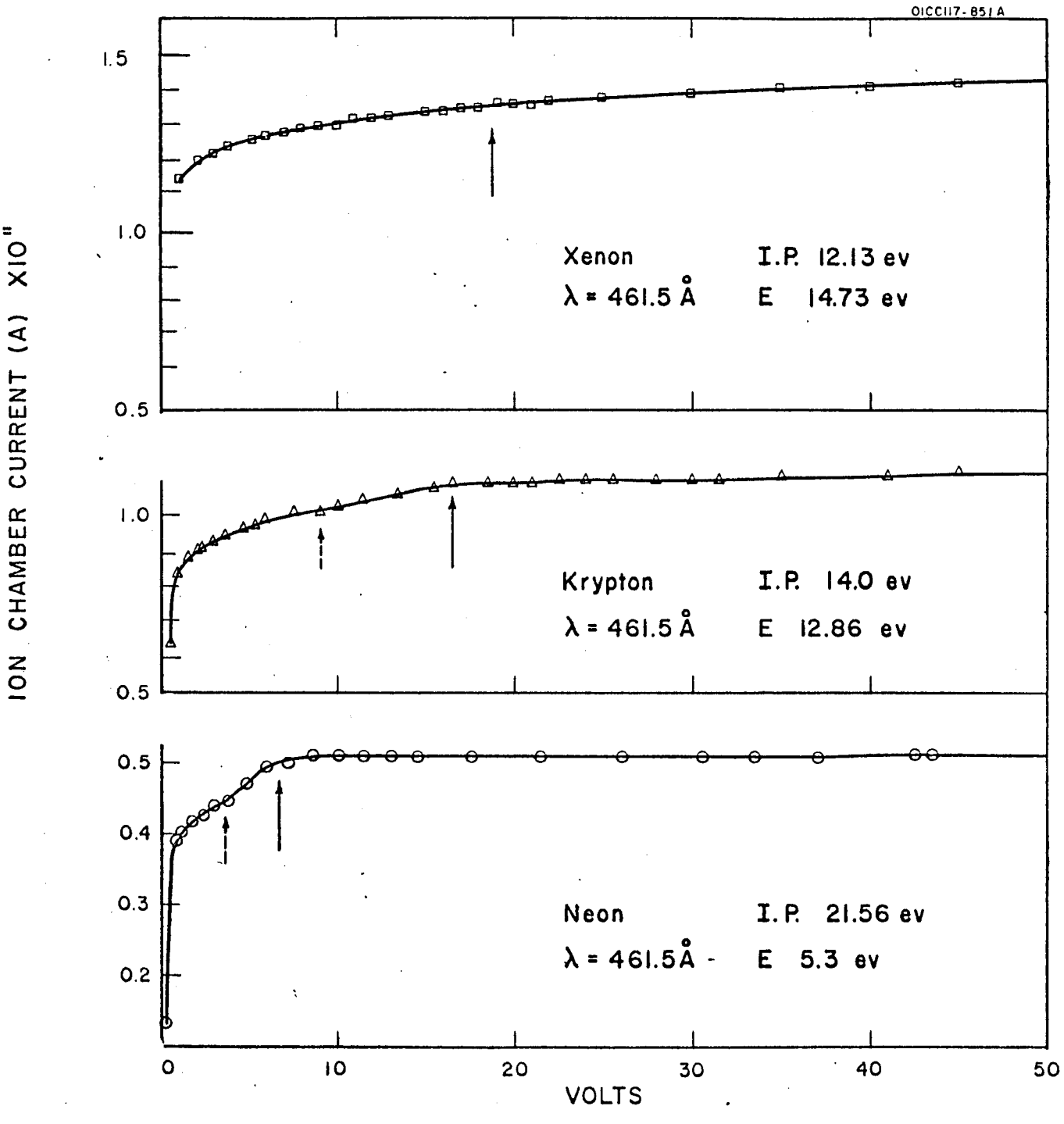

Figure 4. Ion chamber currents as a function of voltage for xenon, krypton and neon at 461.5 Å. In each case, the dashed vertical arrow indicates the voltage necessary to commence electron retardation whereas the solid arrow indicates the voltage necessary to complete electron retardation. E represents the energy of the ejected electron due to radiation of wavelength λ.

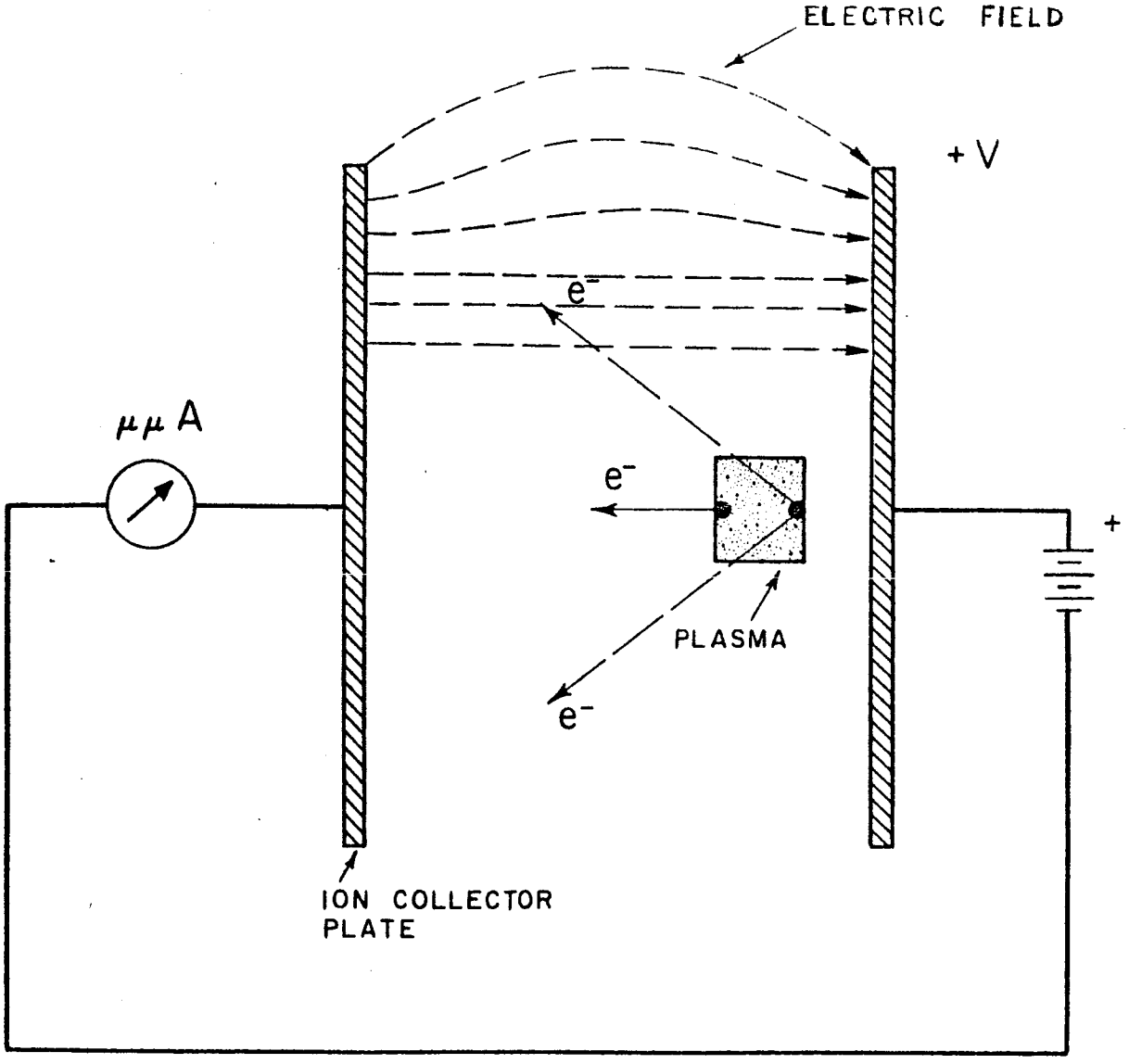

Figure 5. Typical electron trajectories for which the electrons will strike the ion collector plate if a sufficiently high retarding potential is not used.

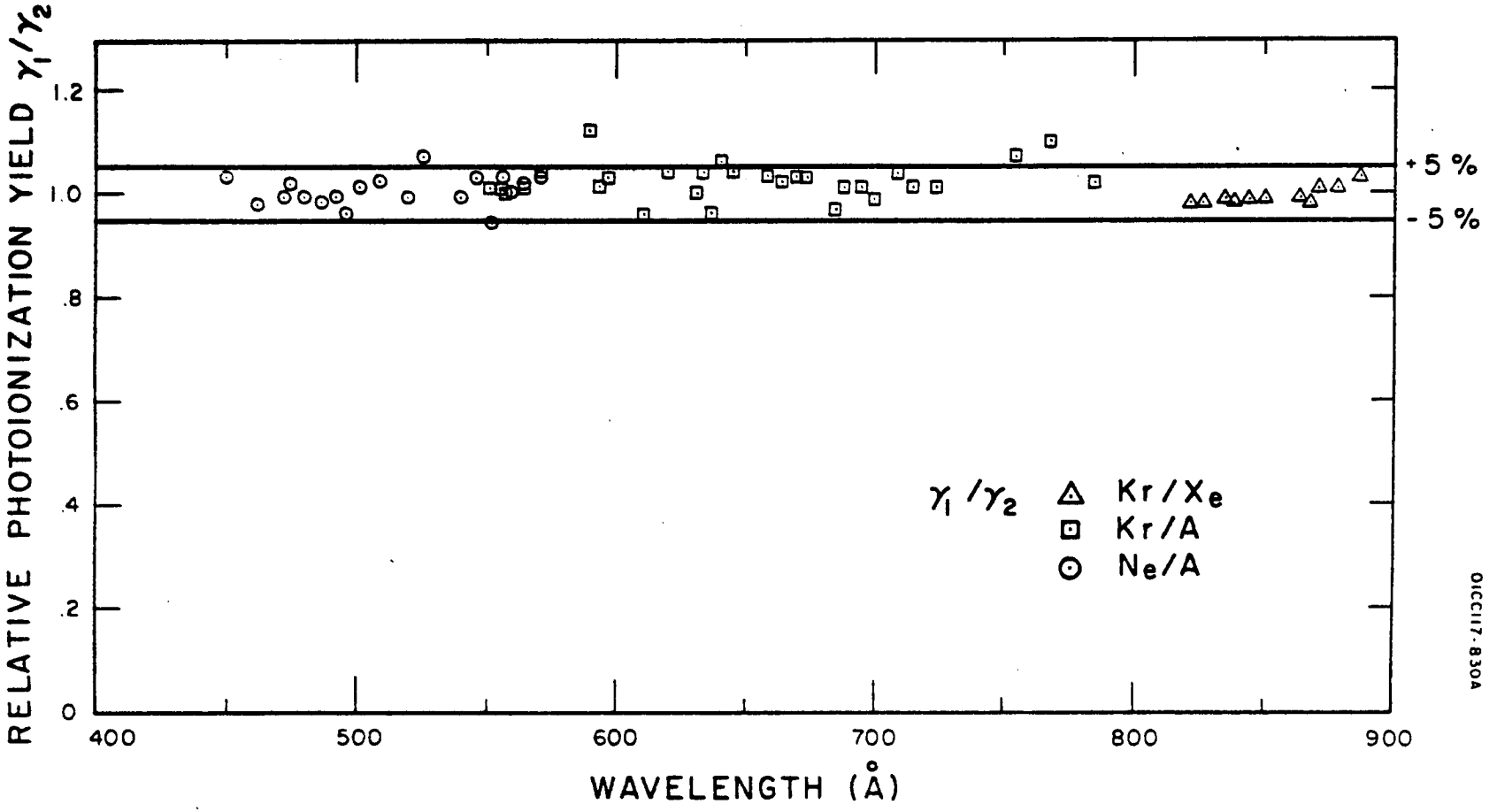

Figure 6. The relative photoionization yield of the rare gases in the region 400 - 900 Å. Kr/Xe represents the yield of krypton relative to xenon, etc.

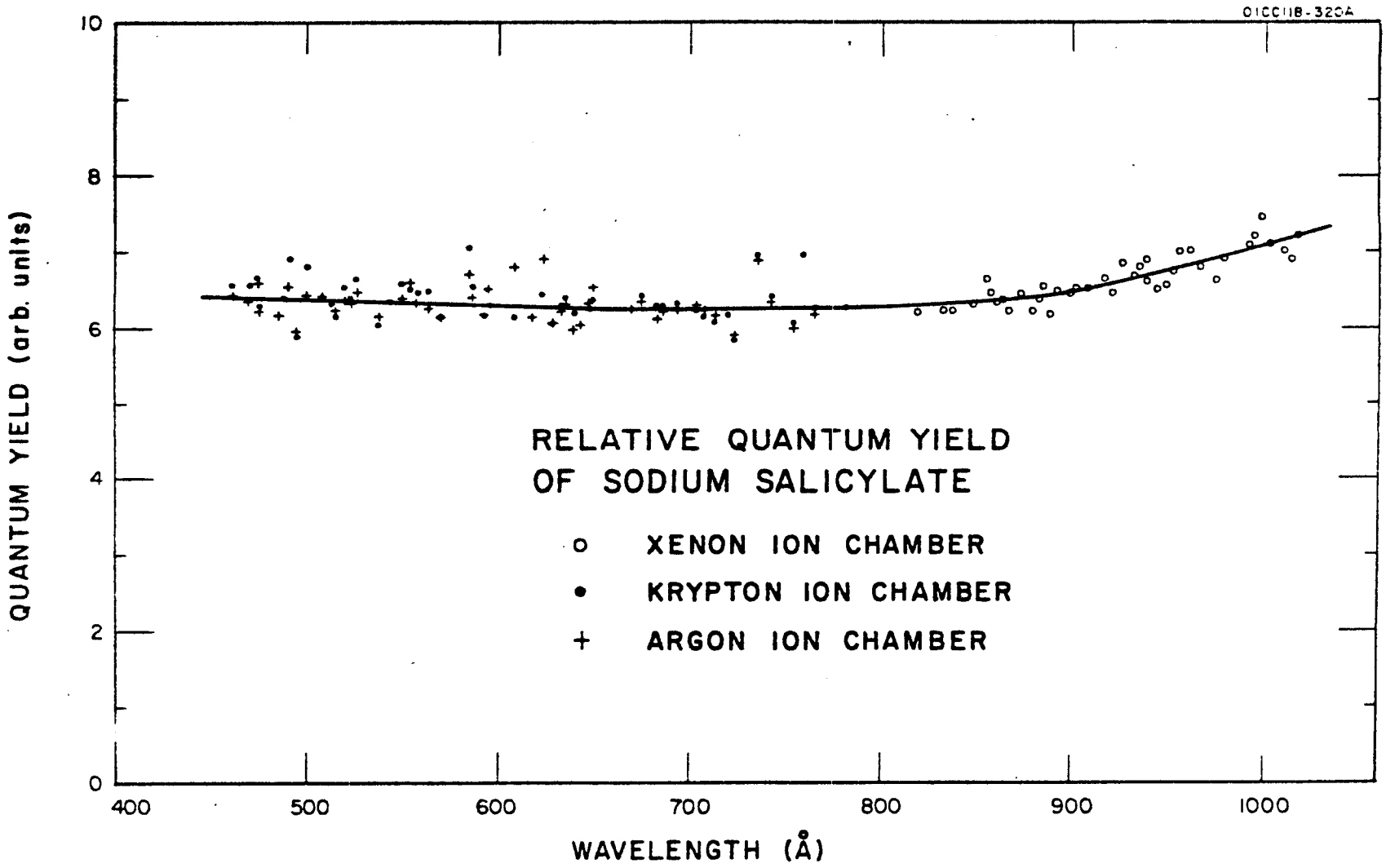

Figure 7. Relative quantum yield of sodium salicylate as a function of wavelength in the range 400 - 1000Å. The intensity of the incident radiation was measured by an ion chamber filled with a rare gas.

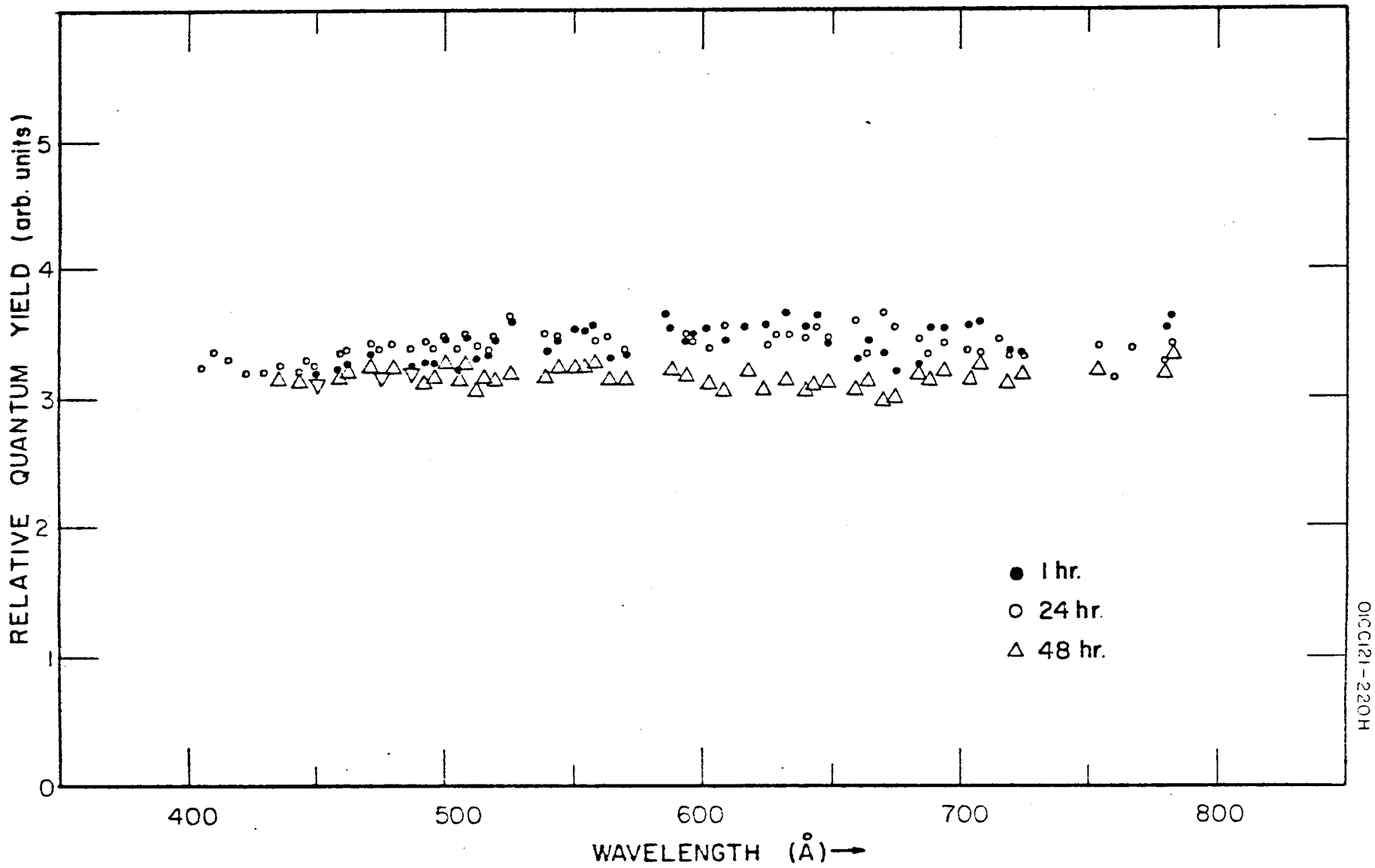

Figure 8. Relative quantum yield of sodium salicylate as a function of wavelength in the range 400 - 800 Å. The intensity of the incident radiation was measured with an argon ionization chamber. The solid data points represent results on a coating 1 hour old, the open circle points 24 hours old, and the triangle points 48 hours old.

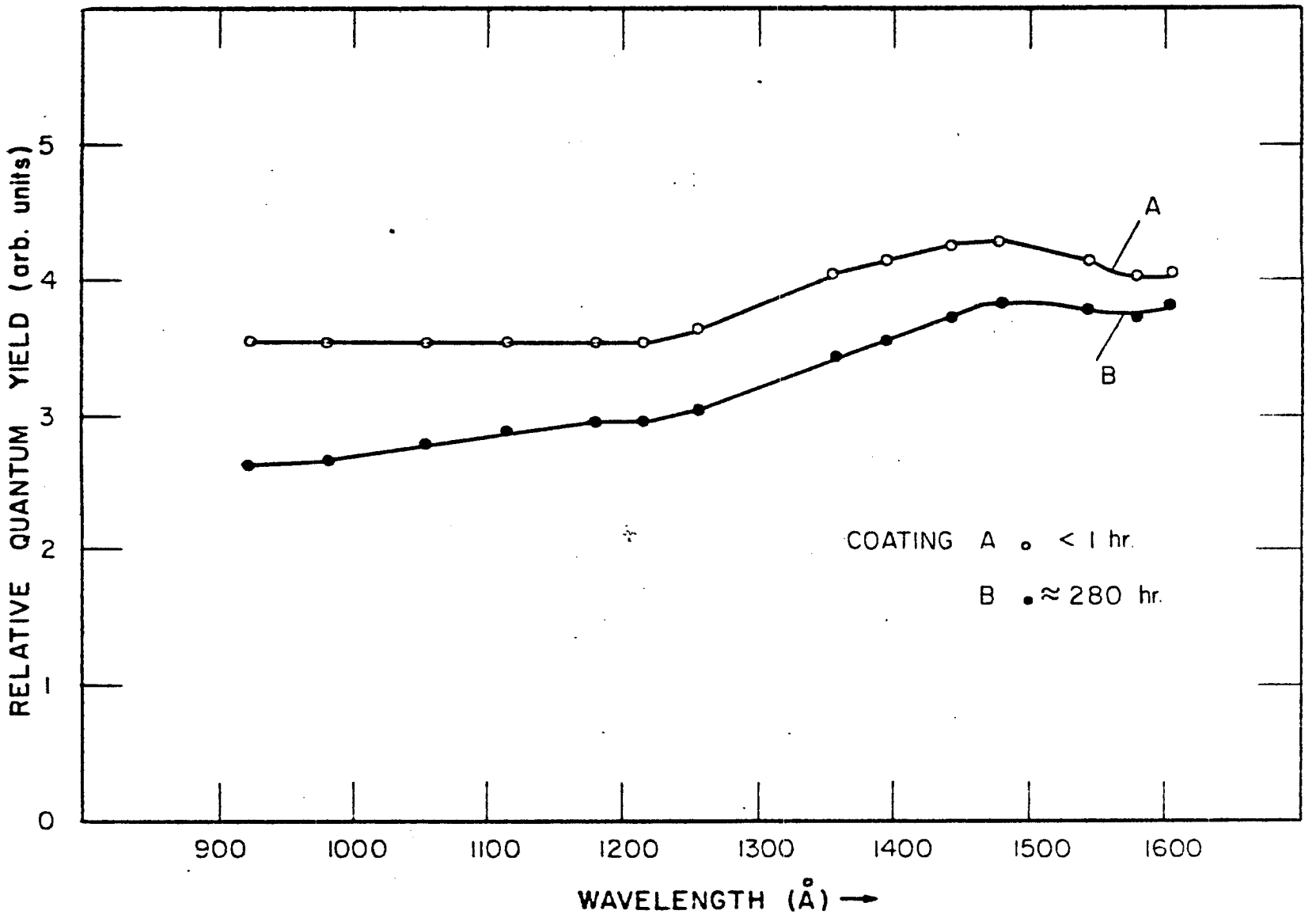

Figure 9. Relative quantum yield of sodium salicylate in the spectral range 900 - 1600 Å. The yield was measured for two different coatings relative to a thermopile: Coating A less than one hour old; Coating B approximately 280 hours old.

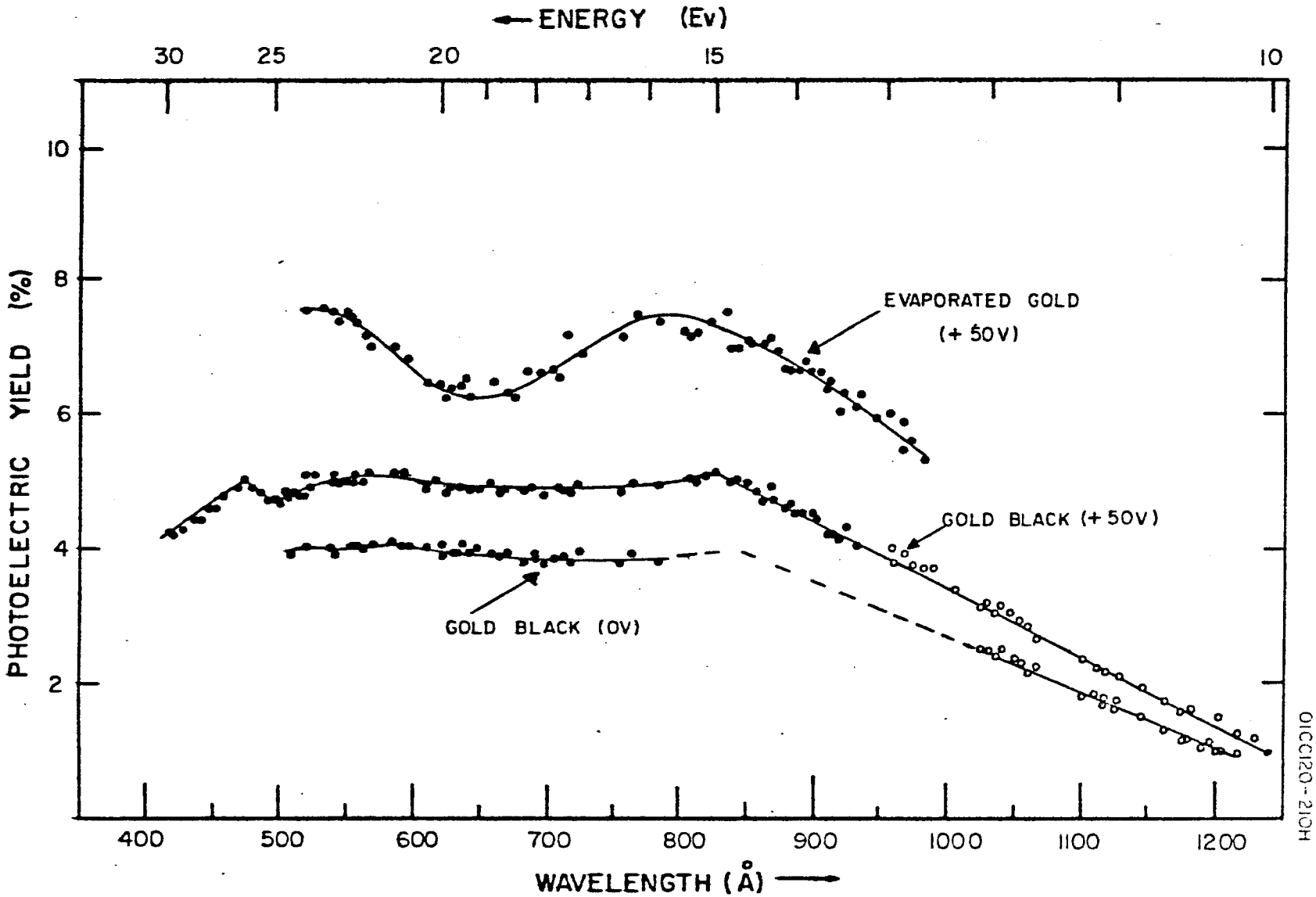

Figure 10. The photoelectric yield of gold.

The gold samples were all made from 99.99% pure gold wire. The evaporated gold sample had a metallic lustre and was prepared at a pressure of 10^{-5} torr while the gold black was evaporated in an atmosphere of nitrogen at a pressure of 1 torr and had a black velvet-like texture. The numbers in parentheses represent the electron collector voltages. The open circle data points were obtained relative to a sodium salicylate freshly-coated photomultiplier while all other data points were obtained using the rare gas ionization chamber.

GCA Technical Report No. 63-13-N

PLANETARY AERONOMY XIV: ULTRAVIOLET ABSORPTION OF SO_2: DISSOCIATION ENERGIES OF SO_2 AND SO

P. Warneck, F. F. Marmo and J. O. Sullivan

May 1963

Contract No. NASw-701

GEOPHYSICS CORPORATION OF AMERICA
Bedford, Massachusetts

Prepared for

NATIONAL AERONAUTICS AND SPACE ADMINISTRATION
Headquarters
Washington 25, D. C.

This paper has been accepted for publication in the Journal of Chemical Physics.

TABLE OF CONTENTS

Ultraviolet Absorption of SO_2: Dissociation Energies of SO_2 and SO

P. Warneck, F. F. Marmo and J. O. Sullivan

•

ABSTRACT

The absorption intensities of SO_2 were measured in the wavelength region 1849-3150 Å employing the hydrogen continuum as the source and at selected wavelengths utilizing the mercury line spectrum. The pressure dependence of the absorption intensity was investigated at 1849, 2537 and 3131 Å. The existence of an absorption continuum commencing at 2280 Å has been established and attributed to the dissociation of SO_2 forming SO and a ground-state oxygen atom. The onset of the continuum provides an upper limit value to the dissociation energy of SO_2. The implications upon the SO_2 and SO dissociation energies are discussed.

I. INTRODUCTION

The complex absorption spectrum of sulfur dioxide in the near and in the vacuum ultraviolet spectral region has been repeatedly studied with the aim of classifying band systems and making vibrational analyses. Specifically, in the wavelength range above 2000 Å, this has been nearly satisfactorily achieved by Duchesne and Rosen[1] and by Metropolis,[2] while the theoretical implications have been discussed by Mulliken[3] and by Walsh.[4] However, there appear to be no available data on quantitative absorption coefficients, except for the 1050 - 2100 Å spectral region, studied by Golomb et al.[5] In the present work, measurements of the SO_2 absorption intensities were performed at room temperature using the photomultiplier technique and covering the wavelength region 1849 - 3150 Å.

The available spectral resolution was insufficient to obtain new information concerning the involved band systems, especially in view of the considerable fine structure exhibited on photographic plates.[1] However, the photomultiplier technique is well suited for a study of any underlying continua. Thus, an important observation in the present work appears to be the finding of an absorption continuum commencing at 2280 Å. Part of this continuum can be discerned in the previously published data,[5] which also suggest the existence of a second continuum at shorter wavelengths, with the onset at 1680 Å. Since in this spectral region continua commonly arise from photodissociation processes, the observed long wavelength onset of a continuum provides an upper limit

estimate for the dissociation energy of the process involved. For the two continua mentioned with onsets at 2280 and 1680 Å, the corresponding upper limits to the dissociation energies are 125 kcal and 170 kcal, respectively. It is interesting to note that the energy difference (45 kcal) between the two onsets is close to the energy required to excite the ^1D state of atomic oxygen. This factor suggests that the observed continua may be interpreted as arising from the dissociation processes:

$$SO_2 + h\nu \rightarrow SO + O(^3P); \quad D(SO_2) \leq 125 \text{ kcal} \qquad (1)$$

$$SO_2 + h\nu \rightarrow SO + O(^1D); \quad D(SO_2) \leq 170 \text{ kcal.} \qquad (2)$$

One purpose of the present work is to show that it is reasonable to associate processes (1) and (2) to the observed continua. The importance of such data becomes evident when it is considered that the actual SO_2 dissociation energy is presently not well known and has been the subject of some controversy. Thus, after giving a description of the experiments and their results, the facts pertaining to the dissociation energies of SO_2 and the related molecules SO and S_2 will be discussed in a subsequent section.

II. EXPERIMENTAL

The principal experimental arrangement has been described.[6] In the present experiments a McPherson 2.2 m UV grating monochromator was employed in conjunction with an EMI 9514 photomultiplier detector viewing a sodium salicylate-coated glass plate. The absorption cell was 12.4 cm long, fitted with LiF windows at both ends, and mounted between detector and exit slit. With a 600 lines/mm grating and slit widths of 100 microns, the theoretical resolution was 0.8 Å. In practice, a resolution of 1 Å was observed. In order to avoid the overlapping and interference of the first and second order spectra above 2000 Å, a quartz plate was interposed between the absorption cell and the exit slit, resulting in a short wavelength cutoff at approximately 1600 Å and a long wavelength limit around 3200 Å.

Two types of light sources were employed: (1) A windowless hydrogen discharge tube, operated at 0.5 amps and 500 volts DC, furnished the well-known hydrogen continuum which provided a suitable background for recordings of the total absorption spectrum; (2) To establish the presence of true absorption continua, additional measurements were performed at specific wavelengths utilizing the line spectrum emitted from a Hanovia Mercury Utility Lamp. In this case, the entrance section of the monochromator was sealed off by means of a quartz window. Cooling the lamp with a fan considerably improved its radiation output in the ultraviolet, making the lines at 1849, 2537 and 3131 Å sufficiently intense to study at these wavelengths the pressure range.

Although the contribution of scattered light to the over-all signal received by the photomultiplier was generally negligible, allowance had to be made for it when the cell pressure was so high that it caused a decrease in the incident intensity by a factor of more than one thousand.

When such discrete line sources are employed, the apparent absorption coefficient decreases with increasing pressure in the case of discrete absorption; whereas, for a truly continuous absorption, the absorption coefficient does not vary sensitively with pressure. This behavior is due to the restricted resolution. For the case that both discrete and continuous absorption occur together, generally the apparent absorption coefficient decreases with increasing pressure until an upper limit value for the continuum is established. Finally, for very diffuse structure, the behavior is intermediate between the two cases discussed.

Matheson "bone dry" sulfur dioxide was used without further purification. A sample subjected to mass spectrometric analysis showed less than 1% impurity of either N_2 or CO, which should not alter absorption measurements in the considered spectral region. Neither detrimental water vapor nor SO_3 were observed. Pressures in the absorption cell were determined with a silicone oil manometer up to 25 mm Hg, while higher pressures were read on a Wallace and Tiernan No. FA129 instrument.

III. RESULTS

Intensities of absorption are shown in Figures 1 and 2 for the indicated wavelength regions. The data are expressed by the absorption coefficient k in reciprocal centimeters defined by $I = I_o \exp(-kx)$, where I_o and I are the incident and transmitted intensities and x is the layer thickness of the absorbing gas reduced to NTP. In general, absorption intensities obtained at various pressures (ranging from 2 mm Hg to 10 mm Hg) exhibited little pressure effect as long as less than 90% of the incident radiation was absorbed in the cell. Also, under these conditions, good agreement was observed between results obtained with the mercury line source on one hand and the hydrogen lamp on the other. Consequently, most k-values were derived by averaging measurements at several pressures. However, at the absorption maxima some pressure variation did occur and in this case, the values given are those obtained at the lowest cell pressures. Accordingly, the presented absorption coefficients have to be regarded as apparent ones, owing to the limited spectral resolution employed.

The spectrum shown in Figures 1 and 2 suggests the presence of two continua (overlapped by bands), one in the spectral region below 2280 Å and the other above 2400 Å. Only the first is energetically compatible with the approximately known energy value for SO_2 dissociation (vide infra). The data above 2400 Å give the appearance of a continuum but are really due to the restricted spectral resolution and a considerable overlapping of the involved bands. This view is compatible with the existent spectroscopic data[7] and the present absorption experiments performed at higher

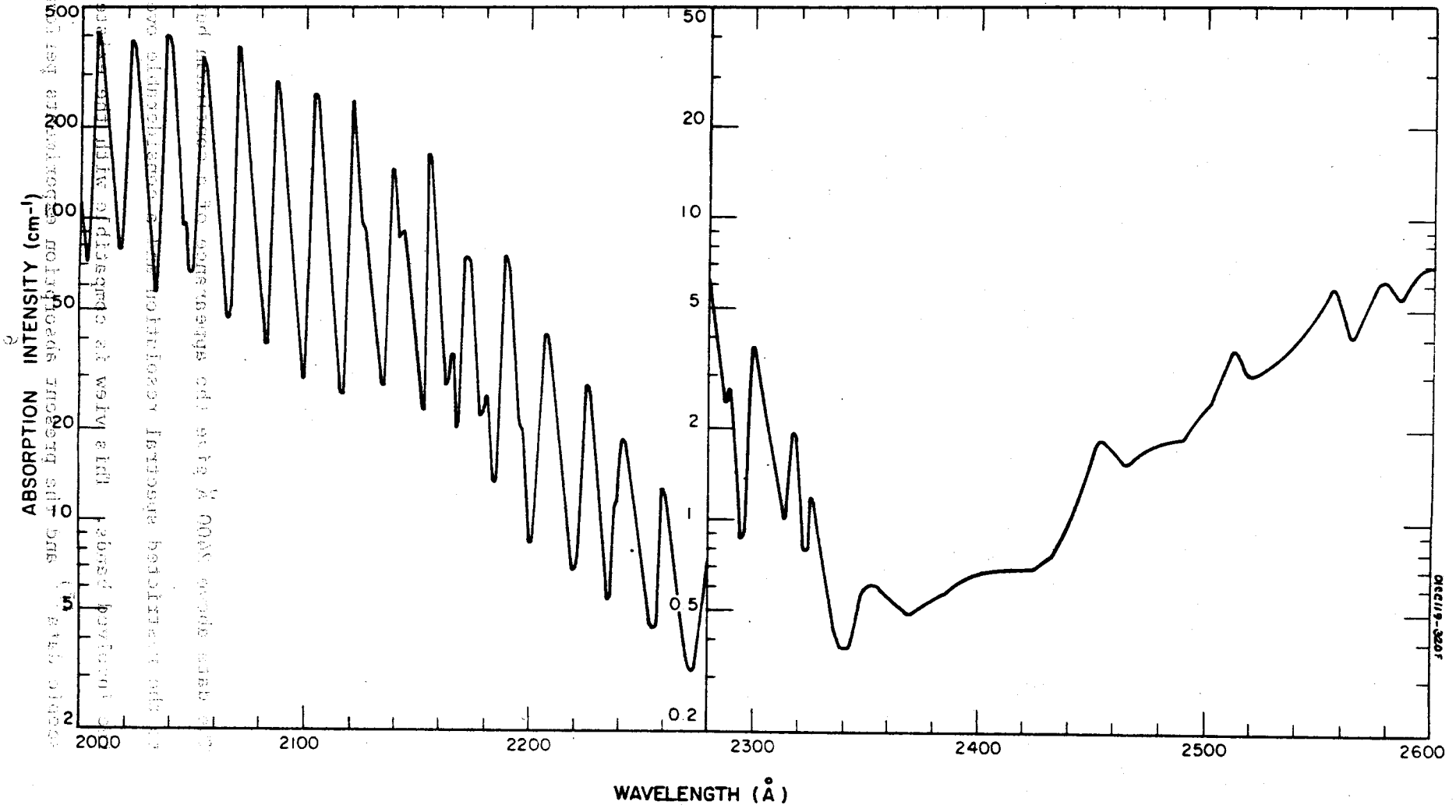

Figure 1. Absorption Intensities of SO_2 at 2000-2600 Å.

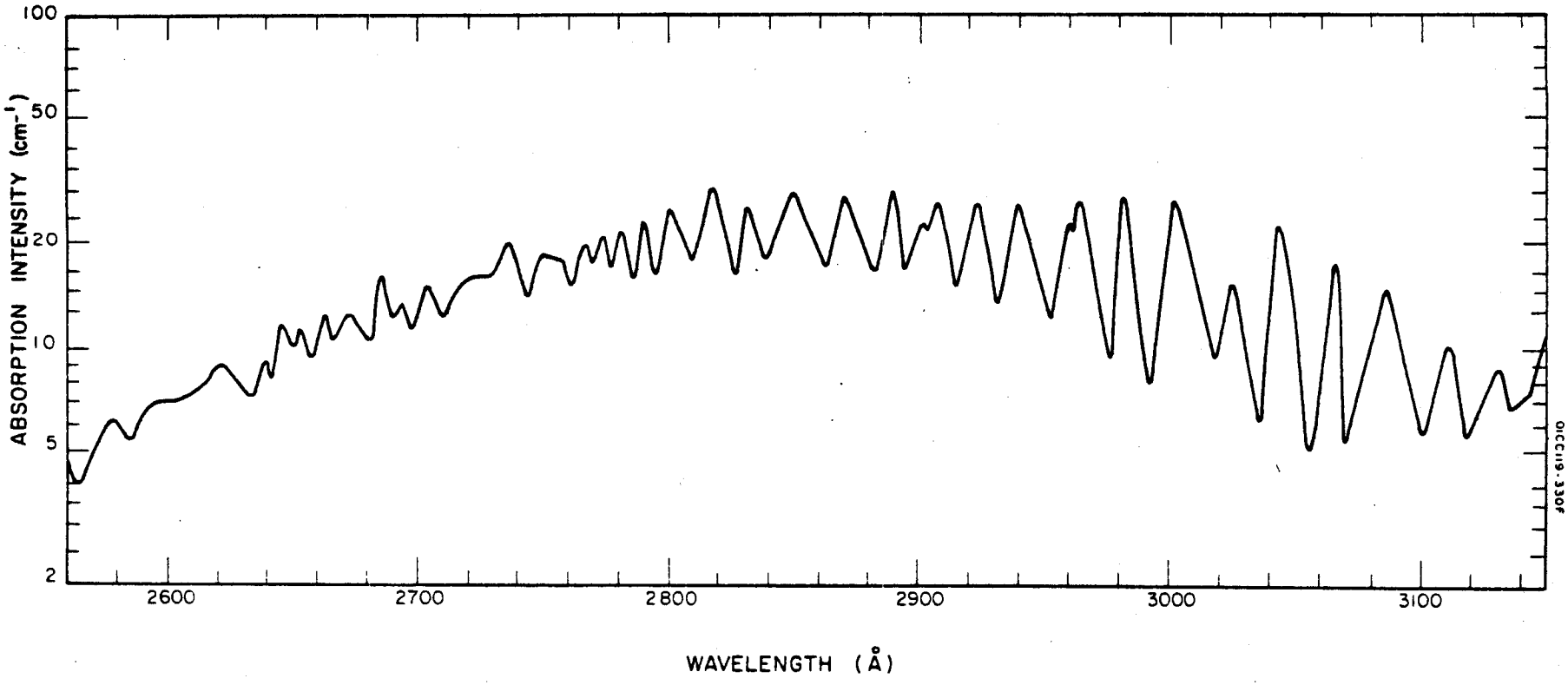

Figure 2. Absorption Intensities of SO_2 at 2560-3150 Å.

pressures, with the mercury light source at the discrete wavelengths 1849 Å, 2537 Å and 3131 Å.

Characteristically, in these experiments the amount of incident radiation absorbed in the cell was more than 90%. At 1849 Å, as shown in Figure 3, the apparent absorption coefficient at first decreases with increasing pressure and then becomes essentially independent of pressure. This behavior shows the presence of a discrete absorption spectrum, but it also makes evident that in the region below 2280 Å the values at the band mimima can be ascribed mainly to a true continuum. It is also interesting to note that with the discrete 1849 Å source the measured absorption coefficient approaches a value for the continuum of only 28 cm^{-1} as compared to the higher value of 75 cm^{-1} previously reported.[5] This apparent discrepancy can be ascribed to the insufficient resolution obtained in the reported experiments with the hydrogen background source. Thus, it appears that a true continuum exists in the 1700 - 2300 Å region with an upper limit absorption coefficient of 28 cm^{-1} at 1849 Å.

At 2537 Å, a decrease of the apparent k-value was observed, starting at a pressure of about 150 mm Hg. However, in this case, the line intensity was insufficient to give a strong enough signal for accurate measurements above 300 mm Hg. At this pressure, the apparent k-value was only 2.3 cm^{-1} (compared to 4.2 cm^{-1} at lower pressures). The apparent absorption coefficient probably decreases further with increasing pressures, suggesting that no continua exist at 2537 Å. Nevertheless, if the absorption at this wavelength should be in part continuous, the upper limit for the k-value of the continuum would be 2.3 cm^{-1}. For the 3131 Å case, no

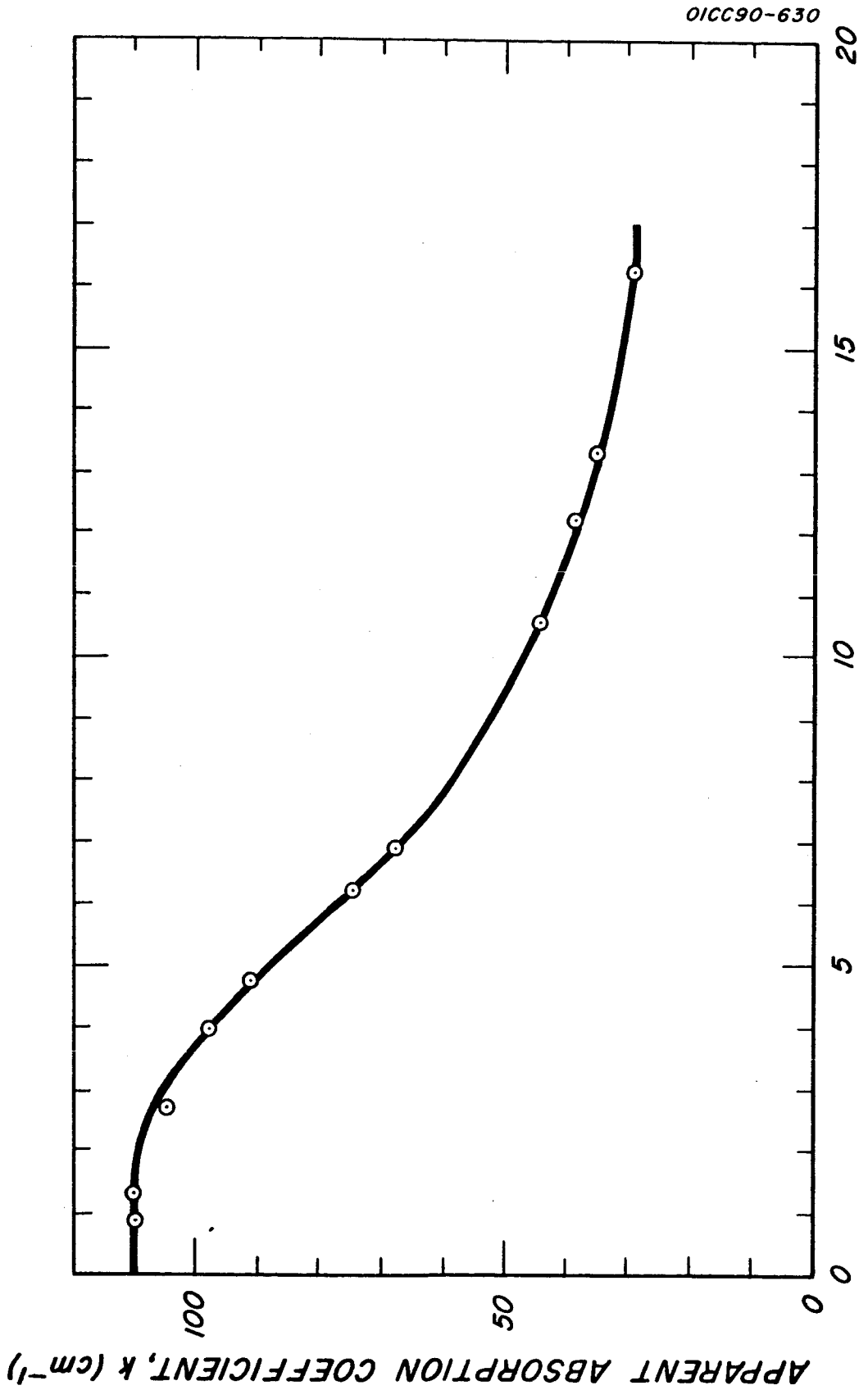

Figure 3. Pressure Variation of SO_2 Absorption at 1849 Å.

sensitive k-value decrease with pressure was observed owing to the insufficient intensity of the source. However, Figure 2 and energetic considerations preclude a continuum in this spectral region.

While the available evidence disfavors the existence of a continuum beyond 2500 Å, there can be no doubt about the reality of the continuum observed below 2280 Å. In Figure 4 are plotted the bases of the overlying bands versus wavelengths making use also of the data of Golomb et al.[5] The continuum is found to be quite symmetric in appearance, the maximum lying at 1915 Å and the observed long wavelength onset at 2280 Å. Conventional computation gives an f-number of 0.0294, but this is probably too high because of the insufficient spectral resolution employed. If it is taken into account that with increasing pressure the 1849 Å apparent absorption coefficient decreases from k = 75 to k = 28 cm^{-1}, the corrected value is reduced to f = 0.011.

Also shown in Figure 4 is the continuum located below 1700 Å. Since little overlapping occurs between the two continua, the experimental long wavelength onset of the 1300 - 1700 Å continuum could be reliably estimated to lie at 1680 Å whereas the maximum occurs at 1485 Å. The superposition of intense bands on the short wavelength slope of the continuum makes the obtained f-values somewhat ambiguous. The largest possible f-value is f = 0.0473, while the assumption of a symmetric continuum gives f = 0.035.

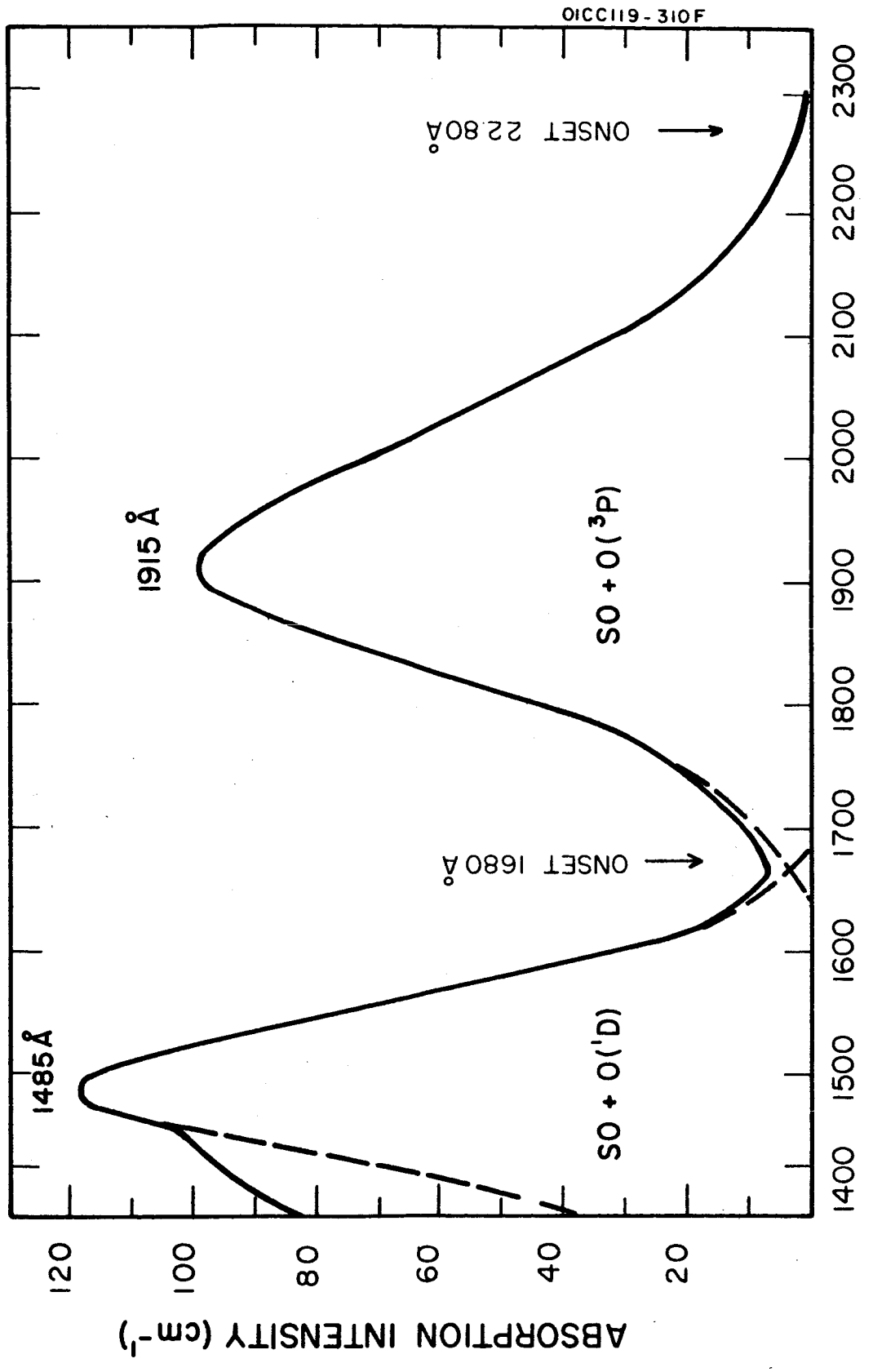

Figure . Absorption Continua for SO_2.

Undoubtedly, among the various data reported, the recognition of a true continuum in the spectral region 1700 - 2300 Å is most significant because of its implications concerning the dissociation energy of SO_2. This aspect of the results will now be discussed.

IV. THE SO_2 DISSOCIATION ENERGY

Making the reasonable assumption that at least the long wavelength end of the observed continuum is due to only one direct dissociation process, the corresponding upper limit of the dissociation energy can be determined, in principle, from the observed long wavelength onset of the continuum. Although in practice this is not a completely reliable method, in many cases it is the best available method provided the extrapolation is not too extensive.

In the present case, the long wavelength onset obtained for the two continua correspond to energies of 5.43 eV and 7.38 eV, or 125.3 kcal and 170.1 kcal, respectively. In addition, it is found that the energy difference (1.95 eV) is very close to the energy required to excite the ^1D state of atomic oxygen (1.967 eV), which makes is reasonable to associate the long wavelength parts of the two continua with the dissociation processes (1) and (2). Although it is difficult to give a reliable estimate of the errors involved in locating the onsets of the two continua, the derived upper limits of the dissociation energies are believed to be in error by not more than 0.2 eV, which corresponds to about 80 Å at 2280 Å and 50 Å at 1680 Å.

Except for the assignment of a predissociation limit at 1950 Å by Henri[7] which has been refuted,[8] there appears to exist no direct determination of the SO_2 dissociation energy with which the present value could be compared. The energy requirement of Reaction (1) can be calculated from thermochemical data by means of the relation

$$D(SO\text{-}O) = H(SO_2) + 1/2\ D(S_2) + D(O_2) - D(SO) \qquad (3)$$

provided the dissociation energies of the diatomic molecules S_2, O_2 and SO are known in addition to the heat of SO_2 formation from S_2 and O_2 in the gas phase. Unfortunately, only $D(O_2) = 118.0$ kcal[9,10] and $H(SO_2) = 86.3$ kcal[11] are well established, while the dissociation energies of S_2 and SO are still controversial. In both cases, fairly accurate predissociation limits are known from spectroscopic observations, but the lack of information concerning the electronic states of the product atoms precludes the proper choice among several possible values for the dissociation energies. The pertinent facts may be briefly recapitulated.

The predissociation occurring in the main SO emission spectrum is of a type for which the dissociation limit can be accurately established.[9] Martin[12] determined the limit to lie at 5.14 eV, but the SO <u>absorption</u> spectrum recorded by Norrish and Oldershaw[13] has indicated that the numbering of the vibrational levels of the ground state employed by Martin had to be revised, thus raising the predissociation limit to 5.35 eV or 123.5 kcal. If both of the atoms produced are in their ground states, this is also the dissociation energy.[14] On the other hand, if the resulting sulfur atom were in its first excited ^1D state, the dissociation energy would be lower by 1.15 eV (26.5 kcal). From a Birge-Sponer extrapolation of the vibrational levels for the upper state which is assumed to dissociate into $O(^3P)$ and $S(^1D)$, McGrath and McGarvey[15] have recently obtained $D(SO) = 127.1$ kcal in fair agreement with the predissociation limit of Norrish and Oldershaw.

In a similar way, an evaluation of the pertinent spectroscopic data for S_2 admits the possibilities $D(S_2)$ = 4.4, 3.6, or 3.3 eV, corresponding to 101, 83 or 76 kcal, none of which can be ruled out with certainty. The available evidence has been discussed in detail by Gaydon[14] and by Cottrell.[16]

When the various possible values for D(SO) and $D(S_2)$ are combined with the known heats of O_2 dissociation and SO_2 formation according to Equation (3), the array of SO_2 dissociation energies shown in Table I is obtained. Upon inspection it is found that the SO_2 dissociation energies derived with D(SO) = 97 kcal exceed by some 20 kcal the experimentally determined upper limit of $D(SO_2)$ = 125 kcal, thereby ruling out the lowest of the three possible values for D(SO). This leads at once to the acceptance of D(SO) = 123.5 kcal, or the slightly higher value of D(SO) = 127.1 kcal if the latter is shown to be more correct. Accordingly, it is also established that in the observed predissociation of SO, the products are ground state atoms; i.e., $O(^3P)$ as originally suggested by Martin,[12] while the upper state ($^3\Sigma^-$) dissociates into $O(^3P)$ and $S(^1D)$ as it was assumed by McGrath and McGarvey.[15]

For the dissociation energy of S_2, a similar choice is not provided by the present data. This is due to the errors involved in locating the onset of the observed SO_2 dissociation continuum combined with the circumstance that only one-half of $D(S_2)$ enters into Equation (3), thus reducing the spread in $D(SO_2)$. As a consequence, it is also not possible to deduce the SO_2 dissociation energy with exactitude. However, the true value for $D(SO_2)$ will lie within 6.5% of the averaged one, $D(SO_2)$ = 123.3 ± 8 kcal,

TABLE I. SO_2 dissociation energies assuming various values for D(SO) and $D(S_2)$.

	D(OS-O)		
$D(S_2)$	D(SO) = 127.1	D(SO) = 123.5	D(SO) = 97
101	127.7	131.3	157.9
83	118.7	122.3	148.9
76	115.3	118.9	145.3

which happens to coincide with the measured onset of the dissociation continuum.

While the preceding usage of the terms "SO_2 dissociation energy" and "$D(SO_2)$" referred to the energy required to rupture the OS-O bond as characterized by Reaction (1), one must recognize the existence of the alternative mode of dissociation

$$SO_2 + h\nu \rightarrow S + O_2 \quad . \tag{4}$$

Although this process would require the breakage of two bonds, it is not permissible on this ground to exclude the reaction a priori. In the similar case of N_2O photodecomposition, it has been shown[17] that the center nitrogen atom can be ejected with some probability even though the energy is insufficient for a dissociation into three atoms. Neither can Reaction (4) be excluded for energetic reasons. However, it may not be reasonable to associate the appearance of a true absorption continuum to Reaction (4) because the breakup of the SO_2 molecule into O_2 and S must necessarily be preceded by an atomic rearrangement in the excited state, which by its nature resembles a unimolecular decomposition rather than direct dissociation along a repulsive state. The absorption spectrum would be diffuse owing to perturbations from other crossing potential curves, but would not display a true continuum. This view is still compatible with the results of the photodecomposition referenced above,[17] since in that case the interest lay in the decomposition products. The

interpretation of absorption spectra, on the other hand, deals with the initiating step in the photodecomposition. Consequently, the given argument tends to confirm the assignment of the absorption continua to Processes (1) and (2) which describe the direction dissociations.

REFERENCES

1. Duchesne, J. and B. J. Rosen, J. Chem. Phys. 15, 631 (1947).

2. Metropolis, N., Phys. Rev. 60, 295 (1941).

3. Mulliken, R. S., Rev. Mod. Phys. 14, 204 (1942).

4. Walsh, A. D., J. Chem. Soc., 2266 (1953).

5. Golomb, D., K. Watanabe and F. F. Marmo, J. Chem. Phys. 36, 958 (1962).

6. Watanabe, K., J. Chem. Phys. 22, 1564 (1954).

7. Henri, V., Leipziger Vortrage, 131-54 (1931).

8. Price W. C. and D. M. Simpson, Proc. Roy. Soc. A165, 272 (1937).

9. Herzberg, G., Molecular Spectra and Molecular Structure (D. Van Nostrand and Company, Inc., Princeton, 1957), Vol. 1.

10. Brix, D. and G. Herzberg, J. Chem. Phys. 21, 2240 (1953).

11. Bulletin 542, U. S. Bureau of Mines (1954).

12. Martin, E. V., Phys. Rev. 41, 167 (1932).

13. Norrish, R. G. W. and G. A. Oldershaw, Proc. Roy. Soc. (London) A249, 498 (1958).

14. Gaydon, A. G., Dissociation Energies (Dover Publications, New York, 1950).

15. McGrath, W. D. and J. F. McGarvey, J. Chem. Phys. 37, 1574 (1962).

16. Cottrell, T. L., The Strengths of Chemical Bonds (Academic Press Inc., New York, 1958).

17. Doehring, J. P. and B. Mahan, J. Chem. Phys. 34, 1617 (1961).

LIST OF FIGURES

Observed and Predicted New Autoionized Energy Levels in Krypton, Argon, and Xenon

James A. R. Samson
Physics Research Division, Geophysics Corporation of America, Bedford, Mass.

ABSTRACT

The absorption spectrum of argon and krypton has been investigated between 400 - 600Å. Discrete structure is observed which can be related to the excitation of an inner s electron. Configuration interactions between the discrete excited levels and the overlapping ionization continuum leads to autoionization of the energy levels, as evidenced by the fact that the measured photoionization yield within the discrete structure is 100%.

The first member of the series is observed at 466Å for argon and 497Å for krypton with a predicted value of 593Å for xenon.

The Rydberg series $\nu = 235\ 832 - R(n-1.53)^2$, n = 4, 5, --- etc. describes the argon data while similar series are predicted for krypton and xenon with quantum defects equal to 2.53 and 3.53, respectively, and using the appropriate term value for their respective N_1 and O_1 absorption edges.

This paper has been accepted for publication in The Physical Review (December 1963).

OBSERVED AND PREDICTED NEW AUTOIONIZED ENERGY LEVELS IN KRYPTON, ARGON, AND XENON

James A. R. Samson
Physics Research Division, Geophysics Corporation of America, Bedford, Mass.

The photoionization cross sections of argon and krypton have been measured between 400 - 560Å. In both gases discrete structure is observed superimposed on the photoionization absorption continuum. The structure in argon can be identified with the new autoionized energy levels recently observed spectroscopically by Madden and Codling,[1] while that of krypton has not previously been reported. The structure in the krypton photoionization cross sections is assumed also to be due to autoionized energy levels, since the photoionization yields for the discrete structure in both argon and krypton were measured and found to be 100%.

The anomolous nature of the autoionized lines in showing a decrease in absorption with no accompanying increase is apparently allowed in the Fano theory of autoionization.[2]

The cross section measurements were made on a 1/2 M Seya-type vacuum monochromator with a 2.5Å band pass. The light source consisted of a high voltage repetitive spark discharge in argon which produced an extremely dense line spectrum above 400Å. The absorption cell consisted of two ionization chambers in series and of identical lengths, d. The absorption coefficient, μ, is then given by

$$\mu = \ell n(i_1/i_2)/d,$$

where i_1 and i_2 are the ion currents produced, respectively, in the two ion chambers. A detailed discussion of this technique is described in another paper.[3] The gas pressure was varied from 0.05 - 0.5 Torr and the effective absorption length, d, was 10 cm. The major advantage of this technique in the measurement of absorption coefficients is that i_1 and i_2 (and hence μ) are measured simultaneously and are, therefore, independent of any changes in light source intensity.

The photoionization cross sections, reduced to S.T.P., are shown in Figures 1 and 2 for argon and krypton, respectively. With the exception of the discrete structure the cross sections are pressure independent (± 5%) over a pressure range of 0.05 - 0.5 Torr.

There exist very little data on the photoionization cross sections of krypton and argon between 400 - 500Å, with the exception of the work on argon by Po Lee and Weissler[4] who used photographic techniques to measure the cross sections. Where data exist, there is agreement within 10%.[5,6]

The vertical lines in Figure 1 represent the positions of the autoionized lines in argon discovered by Madden and Codling using the continuum radiation from a 180 Mev synchrotron.[1] It can be seen that the discrete absorption structure coincides exactly with the first three terms of their series. In the present work these lines appear at 466, 442.8 and 434.8Å. There is an uncertainty of ±0.5Å in the wavelength determination. The line widths shown here are instrumental, reflecting the 2.5Å band pass of the monochromator. The vertical arrow represents the M_1 edge at 424Å as obtained from spectroscopic data.[7] The experimental value of 422Å is in good agreement with this value.

The autoionized lines observed in krypton appear at 471.8 and 497Å with the suggestion of one at 464Å. A sudden discontinuity in the curve occurs at 449Å, in good agreement with the spectroscopic value of 450.5Å for the N_1 edge of krypton,[8] represented by the vertical arrow in Figure 2.

It seems likely that the autoionized lines in argon and krypton are due to the excitation of the inner s electron terminating with its ejection at the M_1 and N_1 edges, respectively. If this is the case, the following Rydberg series for argon can be fitted to the data of reference 1 and to the first three terms of the present work.

$$\nu = 235832 - R/(n - 1.53)^2 \quad n = 4,5 \ldots, \text{ etc.}$$

Table I compares the observed wavenumbers to those calculated from the above series. The observed data were obtained from measurements made on an enlarged photograph, taken from reference 1, and, thus, are not so precise as their original data.

In order to fit a Rydberg series to the krypton data and thereby predict the higher terms of the series, the following system was adopted: If we assume that the first observed term in krypton is indeed the first member of the series $4s^2rp^6 - 4s4p^6np$, we can then determine the quantum defect for n = 5 and 6. Comparing these values with those deduced from reference 1 and also to the alkali metals we might expect to find a relationship between the various quantum defects enabling us to predict a quantum defect for the higher members of the krypton series. These quantum defects are tabulated in Table II. It can be seen that there is a very striking relationship, not only in the quantum defects between the rare gases but also compared to the alkali metals. The main features are, (i) that the quantum defect increases approximately by unity

Table I. Observed wavenumbers in argon for the transition $3s^2 3p^6 - 3s3p^6 np$ compared to the calculated values given by $\nu = 235832 - R/(n-1.53)^2$.

n	ν obs.	ν calc.
4	214 500	217 845
5	225 700	226 718
6	229 900	230 340
7	232 000	232 164
8	233 200	233 211
9	233 900	233 865
10	234 300	234 302
11	234 600	234 608

Table II. Observed quantum defects of the rare gases compared to those of the alkali metals. Numbers in italics indicate predicted values.

Term	Quantum Defects								
	Ne[a]	Na	A[b]	A[a]	K	Kr[b]	Rb	Xe	Cs
3p	0.86	0.883	...	...	...	...	...	...	...
4p	.85	.867	1.73	1.73	1.77	...	...	...	...
5p	.8	.862	1.7	1.7	1.74	2.7	2.71	...	...
6p	.8	.860	1.7	1.7	1.73	2.7	2.67	3.67	3.65
7p	.6	.859		1.6	1.72	...	2.66	...	3.60
8p	.6	.858		1.6	1.72	...	2.66	...	3.59
				...		...		...	
				...		...		...	
∞				1.53		2.53		3.53	

a These values were deduced from an absorption spectrum in Reference 1. The accuracy in the quantum defect for the first term is approximately ± 0.01; however, for higher terms the inaccuracies increase to probably as much as ± 0.1.

b Present work.

in steps going from neon to argon to krypton and (ii) the quantum defect of a rare gas is essentially equal to that of the alkali metal next to it in the periodic table and whose final state transition is the same as that of the rare gas. The similarity appears reasonable since we are essentially comparing the binding energies of similar electrons in closely related atoms. The quantum defect for the rare gases, however, does vary more rapidly than that of the alkali metals, probably due to the interaction between the discrete states and the continuum. Since the quantum defects in argon and krypton differ by unity in the first two terms we will assume this difference continues for higher members and thus predict the following Rydberg series for krypton:

$$\nu = 221917 - R/(n-2.53)^2 \quad n = 5,6 \ldots, \text{ etc.}$$

Similarly, we should expect from (i) above that the transition $5s^2 5p^6 - 5s5p^6 6p$ in xenon would have a quantum defect of 3.7 and from (ii) a value of 3.65. Assuming a mean value of, say, 3.67 the predicted term level would be approximately at 168500 cms^{-1} (593Å). Following the same reasoning as for krypton the higher terms in xenon are predicted to follow the Rydberg series,

$$\nu = 188708 - R/(n-3.53)^2 \quad n = 6,7 \ldots, \text{ etc.}$$

A search for this series is currently under way.

It is a pleasure to acknowledge the many helpful discussions with Professor A. Dalgarno and Dr. A. Naqvi.

REFERENCES

1. R. P. Madden and K. Codling, Phys. Rev. Letters 10, 516 (1963).

2. U. Fano, Phys. Rev. 124, 1866 (1961).

3. J. A. R. Samson, J. Opt. Soc. Am., to be published.

4. Po Lee and G. L. Weissler, Phys. Rev. 99, 540 (1955).

5. N. Wainfan, W. C. Walker, and G. L. Weissler, Phys. Rev. 99, 542 (1955).

6. A. Pery-Thorne and W. R. S. Garton, Proc. Roy. Soc. (London) 76, 833 (1960).

7. C. E. Moore, Atomic Energy Levels,National Bureau of Standards, Circular No. 467 (U. S. Government Printing Office, Washington, D.C., 1949), Vol. I.

8. C. E. Moore, Atomic Energy Levels, Vol. II, 1952.

LIST OF FIGURES

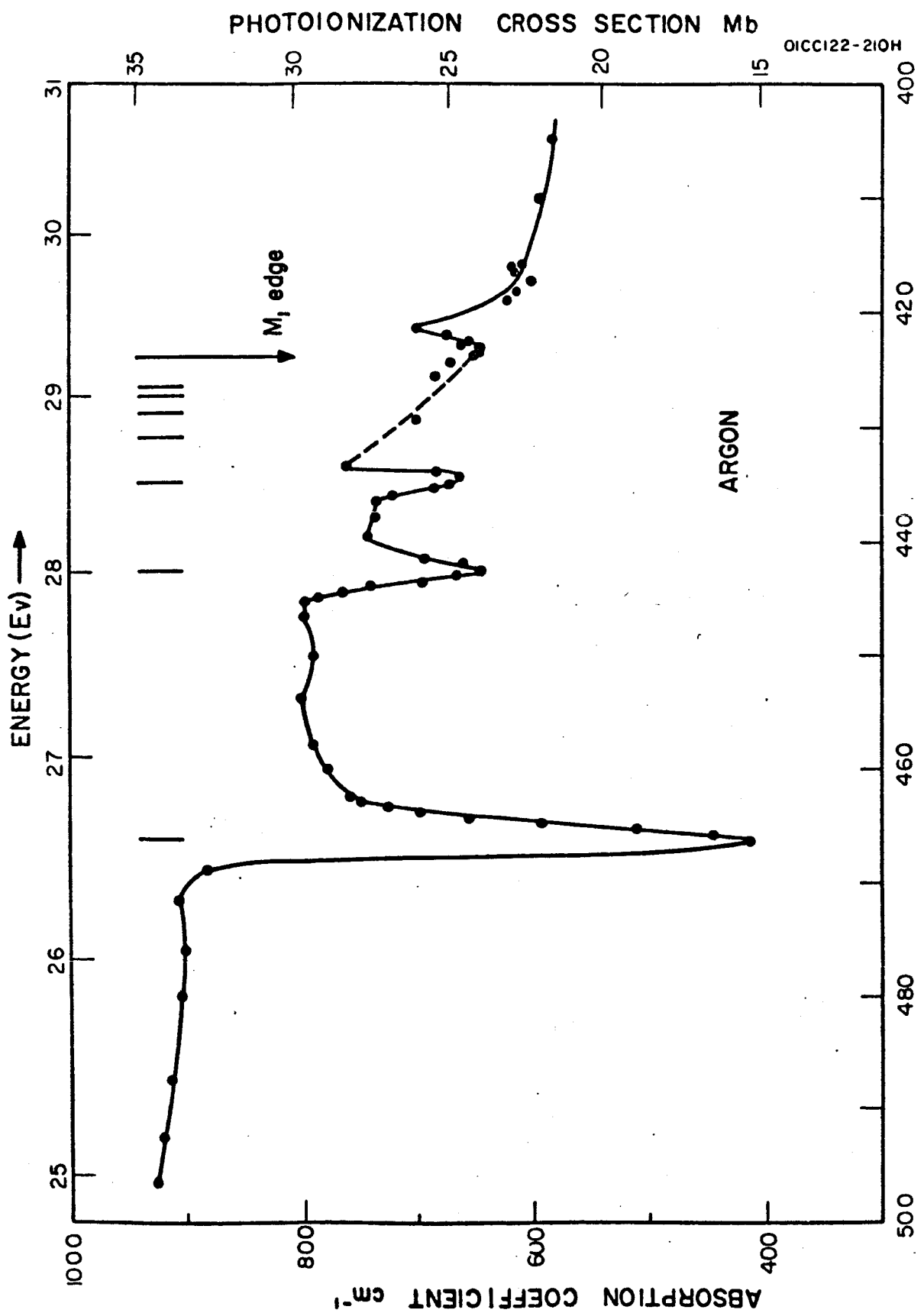

Figure 1. Photoionization cross sections for argon between 400-500 Å. The vertical lines represent the positions of the autoionized series reported in Ref. (1), while the vertical arrow indicates the position of the M_1 edge due to the removal of an s electron.

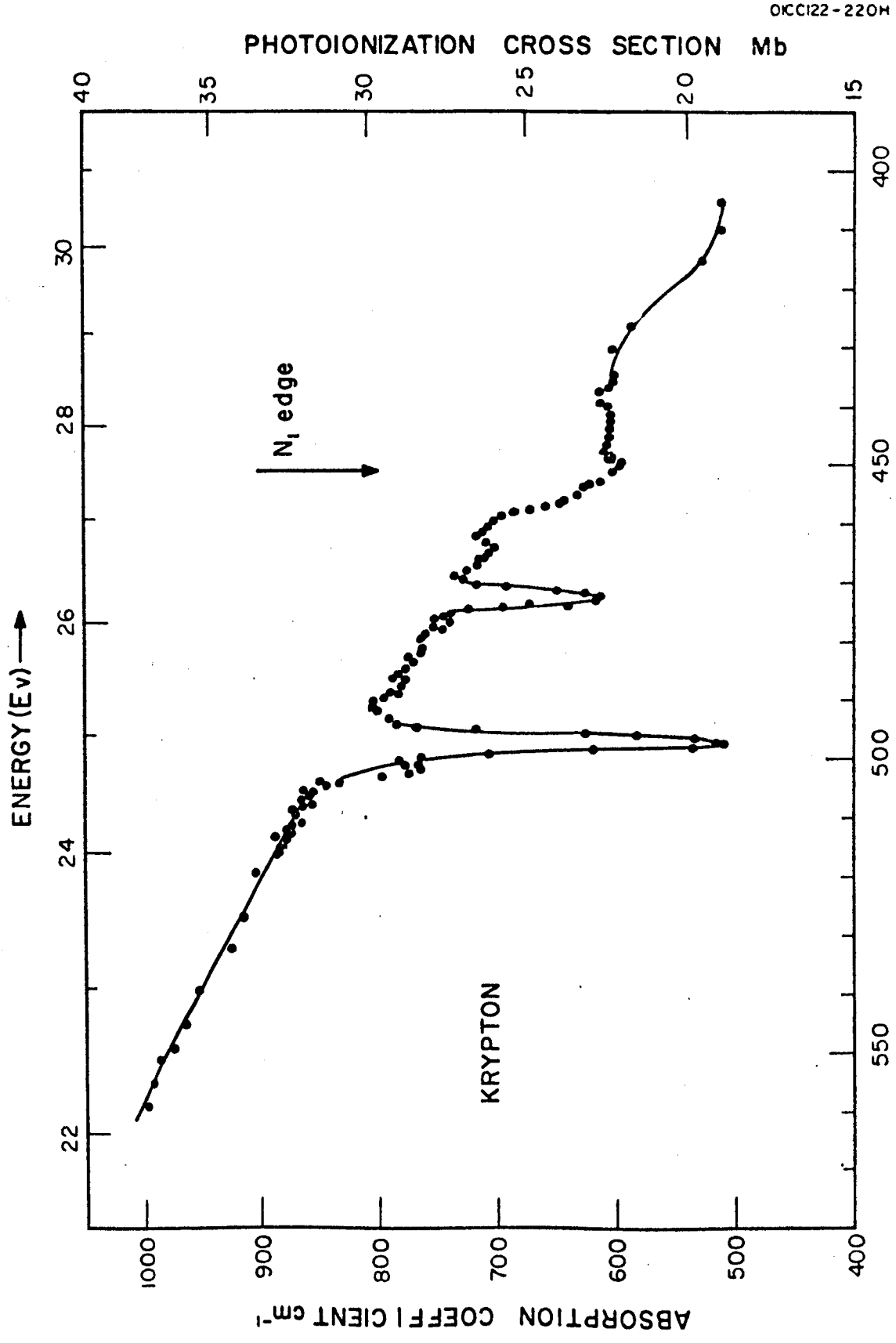

Figure 2. Photoionization cross sections for krypton between 400-560 Å. The vertical arrow indicates the position of the N_1 edge due to the removal of an s electron.